MORPHOLOGICAL CHARACTERIZATION OF DYNAMIC DENDRITE GROWTH IN THE AWAKE DEVELOPING BRAIN

by

Sharmin Hossain

A THESIS SUBMITTED IN PARTIAL FULFILLMENT OF
THE REQUIRMENTS FOR THE DEGREE OF

DOCTOR OF PHILOSOPHY

in

THE FACULTY OF GRADUATE AND POSTDOCTORAL STUDIES

(Neuroscience)

THE UNIVERSITY OF BRITISH COLUMBIA

(Vancouver)

December 2014

Abstract

Precise wiring between dendrites and axons during brain development is a critical requirement for forming proper neuronal connectivity, a prerequisite to generate correct brain function. Establishing this highly complex physical network entails forming precise patterns of dendritic and axonal arborization as well as correct targeting of these processes to appropriate brain regions. As compared to our current understanding of axonal development, relatively little is known regarding the structural organization and of dendritic arbor growth during dendritogenesis. Two major obstacles in studying dendritogenesis *in vivo* are technical challenges in observing the dynamic behavior of these structures in the developing brain, and post-imaging analyses of their complex growth patterns. Here, we used *in vivo* rapid time-lapse imaging in the intact and awake vertebrate brain to observe dynamic dendritogenesis and analyzed components of growing dendritic arbors of individual neurons to elucidate how short-term growth behaviors culminate to produce the dendritic arbor patterning of mature neurons. Of particular interest, this work establishes that dendritic growth cones exist on all growing dendrites, but due to their dynamic nature, they have been grossly under-reported in previous *in vivo* studies. In this study, I find that dendritic growth cone morphology correlates with branch behavior, report differences in two different dendritic filopodial populations *in vivo*, and describe how dendritic growth behavior changes over neuronal maturation. Further, we have developed a novel analysis tool called Dynamo to accurately track and analyze dendritic components. I have used this tool to screen three candidate guidance cue molecules, including ephrin-A1, ephrin-B1, and slit2, for their potential role in regulating dynamic behavior of growing dendrites, and found that slit2 exposure decreases branch motility and increases branchtip filopodial motility *in vivo*. I also find that neurons located in the caudomedial tectum project their dendrites in a biased rostral orientation to reach the tectal neuropil, and that interfering with the Slit receptor

Robo3, prevents this biased dendrite growth. These findings provide novel insights into how dendrites develop *in vivo* in the awake vertebrate brain.

Preface

A version of Chapter 2 has been published as **'Dynamic morphometrics reveals contributions of dendritic growth cones and filopodia to dendritogenesis in the intact and awake embryonic brain' (Developmental Neurobiology, 2012. Apr;72(4):615-27).** For this chapter, I was responsible for all work, including research design, conducting experiments, data analysis and writing the manuscript, except as follows: Dr. Kurt Haas provided feedback on project design and edited the manuscript, and Dr. Sesath Hewapathirane conducted the experiments for Figure 7E, F, and G, while I analyzed data and made the figure.

Chapter 3 is previously unpublished. This chapter describes development and features of a novel program, called Dynamo, to trace neurons and analyze dendritic arbor growth. Kaspar Podgorski and I contributed equally as primary authors to project research, design, and implementation. In addition, a lab intern, Steffen Kaiser, supervised by Kaspar and me, contributed to the Analysis and Documentation component.

Chapter 4 is previously unpublished. I was responsible for all aspects of this work, except as follows: An undergraduate intern under my supervision, Kristel Leung, conducted experiments for 2 n's for the ephrin-A group for Figure 14,Figure 15, and Figure 16, and I performed experiments for 2n's for this group and all experiments for all other groups. I was solely responsible for data analysis and making figures.

All animal experiments included in this dissertation were approved by University of British Columbia Animal Care Committee and were conducted according to Protocol A11-0332.

Table of Contents

List of Tables

List of Figures

List of Abbreviations

AMPA: α-amino-3-hydroxy-5-methyl-4-isoxazolepropionate

APV: (2*R*)-amino-5-phosphonovaleric acid

BDNF: Brain-derived neurotrophic factor

CAM: Cell adhesion molecules

CAMK: Calcium/calmodulin-dependent protein kinase

cAMP: Cyclic adenosine monophosphate

cGMP: Cyclic guanosine monophosphate

CSPG: Chondroitin sulphate proteoglycan

CNQX: 6-cyano-7-nitroquinoxaline-2,3-dione

CNS: Central nervous system

DRG: Dorsal root ganglion

DSCAM: Down syndrome cell adhesion molecule

EGF: Epidermal growth factor

EM: electromicrographs

FGFP: Farnesylated enhanced green fluorescent protein

FNIII:Fibronectin type III

GSK3: Glycogen Synthase Kinase 3

GUI: Graphical user interface

Ig: Immunoglobulin

LRR: Leucine-rich repeat

MAPK: Mitogen-activated kinase

NGL: Netrin G ligand

NGF: Nerve growth factor

NMDA: n-methyl-d-aspartate

OT: Optic tectum

PI3K: phosphoinositide 3-kinase

PIP3: phosphatidylinositol 3,4,5 triphosphate

RGC: Retinal ganglion cell

RTK: Receptor tyrosine kinase

SC: Superior colliculus

SCE: Single-cell electroporation

TDBL: Total dendritic branch length

Acknowledgements

I would first like to thank my supervisor Dr. Kurt Haas, for his guidance, support, and patience, and for providing me with substantial freedom to be creative. I believe I have become stronger as a person as well as a researcher in the Haas lab, and most importantly, learned that in life, impossibility is a relative term. I would also especially like to thank my committee members, Dr. Tim O'Connor, Dr. Shernaz Bamji, and Dr. Jane Roskams for their invaluable time and input in my project design. Special thanks go to Dr. Kurt Haas and Dr. Tim O'Connor for their mentorship and consideration when life took some unexpected turns.

Thank you to my lab mates, including Dr. Blair Duncan, Dr. Sesath Hewapathirane, Dr. Xuefeng Liu, Dr. Derek Dunfield, Dr. Simon Chen, and Kasper Podgorski, for leaving me with one of the most memorable periods of my life. You were truly there for me every step of the way, and not just as colleagues, as friends you have gone above and beyond. Every one of you, in unique ways, has inspired me in more ways than I can express in words. I also want to express my sincere gratitude to some terrific friends and colleagues, including Dr. Ted Dobie, Dr. Tabrez Siddiqui, Dr. Kevin She, and Dr. Ainsley Coquinco for their expert advice and delightful conversations. Also, thanks go to Dr. Wun Chey Sin and Dr. Steve Bond for their help and advice with molecular biology and biochemistry, and to Jamie Boyd, Shay Neufeld, Steffen Kaiser, Ran (Richard) Liu for help with analysis. In addition, I feel very privileged to have had the opportunity to mentor several dedicated and brilliant students, including Kristel Leung, Lisa Zhou, Christina Sun, Vincent Ye, Mark Ventura, Sharukh Bakar, and Minh Nguyet Nguyen, without whom my work would not have been half as enjoyable. You have taught me to love teaching!

Finally, I would like to take this opportunity to thank my mother Dr. Bilquis Banu, who taught me to love learning, my father Mohamed Anwar Hossain, who taught me the meaning of perseverance, and my dearest brother Raged Anwar, for keeping me grounded in reality.

For my parents,

this work is but a pebble in the beach of debt owed to you

Chapter 1: Introduction

The development of functional brain circuits is one of the most critical and complex events in early life. Establishing the framework of mature human brain connectivity involves formation of appropriate synaptic contacts between 100s of billions of growing neurons. The structure and spatial location of each brain neuron's dendrites and axons, the primary input and output structures respectively, forms the physical network that determines the type and number of contacts that can be formed, and therefore directly influences neural circuit function. Thus, understanding the structural and orientation development of dendrites and axons is a fundamental goal in developmental neurobiology. To this end, axonal growth has been extensively studied (Bentley and O'Connor, 1994). However, due to technical challenges in observing developing dendrites in the intact immature brain, and an entrenched focus on questions of axonal pathfinding, investigation of dendrite development and guidance remains in its infancy (Georges et al., 2008). A comprehensive understanding of dendrite development in the intact immature brain is necessary to understand how functional neural connectivity is established. Furthermore, as abnormal dendrite growth has been observed in several neurodevelopmental disorders, including Down syndrome, Rett syndrome, fragile X syndrome, and febrile seizures, deeper insight into normal and abnormal dendrite development may resolve how aberrant dendritogenesis affects the pathophysiology of these disorders (Hewapathirane et al., 2008; Kaufmann and Moser, 2000; Purpura, 1975).

1.1 Generation of neuronal polarity involves axon-dendrite specification

A critical step in neuronal morphogenesis is to break from the symmetry of a newly differentiated neuron and formation of dendrites and axons as morphologically, molecularly, and functionally distinct compartments. Embryonic hippocampal neuron culture has been widely

used to investigate generation of neuronal polarity. In dissociated embryonic hippocampal cultures, neurons progress through several morphological stages. Initially, soon after transplanted neurons adhere to the substrate, they begin to sprout lamellipodia around the soma (Bradke and Dotti, 2000; Craig and Banker, 1994; Dotti et al., 1988). Next, several small 'neurites', a general term used to denote both undifferentiated axons and dendrites in culture appear from the soma. These processes are tipped with growth cones, which are highly dynamic structures at the ends of neuronal processes consisting of a web-like lamella or high filopodial turnover (Bartlett and Banker, 1984a, b; Bray, 1973). Several hours later, axon initiation occurs as one of these neurites begin to extend more rapidly compared to the other neurites and begin to differentiate into an axon while the remaining neurites become dendrites, giving rise to neuronal polarity. Ensuing growth and refinement of both axons and dendrites give rise to the mature neuronal architecture. In the case of mammalian excitatory synapses, maturation of dendrites generally also involves formation of dendritic spines, small "door-knob" shaped protrusions that receive excitatory inputs.

In dissociated neuronal cultures, neurons lack endogenous extracellular cues, yet somehow they still form a single axon from multiple equipotential neurites. The prevailing hypothesis on the underlying mechanism of this phenomenon states that axon initiation in culture occurs through a stochastic and spontaneous process that results in symmetry breaking among multiple neurites (reviewed in Craig and Banker, 1994; reviewed in Lalli, 2014). Initially, all growing neurites undergo alternating periods of elongation and retraction, and during this period, all neurites remain at a similar length. From the molecular perspective, it has been proposed that an underlying negative feedback loop is present, such that each growing neurite sends intracellular signals to the soma, which prevents all other neurites from extending too far. In hippocampal cultures, this balance is maintained for approximately one day, after which by a stochastic mechanism, one neurite extends and becomes longer than the other ones (reviewed

in Andersen and Bi, 2000). Once this occurs, a positive feedback loop causes this neurite to extend farther, and simultaneously, this 'stronger' neurite exerts a greater negative feedback loop on the other growing neurites, preventing them from becoming axons as well. The molecular cues that may underlie these positive and negative feedback loops are not yet known, although it has been proposed that Rho GTPases, which act as molecular switches that regulate the actin cytoskeleton, may play a role (Andersen and Bi, 2000). Interestingly, axon specification in the case of hippocampal neurons in culture is not permanent, but rather a flexible event (Goslin and Banker, 1989). *Goslin et al.* demonstrated that transecting the growing axon at a position that makes it equal length or shorter than one of the other neurites leads to a different neurite taking on axonal properties.

Molecular mechanisms underlying axon initiation are beginning to be elucidated (reviewed in Lalli, 2014; Zhou and Snider, 2006). Molecules in the extracellular environment activate intracellular signaling cascades within the growing neuron, which ultimately impinge on either actin or microtubule dynamics or membrane delivery to the nascent axon. A key intracellular pathway in axon initiation involves phosphoinositide 3-kinase (PI3K) activation in the developing growth cone of the growing neurite, which leads to phosphatidylinositol 3,4,5 triphosphate (PIP3) accumulation in that neurite, which in turn inactivates Glycogen Synthase Kinase 3 (GSK3). GSK3 phosphorylates several microtubule-binding proteins, including CRMP2, Map1b, and Tau, which prevents them from binding to microtubules. Thus, GSK3 inhibition via PI3K activation leads to binding of these microtubule-associated proteins (MAPs), leading to microtubule stabilization, which in turn allows axon initiation. PI3K activity is highly localized to the tips of growing axons, and this polarized distribution of its activity is necessary for axon formation (Shi et al., 2003). In rat hippocampal neurons in culture, GSK-3β is differentially distributed in axons versus dendrites, and enhanced GSK-3β activity inhibits axon formation, whereas decreased GSK-3β activity leads to formation of multiple axons (Jiang et al.,

2005). Another pathway critically involved in neuronal polarity involves the PAR complex, which consists of the PAR-3, Par6, and aPKC (atypical protein kinase C) proteins have been implicated in various events involving cellular polarity (reviewed in Kemphues, 2000). Activation of the PAR complex leads to delivery of membrane precursor vesicles to the growing axons in *Drosophila* as well as microtubule stabilization in rat hippocampal neurons (Chen et al., 2006; Wang et al., 2011). Moreover, interfering with a downstream effector of the PAR complex, Tiam1, leads to development of multiple axons in neuronal cultures (Nishimura et al., 2005).

Recent experiments suggest that *in vitro* mechanisms of neuronal polarization do not necessarily reflect how neurons develop *in vivo* (reviewed in Lalli, 2014; Zolessi et al., 2006). In contrast to rat hippocampal neurons and zebrafish RGCs cultured *in vitro*, RGCs *in vivo* do not extend multiple neurites at random orientations around the cell body prior to axon initiation. Instead, they extend a single neurite, which extends rapidly and invariably forms the axon. RGCs developing *in vivo* have access to extracellular cues from the surrounding tissue, namely the retinal neuroepithelial environment, and this study suggests that these cues direct the proper orientation and location of axon initiation. Interestingly, if RGC neurons are ectopically transplanted in mutant zebrafish larvae with disrupted orientation of the retinal neuroepithelium, neuronal polarity is perturbed, resulting in axons initiating from aberrant locations. In this study, Zolessi *et al.* suggest that in the absence of the natural extracellular cues, neurons may be forced to resort to artificially use available intrinsic mechanisms to compensate and generate a method of axon initiation, highlighting the necessity for investigating neuronal polarity in other *in vivo* systems.

1.2 Dendritic architecture underlies functional neural circuit development

Neuronal dendritic architecture encompasses myriad shapes, sizes, and complexity,

which correlates with the diverse functionality of different types of neurons (Wong and Ghosh, 2002). Despite this diversity, a common theme in dendritic growth patterns is that dendrites often have spatial orientation bias that increases the probability of contacts with the appropriate presynaptic axons. Purkinje cells of the cerebellum, for example, have complex and elaborate dendritic arbors which receive and integrate over 100,000 synaptic inputs, and provide the only source of output for the entire cerebellar cortex (Apps and Garwicz, 2005). The dendritic arbors of these neurons are preferentially orientated towards the inputs from their primary presynaptic partners, the parallel fibers from granule cells. Similarly, retinal ganglion cells (RGC) in the vertebrate project their dendrites to “ON” or “OFF” regions of the inner plexiform layer of the retina correlating with the way the neuron responds to a light stimulus (Nelson et al., 1978).

Whereas the location of dendritic arbors influences which synaptic inputs are received, dendritic arbor length, width, and branching complexity shape intraneuronal information processing. Dendrites are the sites for most excitatory inputs onto neurons in the CNS. In a given neuron, both excitatory and inhibitory synaptic inputs from various regions of the dendrite propagate down the length of the dendrites and integrate at the soma to produce an all-or-none action potential output for the neuron. This output is also affected by inputs, usually inhibitory, received at the soma or the axon hillock. The distance of a synaptic input to the soma and dendritic morphology influence how the signal decays as it propagates toward the soma and thus how much the signal contributes to synaptic integration with other inputs. Given that the spatial location of dendrites determine which presynaptic partners the neuron can receive inputs from, and dendritic architecture influences information processing at the level of individual neurons, dendrite growth has a profound effect on neural circuit formation and function.

1.3 Dendritogenesis occurs via dynamic net branch growth

Given the integral role of dendritic architecture to neural connectivity and information

processing, it is critical to understand how immature neurons elaborate their dendrites during development to establish their final dendritic morphology. During brain development, new neurons are generated when neural progenitor cells divide asymmetrically to give rise to a new neuron and another neural progenitor cell (Gotz and Huttner, 2005). Depending on the brain region and neuron types, these newly generated neurons often have to migrate to their final target region before they can begin to form neuronal processes.

1.3.1 Misconceptions of constant dendrite growth resulted from static images

From the 1890's, with the advent of the Golgi stain (1890's) and the electron microscope (1930's), to the 1990's, *in situ* observations of dendrite growth were conducted in fixed tissue by observing neurons at different developmental stages with neuronal stains (Golgi, antibodies, dye injections) and electromicrographs (Fox et al., 1976; McAllister, 2000; Purpura, 1975). Due to the static nature of these observations and comparison across neurons, until the 1990's, dendritogenesis was thought to occur in a consistent manner similar to branches on trees, with a steady increase in dendrite growth and branching (Cano et al., 1989; Mathers, 1977, 1979).

1.3.2 Time-lapse imaging reveals dynamic fluctuations of developing arbors

In contrast to these static observations, however, live cell time-lapse imaging has invalidated this "steady growth" view of dendrite formation to reveal that dendritogenesis is a dynamic process, which consists of branch addition, elongation, retraction, and selective stabilization. Net branch growth over time, rather than a steady increase in branch length results in increased dendrite growth over neuronal maturation. This modern perception of dynamic growth initially emerged from *in vitro* examination of neurites. However, although dissociated primary cultures and organotypic slice cultures have offered significant insight into how neurites

differentiate into dendrites and axons, it is important to understand the similarities and differences between these systems and neurons that mature *in vivo* in their native environment, the intact brain.

1.3.3 Developing dendrites *in vivo* feature branches, filopodia, and growth cones

The advent of two-photon microscopy, adaptation of fluorescent molecules to live-cell imaging, and the development of single-cell electroporation has allowed observation of novel aspects of dendrite growth *in vivo* (Haas et al., 2001). A developing dendritic arbor has several notable morphological components, including dendritic filopodia, dendritic branches, and dendritic growth cones (DGCs) (Hossain et al., 2012; Wu et al., 1999). Filopodia are short, highly dynamic, actin-rich processes that are typically less than 10µm in length. DGCs are typified by motile structures located at dendritic branchtips, consisting of lamellipodia or dynamic branchtip filopodia (Hossain et al., 2012; Portera-Cailliau et al., 2003). Dendritic branches consist of dendritic shafts, composed of a cytoskeletal core of microtubule, which confer branch stability, and cortical actin surrounding this core. Dendritic branches *in vivo* display several different morphologies, with some demonstrating higher order branching, some decorated with dendritic filopodia or DGCs, whereas others consisting of long shafts devoid of DGCs or filopodia. Importantly, individual dendrites often assume varying morphologies over time.

In the intact brain, dendritogenesis proceeds through several distinct phases (Wu et al., 1999). Similar to cultured neurons, newly differentiated neurons *in vivo* generate several undifferentiated processes that protrude out of the neuronal soma, of which one or more processes become axons through a process called axon initiation (Wu et al., 1999). Interestingly however, unlike in dissociated neurons, lamellipodia ruffles surrounding the soma in newly differentiated neurons has not been reported *in vivo*, suggesting that it may be an artifact of

substrate adhesion by dissociated neurons or specific to neuronal types. Following axon initiation, the remaining processes become dendrites through highly dynamic extension, retraction and selective stabilization. This dynamic phase of dendritogenesis continues through three distinct stages. First, there is an initial stage of filopodia turnover with little to no stabilization or net growth of dendrites. Second, a phase of rapid dendrite growth occurs, with continued extension and retraction but with increased selective stabilization, which results in a dramatic increase in total dendritic branch length (TDBL). Finally, refinement of dendritic filopodia and branches occurs, which involves motility and turnover of processes with little to no increase in TDBL.

In past studies of dendritogenesis, attention has been focused on dendritic filopodia and branches, whereas DGCs have been largely ignored due to difficulty in identifying and observing these structures *in vivo*. Dendritic filopodia have been studied extensively for their role in forming dendritic spines, which begin to develop following the termination of most major dendrite development, and receive most excitatory synaptic inputs in the mature CNS. However, filopodia also exist in immature neurons undergoing dendritogenesis, and their role during this developmental period is less well known. Recent studies have implicated dendritic filopodia in cell-adhesion and synaptogenesis (*in vivo* in *Xenopus laevis* tectal neurons and *in vitro* in cultured cortical neurons), and in serving as precursors to new dendritic branches in cultured hippocampal neurons (Chen et al., 2010; Kayser et al., 2008; Ziv and Smith, 1996).

Observation of pyramidal neurons from developing mouse cortical slices demonstrates existence of two different types of dendritic filopodia, namely interstitial filopodia along dendritic shafts and branchtip filopodia (Portera-Cailliau et al., 2003). Interstitial filopodia are less stable than branchtip filopodia in terms of motility and turnover, and maturation of these neurons over developmental periods of postnatal day 2 (P2) to postnatal day 12 (P12) leads to increased stability of interstitial filopodia.

Unlike the elaborate lamellipodia observed on the neurites of dissociated neuronal cultures, in the study conducted by Portera-Cailliau et al., DGCs in acute mouse cortical slices were not observed to have lamellipodia; instead, they consisted of branchtips with high filopodial density and motility (Portera-Cailliau et al., 2003). In contrast to the dearth of knowledge available for DGCs, axonal growth cones (AGCs), which are dynamic structures located at the tips of growing axons that sense cues in the environment and steer axons in the appropriate direction, have been studied extensively. Interestingly, Portera-Cailliau et al. describe notable comparisons between DGCs and AGCs observed in acute slices, such as: both DGCs and AGCs contained highly dynamic branchtip filopodia with a higher density as compared to interstitial regions; AGC filopodia were longer and had higher density as compared to DGC filopodia; and importantly, whereas AGCs displayed both lamellipodia and filopodia, DGCs contained only filopodia.

Whether DGCs exist in the developing brain *in vivo*, and if so, characterization of their morphological components (i.e. lamellipodia, branchtip filopodia), behavior, and function in the formation of dendritic architecture remain major unresolved issues in understanding the morphological development of the immature brain.

1.4 Factors that influence dendrite growth

Dendrite growth is influenced by each neuron's intrinsic genetic program and by external factors, such as cues in the environment or neuronal activity. Current knowledge on the contribution of each of these influences on dendritic patterning have emerged from diverse techniques, including genetic manipulation of identified neurons in invertebrates, culturing mammalian neurons in the absence of neuronal activity or extracellular cues, and altering vertebrate neuronal activity while imaging single neurons in the intact brain (Bartlett and Banker,

1984a, b; Haas et al., 2006b; Parrish et al., 2006).

1.4.1 Genetic factors

Low-density dissociated hippocampal neuronal cultures (1500 – 2000 viable cells/cm^2) allow visualization of dendritogenesis while neurons are isolated from their endogenous environment, allowing analysis of dendrite growth with minimal influence from extracellular growth factors and cues or inter-neuronal communication (Bartlett and Banker, 1984a, b). In this environment, neurons arborize with recognizable dendritic growth patterns and look qualitatively similar to hippocampal neurons observed *in situ,* which suggests the presence of genes that regulate neuron type-specific dendritic arborization.

Identity of several genes involved in dendritic arborization has been revealed in *Drosophila* in a screen for genes that affect branching complexity (Grueber et al., 2003; Kim et al., 2006a; Li et al., 2004; Moore et al., 2002; Parrish et al., 2007; Parrish et al., 2006; Sugimura et al., 2004). *Drosophila* has identified classes of neurons that vary in their branching complexity. Specifically,these include “external sensory” neurons that have a single unbranched dendrite, and “multiple dendrite” neurons that have more complex and branched dendritic arbors. Dendritic arborization (da) neurons are multiple dendrite neurons that are categorized into classes I to IV in order of increasing branching complexity. Genetic screens have revealed that the presence of *hamlet*, a transcription factor containing a zinc finger motif, inhibits neurons from adopting multiple dendrite morphology, and instead, promotes the acquisition of simpler external sensory dendritic arbors (Moore et al., 2002). Similarly, levels of the proteins Cut, Abrupt, and Spineless, influences the level of branching complexity among the four different classes of da neurons (Grueber et al., 2003; Kim et al., 2006a; Li et al., 2004; Sugimura et al., 2004). Cut, for example, is absent from the Class I neurons, present at low levels in Class II

neurons, and at higher levels in Class III and IV neurons. Gain and loss-of-function experiments have demonstrated that increasing and decreasing levels of Cut increases and decreases branch complexity respectively (Grueber et al., 2003). In contrast, Abrupt is present only in Class I neurons and reduces branch complexity when ectopically expressed in Class IV neurons (Li et al., 2004; Sugimura et al., 2004). While Cut and Abrupt seem to push dendritic complexity toward more complex or simple arborizations respectively, Spineless, another transcription factor, is present at equal levels in all four classes of da neurons. However, in Class I and II neurons which have simple arbor morphology, Spineless limits branch complexity, whereas in the more branched Class III and IV neurons, Spineless increases branch complexity. This phenomenon is exemplified in mutant *Drosophila* with compromised Spineless function because da neurons in these mutants have similar branch complexities (Kim et al., 2006a).

1.4.2 Extracellular factors

Although in low-density hippocampal cultures, neurons are able to elaborate dendrites in the near absence of neuronal activity and extracellular cues, both *in vivo* and *in vitro* studies demonstrate that activity extracellular environmental factors, including neurotrophic factors and guidance cues, significantly influence dendritogenesis.

1.4.2.1 Neurotrophic factors

Neurotrophic factors constitute a family of molecules that induce survival and growth of immature neurons as well as play a role in mature neuronal survival and regrowth following injury. Among these molecules, nerve growth factor (NGF), brain-derived neurotrophic factor (BDNF), neurotrophin-3 (NT-3), and neurotrophin-4 (NT-4) affect various aspects of dendrite growth (McAllister, 2000). In developing rat sympathetic ganglion neurons, prolonged systemic

treatment (1-2 weeks) with NGF increases TDBL and dendritic branching (Ruit et al., 1990; Snider, 1988). Conversely, treatment with NGF antiserum decreases TDBL. In the CNS, application of several neurotrophins, including NGF, BDNF, NT-3, and NT-4, in organotypic slices increase branch complexity and length of developing cortical pyramidal neurons (McAllister et al., 1995). Interestingly, the specific neuronal growth pattern varies depending on the cortical layer and the type of dendrite (basal versus apical). Basal dendrites of neurons in layer 4, for example, respond strongly to BDNF only, whereas layer 5/6 neurons respond to NT-4, and apical dendrites respond to several different neurotrophins. Moreover, dendrites of pyramidal neurons overexpressing BDNF are more destabilized, with increased basal dendrite sprouting and increased dendritic spine retraction, as compared to control neurons (Horch et al., 1999).

These neurotrophins signal through Trk receptors, a family of high-affinity tyrosine kinase receptors. Specifically, TrkA, TrkB, and TrkC, are receptors for neurotrophins NGF, BDNF and NT-4/5, and NT-3, respectively (reviewed in Cohen-Cory and Lom, 2004; Patapoutian and Reichardt, 2001). In *Xenopus* tadpoles RGC neurons are exposed to two different sources of BDNF; locally from nearby retinal neurons and distally from RGC axonal target neurons in the tectum. Interestingly, dendritic effects on RGCs in response to BDNF vary depending on the source of this neurotrophin (Cohen-Cory and Lom, 2004; Lom and Cohen-Cory, 1999). Whereas locally administered BDNF limits dendritic branching, BDNF application to the tectum stimulates branching. This contradictory result is likely because BDNF application to the retina acts in an autocrine fashion, to stimulate the same group of cells that secrete this neurotrophin, and tectal BDNF mediates target-derived retrograde signaling via RGC axons. Also in mammalian Purkinje neurons, BDNF differentially affects dendrites based on maturational stage, as exemplified by BDNF-/- mice which have stunted dendritic arbors, although at a later stage, in cultured postnatal Purkinje neurons, BDNF application does not

affect dendritic complexity, but instead, increases dendritic spine density (Schwartz et al., 1997; Shimada et al., 1998). However, as these are two different experimental models, cultured neurons versus immunostained sections, it is possible that these differences are due to the experimental model, rather than maturational stage.

1.4.2.2 Guidance cues

Guidance cues are a group of molecules, initially studied for their role in axonal guidance. Some of these guidance cues have been recently implicated in dendritic growth and guidance in several different species (Furrer et al., 2003; Furrer et al., 2007; Hocking et al., 2010; Kayser et al., 2008; Polleux et al., 2000). During 1940's, Nobel laureate Roger Sperry performed an elegant set of experiments to determine how neuronal axons are guided to their targets. At the time of these experiments, there was a heated debate in the scientific community about how axons find their target destinations. Whereas one scientific camp held that molecules present in the environment direct axons, the other pushed the idea that axons grow randomly and only those that reach the appropriate target remain, whereas axonal connections to aberrant regions perish. In frog, RGC axons from the dorsal and ventral retina project to the ventral and dorsal tectum respectively; similarly RGC axons from the anterior and posterior retina project to the posterior and anterior tectum. Similar connectivity also exists in the mouse, chick, frog and several other species. The lens of the eye projects an inverted image onto the retina, but proper spatial connectivity between retina and tectum and experience dependent learning, allows the image of the external environment projected from the retina to the tectum to be construed accurately. In Sperry's experiments, frog eyes were surgically rotated 180 degrees, thus transecting the optic nerve. After the optic nerve regenerated in these animals, changes in visually guided behavior were assessed. Prior to the surgery, when a fly was presented within the frog's visual fields, a frog directed its tongue properly to the direction

of the fly; however, after surgical manipulation, these frogs wrongly directed their tongues in the opposite direction. The results of these experiments strongly suggested that the retinal ganglion axons had some type of “tag” that allowed them to relocate their original target after surgery although this led to maladaptive behavior. If learning and neural activity were sufficient to form proper connections, the RGC axons from the inverted eyes would be expected to adjust to their rotated positions and form connections to guide adaptive behavior. From the results of this and future experiments, Sperry postulated the “chemoaffinity hypothesis”, which in summary, suggests that axons are guided to their targets by interaction with chemical cues present in the environment. Each neuron has a chemical code, determined by the organism’s gene and cellular differentiation, which regulates how the particular neuron interacts with the cues in the environment (Sperry, 1963) . An extensive body of experiments followed which corroborated the existence and identity of some of these guidance cue molecules that actively aid growth cones to navigate within a complex environment.

Today, we have a wealth of growing knowledge about numerous guidance cues in several regions of the central nervous system (CNS) as well as in several different species. Generally, a molecule is considered a guidance cue if it is expressed at the appropriate time and place to serve an attractive or repulsive guidance function; loss-of-function of the molecule or its receptor causes guidance errors, although this is sometimes difficult to ascertain due to presence of redundant ligands and receptors; and co-culturing neurons with cells expressing the molecule causes axons to turn toward or away from the source of the molecule (reviewed in Song and Poo, 2001).

There are four families of “classical” guidance cue molecules, which collectively refer to a group of conserved families of molecules that were initially identified for their function in axon guidance and have been extensively studied, hence the term “classical” (reviewed in Dickson, 2002). These include netrin, semaphorin, ephrin, and slit.

1.4.2.2.1 Ephrins and Ephs

Guidance cue gradients: Eph/ephrin gradients in retinotopic mapping as an example

Guidance cue molecules have been proposed to be present in directionally oriented concentration gradients in the tissue surrounding axons. Axons sense these molecular cues via guidance cue receptors present on axonal growth cones and formulate an appropriate response, such as growth promotion/attraction or repulsion. A classic example of axon guidance via guidance cue gradients comes from studies of 'retinotopic mapping', a phenomenon involved in the correct wiring of RGC axons from the eye as they travel to their specific target locations within the brain, such that axons from adjacent RGCs in the retina project to adjacent locations within the tectum, hence preserving spatial information. While several guidance cue molecules participate at various steps along this complex and segmented trajectory undertaken by RGC axons, (including netrins, slits, semaphorins, and chondroitin sulfate proteoglycans), ephrins/Ephs (discussed below) and Wnt/Ryk, another ligand and receptor pair shown to participate in axon guidance, have been identified as the primary players responsible for this elegant retinotopic mapping (Lim et al., 2010; Schmitt et al., 2006).

Information from the retina, via RGC axonal projections from the eye to the brain, is mapped to the brain optic tectum (OT) of frog, fish, and chick, which is the anatomical equivalent of the superior colliculus (SC) in mouse, along two orthogonal axes. One set of axes maps the nasal-temporal axis of the retina to the posterior-anterior axis of the OT/SC, while another orthogonal set of axes maps the dorsal-ventral axis of the retina to the lateral-medial axis of SC (equivalent to the ventral-dorsal axis of OT) (reviewed in McLaughlin and O'Leary, 2005).

Specifically, ephrin-A/EphA interactions map the nasotemporal axis of the retina to the

anteroposterior axis of the OT/SC and ephrin-B/EphB interactions coordinates mapping the dorsal-ventral axis of the retina to the ventral-dorsal axis of the OT/SC. In the OT/SC, ephrin-As are present in low to high anterior-posterior gradients, and EphAs are present in the opposite high to low anterior-posterior gradients, although the subtype of ephrin-As and EphAs differ depending on the species (reviewed in McLaughlin & O'Leary 2005, Cheng et al., 1995; Higenell et al., 2011) (reviewed in Mann et al 2004, Mann et al., 2002). In retina, ephrin-A is expressed in a high to low nasal-temporal gradient, and EphA is expressed in reverse, in a low to high nasal-temporal gradient. Once high EphA expressing RGC axons from temporal retina reach the OT, they are repelled by high concentrations of ephrin-A in posterior tectum, which positions these axonal terminals in anterior tectum, whereas RGC axons from anterior retina, which have low EphA concentration, are able to travel further into the posterior tectum. In this manner, each RGC axon's ephrin-A and EphA expression determines at which position along the anterior-posterior axis of OT it will terminate. It is important to note however, that in mouse, axons initially overshoot their targets in the SC and 'back-branching' (interstitial branching along the shaft of an axon) and selective retraction of axonal branches from inappropriate areas lead to proper axonal targeting. A similar mechanism, involving EphB/ephrin-B attractive signaling, patterns the dorsoventral axes (Mann et al., 2002).

Molecular structure

Ephrins were initially identified as membrane-bound ligands for the Eph receptors, which constitute the largest family of receptor tyrosine kinases (RTKs) (Flanagan and Vanderhaeghen, 1998). Eph receptors are proteins with a single transmembrane segment, an extracellular domain consisting of a globular ligand-binding domain, a cysteine-rich region, and two fibronectin type III, and an intracellular domain with a PDZ binding domain and tyrosine kinase

activity. Ephrins are classified into two families, ephrin-A and ephrin-B, based on their molecular structure. While both ephrin families consist of a conserved receptor binding domain (~125 amino acids), ephrin-A molecules have a glycosylphosphatidylinositol (GPI) anchor tethered to the cell membrane, while ephrin-B molecules have a transmembrane and an intracellular domain. Eph receptors are also classified into two subclasses, EphAs or EphBs, based on sequence homology and binding affinities with the ephrin-A and ephrin-B ligands. Thus far, ten EphA receptors (EphA1 - A10), six EphB receptors (EphB1 - B6), six ephrin-A (ephrin-A1 - A6), and three ephrin-B (ephrin-B1 - B3) ligands have been identified. Considerable promiscuity exists among the ligand-receptor interactions within each subclass. For example, ephrin-A2 binds with varying affinities with almost all EphA receptors but not with EphB receptors (Flanagan and Vanderhaeghen, 1998). However, some exceptions to this subclass specific ligand-receptor interaction do exist, as ephrin-B3 and ephrin-A5 can activate EphA4 and EphB2 respectively, although these two receptors are members of their opposite subclasses (Himanen et al., 2004).

Function

In addition to their roles in retinotopic mapping discussed above, Ephs and ephrins are involved in a number of other facets of neural development, including axonal pathfinding in other contexts, generation of cellular boundaries, axon branching, dendritic filopodial motility, dendritic branching, regulating dendritic spine morphology, and synaptic plasticity (Carmona et al., 2009; Filosa et al., 2009b; Kayser et al., 2008; Lim et al., 2008a; reviewed in O'Leary and Wilkinson, 1999; reviewed in Wilkinson, 2001; Xu et al., 2011).

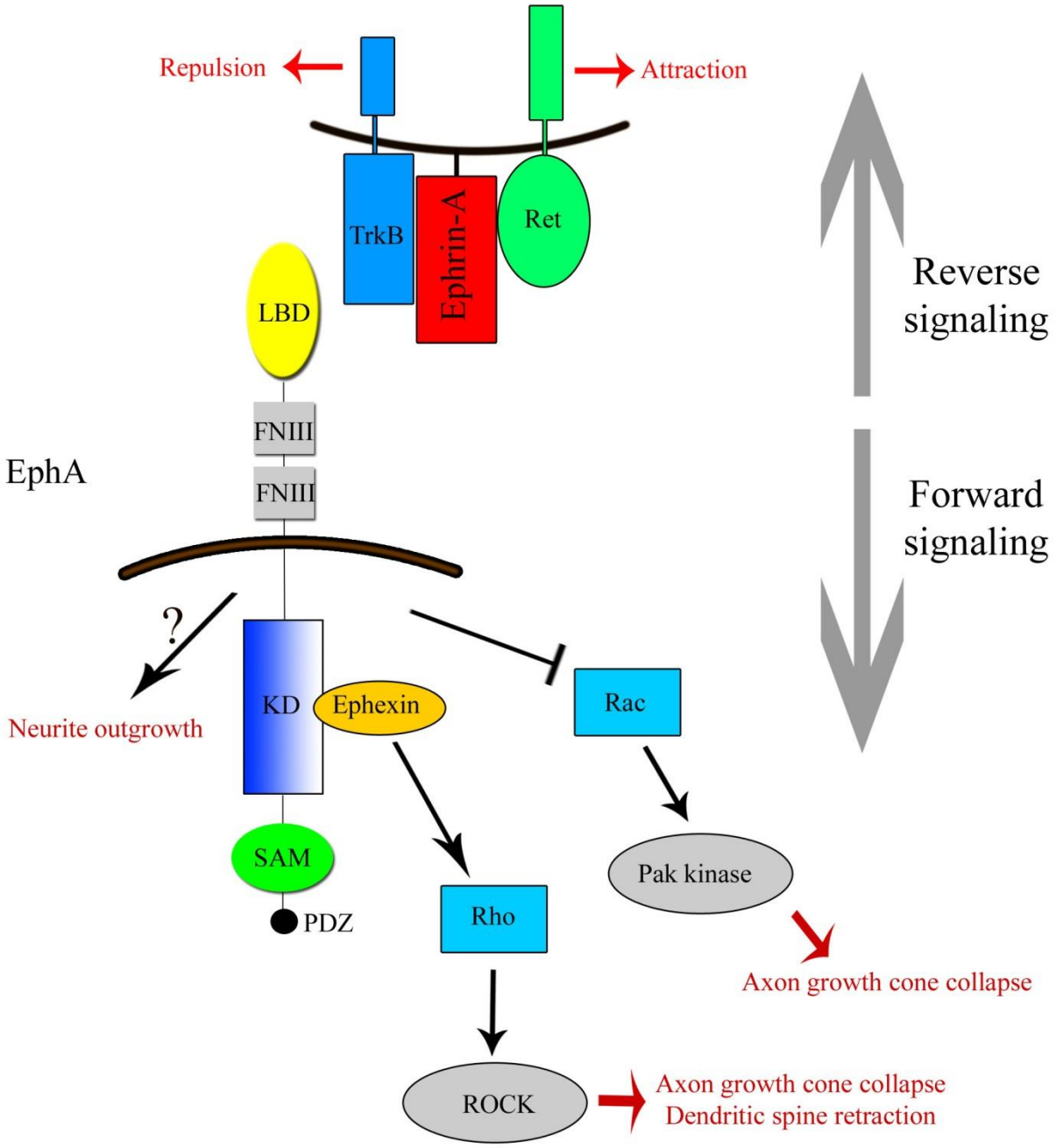

Figure 1. Ephrin-A and EphA.
Schematic of ephrin-A and EphA structures, neuronal function, and signaling. LBD, ligand-binding domain; FNIII, fibronectin type III repeats; KD, kinase domain; SAM, SAM binding domain; PDZ, PDZ-binding domain.

Signaling

Ephrin-A binding to EphA can initiate both “forward signaling”, via EphA intracellular domain, and “reverse signaling”, via ephrin-A interaction with coreceptors (reviewed in Triplett and Feldheim, 2012). Although initially identified as a repulsive factor, it is now understood that ephrin-A/EphA can also induce neurite branching, depending on the cellular context and concentration of ligand. Many of the known Eph signaling pathways impinge on GTPases, including those of the Rho and Ras GTPase families (reviewed in Murai and Pasquale, 2003). Binding of ephrin-A to EphA induces EphA receptor clustering, and this ligand binding is necessary for initiation, but not propagation, of clustering (Wimmer-Kleikamp et al., 2004). Significantly, while pre-clustered ephrins induce Eph receptor phosphorylation, unclustered ligands acts as functional antagonists, thus allowing one to use pre-clustered and unclustered ephrins to study different questions (Davis et al., 1994; Wimmer-Kleikamp et al., 2004). In EphA forward signaling pathway, Ephexin (a GTPase exchange factor), is activated and in turn, activates Rho GTPases and, in some cases, their downstream effectors, Rho-associated kinases or ROCK (Shamah et al., 2001; Wahl et al., 2000). This pathway has been implicated in axonal growth cone collapse and dendritic spine retraction. EphA signaling has also been shown to inhibit Rac, and its downstream effector Pak kinase, also leading to axonal growth cone collapse (Jurney et al., 2002). EphA signaling induces neurite outgrowth in axons from chick nasal retinal explants in a concentration dependent manner (Hansen et al., 2004). In the anterior midbrain, at low concentrations, ephrin-A5 molecules remain unclustered and activate EphA forward signaling, which promotes axon growth (Hansen et al., 2004). In the posterior midbrain however, high concentrations of ephrin-A5 molecules become clustered and trigger reverse signaling mediated axon repulsion. Balance of these attractive and repulsive signals likely influences where RGC axons terminate in the tectum. Since ephrin-A molecules are anchored to the cell membrane by a GPI tether and lack an intracellular domain, their

intracellular reverse signaling is initiated by interaction with coreceptors. Downstream of ephrin-A signaling, p75 and TrkB coreceptors have been shown to mediate repulsion while Ret has been implicated in attraction (Bonanomi et al., 2012; Lim et al., 2008b; Marler et al., 2008).

Ephrin-B/EphB interaction can also mediate both forward and reverse signaling. EphB activation via ephrin-B interaction requires higher order cluster formation (Davis et al., 1994; Schaupp et al., 2014). In fact, unclustered ephrin-B has been used to block endogenous ephrin-B function (Lim et al., 2008a). EphB receptors can signal by activating a different group of GTPase exchange factors, intersectin and kalirin, which also activates Rho GTPases (Irie and Yamaguchi, 2002; Penzes et al., 2003). Intersectin activates Cdc42, and kalirin localizes Rac to sites of EphB-ephrin binding. WASP, an adaptor protein which increases actin branching via Arp2/3 complex, has also been implicated in downstream EphB2 pathway. In combination with these results, two signaling pathways, including intersectin-Cdc42-WASP-actin pathway and kalirin-Rac-Pak-actin pathway, have been proposed in dendritic spine morphogenesis downstream of EphB activation (Irie and Yamaguchi, 2002; Penzes et al., 2003). Other molecules implicated in the Eph receptor signaling pathway include focal adhesion kinase (FAK) and the phosphotyrosine phosphatase Shp2 in integrin mediated cell adhesion, the Rho and FAK-binding protein Cas, as well as other adaptor proteins (i.e. Grb7, Grb2, Grb10, Nck, Shc), although all of these signaling pathways have been studied primarily in non-neuronal cells (Pratt and Kinch, 2002; Stein et al., 1996; Stein et al., 1998).

Ephrin-B receptors activate reverse signaling pathways via their intracellular domain to drive axonal growth cone repulsion, presynaptic development, dendritic spine maturation, synapse formation, and decreased dendritic branching (reviewed in Xu & Henkemeyer 2012, Hoogenraad et al., 2005; Xu et al., 2011). The ephrin-B intracellular domain has a SH2 binding domain and a PDZ binding domain. Upon EphB binding, ephrin-B intracellular region becomes tyrosine phosphorylated, which allows its SH2 binding domain to become associated with the

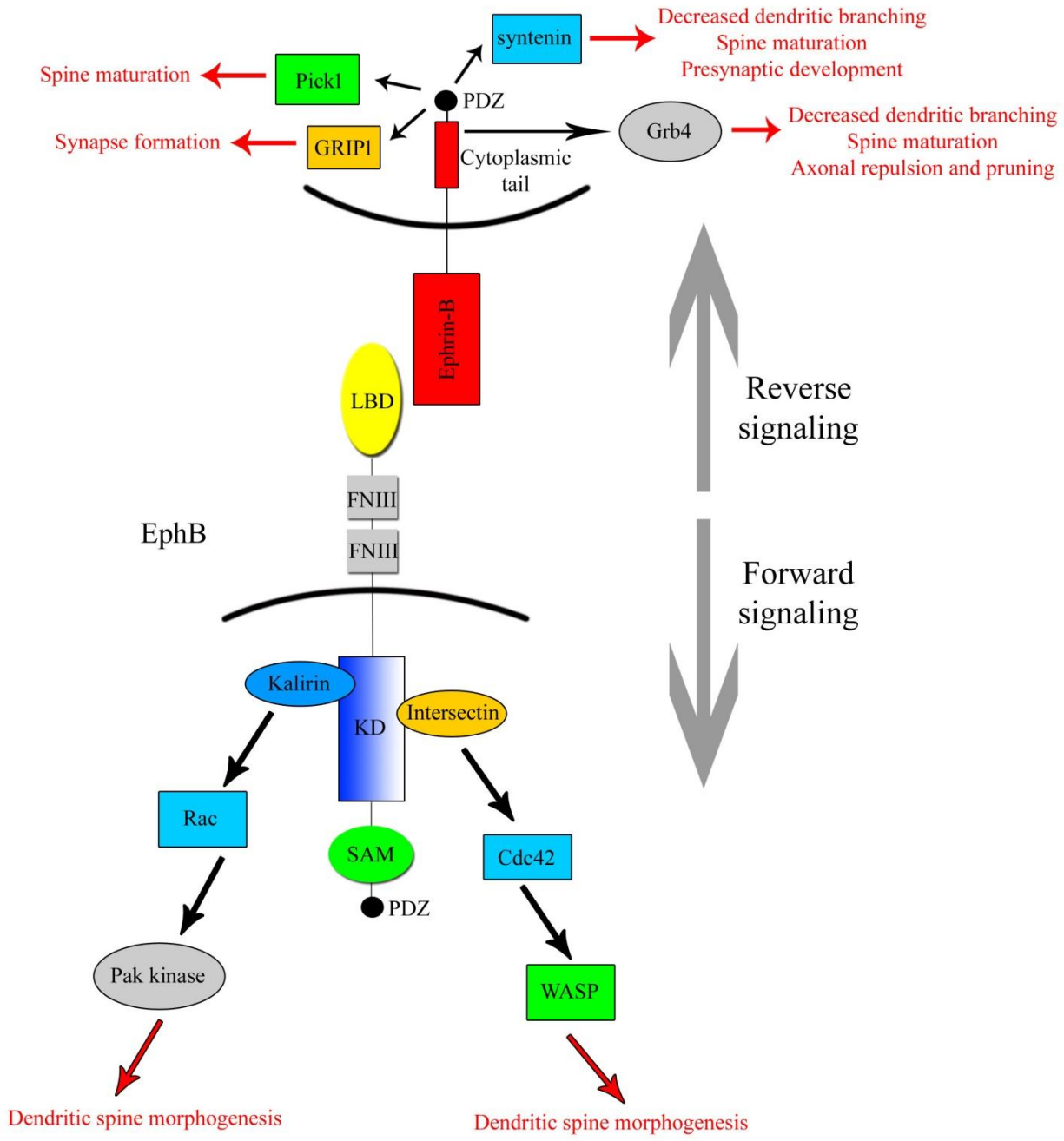

Figure 2. Ephrin-B and EphB.
Schematic of ephrin-B and EphB structures, neuronal function, and signaling. , ligand-binding domain; FNIII, fibronectin type III repeats; KD, kinase domain; SAM, SAM binding domain; PDZ, PDZ-binding domain.

SH2/SH3 adaptor protein Grb4, and its PDZ domain to bind to PDZ containing proteins, such as GRIP1, PICK1, and syntenin (Aoto et al., 2007; Segura et al., 2007; Xu et al., 2011).

1.4.2.2.2 Slits and Robos

Molecular structure

Slit was initially discovered as a gene involved in embryonic patterning defects in *Drosophila* and later as a protein secreted by midline glia in *Drosophila* that acts as a midline repellant for axons (Rothberg et al., 1988; Rothberg et al., 1990). Slits are secreted glycoproteins with an N-terminal signaling domain, four leucine-rich repeats (LRR), variable number of epidermal growth factor (EGF)-like sequences, a laminin-G domain, and a cysteine-rich knot in the c-terminal. Cleavage of slits can generate a short N-terminus peptide and a longer N-terminus protein that can bind to Robo receptors (Nguyen Ba-Charvet et al., 2001; reviewed in Ypsilanti et al., 2010). Thus far three different types of slit genes have been identified. Robo serves as the receptor for slit proteins and was identified in a large-scale genetic screen in *Drosophila* used to search for mutants with midline crossing defects (Kidd et al., 1999; Seeger et al., 1993; reviewed in Ypsilanti et al., 2010). These receptors are a part of the immunoglobulin (Ig) superfamily of cell-adhesion molecules. Most vertebrates have three Robo receptors, with a fourth Robo receptor (zRobo4) expressed in Zebrafish (Bedell et al., 2005; Jones et al., 2008). Most Robo receptors have five Ig motifs, three fibronectin type III domains, a transmembrane domain, and four cytoplasmic domains (reviewed in Chedotal, 2007). These receptors can be alternatively spliced in the 5' region to generate two isoforms, A and B, which vary in their N-terminal region (Camurri et al., 2005). Robo3 also undergoes alternative splicing in the 3' region to generate Robo3.1 or Robo3.2, which differ in their c-

terminal domain. Robo receptors have shown to be involved in mediating both homophilic and heterophilic interactions (Hivert et al., 2002).

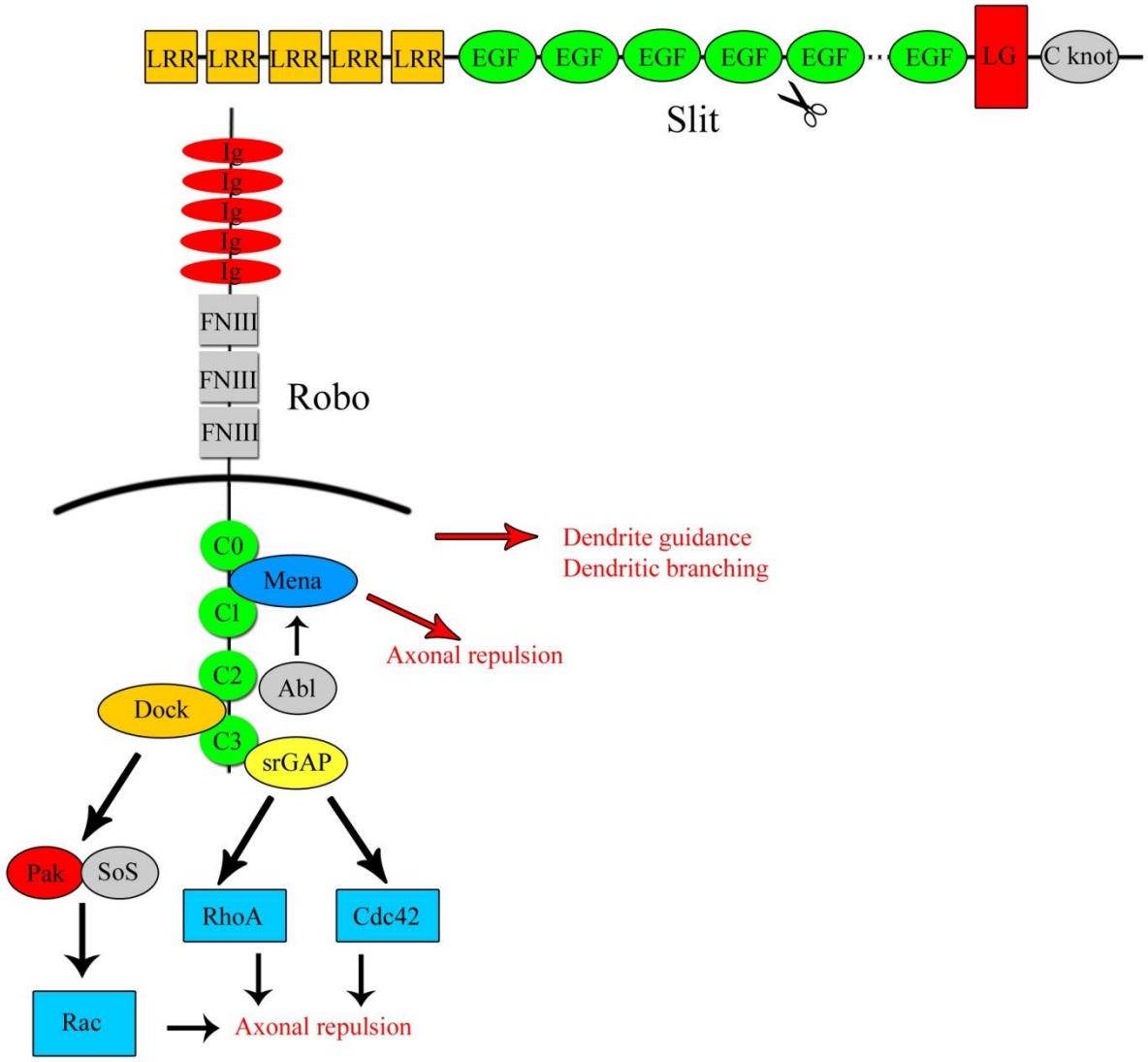

Figure 3. Slit and Robo.
Schematic of slit and Robo structures, neuronal function, and signaling. LRR, leucine rich repeats; FNIII, fibronectin type III repeats; Ig, immunoglobulin motifs; epidermal growth factor (EGF)-like sequences, EGF; LG, laminin-G domain; C-knot, cysteine-rich knot; C0-C3, conserved cytoplasmic domains. Scissors denote cleavage site.

Function

Slit-Robo signaling are involved in a myriad of functions, including axonal and dendritic guidance and branching, axonal and dendritic lamination, organization of axonal projections in the olfactory bulb, cell migration, and regulation of cell adhesion (Andrews et al., 2008; Furrer et al., 2003; Jhaveri et al., 2004; Kidd et al., 1999; Rhee et al., 2002; Xiao et al., 2011). Much of what we understand about the function of slit and Robo in axon guidance comes from experiments in the vertebrate spinal cord and *Drosophila* ventral nerve cord. In the vertebrate spinal cord, commissural neurons are born in the dorsal spinal cord and project their axons ventrally toward the midline, and then cross the midline. In contrast, axons of non-commissural axons do no cross the midline, but instead, project anteriorly in pathways paralleling the spinal cord. In this system, slit serves as a midline chemorepellant for Robo expressing axons. Disrupting all three *slit* genes leads to aberrant axonal stalling or re-crossing by commissural axons (Long et al., 2004). Non-commissural axons are repelled by slit-expressing midline cells and do not cross the midline. In contrast, although Robo is also expressed in commissural axons, posttranscriptional downregulation of Robo receptor activity, by a protein encoded by the *commissureless* (*comm*) gene in *Drosophila*, or by the Robo3 protein in vertebrates, suppress slit-robo repulsive signaling, allowing these axons to cross (Keleman et al., 2002; Keleman et al., 2005; Sabatier et al., 2004; Seeger et al., 1993; Tear et al., 1996). Once these axons cross, downregulation of comm or Robo3 (also known as Rig-1) establishes slit-Robo repulsive signaling to take over, thus preventing aberrant midline re-crossing by these axons. Thus, although traditionally slit-Robo signaling was thought to be repulsive, Robo3 surprisingly antagonizes Robo1 signaling in mouse as *comm* protein antagonizes Robo receptors in *Drosophila* (Chen et al., 2008; Sabatier et al., 2004).

In addition to their roles in axonal guidance, a limited number of more recent studies have also implicated these guidance cues and receptors in dendritic guidance and dendrite

branching in *Drosophila*, *Xenopus*, and Zebrafish. Slit and Robo are involved in both dendrite guidance and dendritogenesis of identified *Drosophila* motor neurons (Furrer et al., 2003; Furrer et al., 2007). In wild type *Drosophila* motorneurons, RP3, aCC, and RP2, have the following stereotypic dendritic orientation: RP3 and aCC neurons project dendrites both ipsilateral and contralateral to the midline, whereas RP2 neurons project dendrites do not cross the midline and project only ipsilaterally (Furrer et al., 2003). In *robo* null mutants (but not in *robo2* or *robo3* mutants), however, RP2 and RP3 neuronal dendrites show abnormal midline crossing and winding around the midline, similar to axonal crossing or re-crossing in *robo* mutants (Seeger et al., 1993), and this phenotype is rescued by cell-autonomous expression of *robo* in each neuron. In contrast to *robo* null mutants, in *comm* mutants RP3 and aCC neuronal dendrites that normally project contralaterally across the midline, instead project ipsilaterally. These results suggest that, as in axons, in dendrites slit-Robo interaction prevents midline crossing by a subset of dendrites in *Drosophila*. In *Xenopus,* slit activity induces RGC dendritic branching in dissociated RGC neurons, and expression of dominant-negative Robo constructs decreases number of branch points and total dendritic branch length, with dominant-negative Robo2 having a stronger effect than dominant-negative Robo3 (Hocking et al., 2010). Similarly, in rat primary dissociated cortical cultures, slit-1 induces dendritic branching, whereas Robo-Fc soluble extracellular domain or transfection of dominant-negative Robo1 or Robo2 receptors (Robo receptors missing c-terminal domain) decrease dendritic branching (Whitford et al., 2002).

Signaling

Slit-Robo binding initiates downstream signaling via proteins that interact with Robo receptor cytoplasmic motifs and signal intracellularly, through direct phosphorylation or recruiting additional proteins, to modify actin. Abelson (Abl) tyrosine kinase and its substrate Enabled (Ena) directly bind to *Drosophila* Robo cytoplasmic domain, and interference of either

Abl or Ena function leads to opposite phenotypes in midline crossing defects (Bashaw et al., 2000). Whereas Abl mediated phosphorylation of Robo intracellular tyrosine residue on the CC0 and CC1 motifs antagonizes Robo signaling, Ena interaction with the CC2 motif is required for proper Robo function. Robo activation also been shown to increase function of srGAP1, a GTPase-activating protein (GAP), which binds to the CC3 cytoplasmic domain of Robo1 and downregulates Cdc42 and upregulates RhoA activity (Wong et al., 2001). Also, the Robo receptor CC2and CC3 domains can bind Dock (a SH3-SH2 adaptor protein) and recruit p21-activated protein kinase (Pak) and Son of Sevenless (Sos), which increases Rac activity and causes axonal repulsion (Fan et al., 2003). This Rac mediated axonal repulsion is surprising since Rac is generally involved in lamellipodia activity and axonal extension, and how this GTPase can mediate both attractive and repulsive behavior remains unknown. Interestingly, Robo can also directly bind to the cytoplasmic domain of the netrin receptor DCC, and silence netrin effects (Stein and Tessier-Lavigne, 2001).

1.4.2.2.3 Netrins and their receptors (DCC/Unc-5, DSCAM, NGLs)

Molecular structure

The first member of the netrin family, uncoordinated-6 (Unc-6) was initially identified in *C. elegans* as a gene implicated in neural development (Ishii et al., 1992), and since then, several types of netrin proteins have also been identified in *Xenopus, Drosophila,* sea anemone, as well as mammals (de la Torre et al., 1997; Harris et al., 1996; Matus et al., 2006; Serafini et al., 1994). Netrins are composed of a family of extracellular proteins from the laminin superfamily that are either secreted or GPI anchored (reviewed in Rajasekharan and Kennedy, 2009). To date, five different mammalian netrins have been identified, including netrins 1, 2, and

4 which are secreted, and netrins G1 and G2, which are GPI anchored at the carboxy-terminal (Nakashiba et al., 2000). The amino-terminal of netrin contains a globular domain VI, followed by domain V with three epidermal growth factor (EGF) repeats. In secreted netrins, the carboxy-terminal (C-domain) contains a high density of basic amino acids that bind heparins with high affinity. In invertebrates, only secreted netrins have been identified thus far. Identified netrin-1 receptors include the DCC/neogenin family, Unc5 (Unc5A-Unc5D in vertebrates), and the Down syndrome cell adhesion molecule (DSCAM). Orthologs of DCC are named Unc-40 and Frazzled, in *C. elegans* and *Drosophila*, respectively. DCC proteins are single-pass transmembrane proteins with four immunoglobulin domains and six fibronectin type III (FNIII) repeats in the extracellular domain and a highly conserved intracellular region with P1, P2, and P3 domains. Unc5 proteins are also transmembrane proteins, with two immunoglobulin repeats and two thrombospondin type-I modules in the extracellular domain. The Unc5 intracellular region contains a ZU-5 domain and a "death domain" involved in apoptotic signaling (Hofmann and Tschopp, 1995). Recently DSCAM, a type I transmembrane receptor with ten immunoglobulin domains and six FNIII repeats in the extracellular domain, has also been shown to function as a netrin-1 receptor (Andrews et al., 2008; Ly et al., 2008). Netrin Gs, on the other hand, has not been shown to interact with these three receptor types, but instead, bind to netrin G ligands (NGLs), NGL-1 and NGL-2, which are transmembrane proteins with LRRs and immunoglobulin domains in the extracellular region (Kim et al., 2006b; Lin et al., 2003).

Function

Although netrins have been mostly studied with regards to their roles cell migration and axon guidance, they also function in cell adhesion, cell survival, tumorigenesis, maturation of cell morphology, synaptogenesis, and dendrite guidance (reviewed in Rajasekharan & Kennedy

2009, Colon-Ramos et al., 2007; Furrer et al., 2003; Jarjour et al., 2008; Kennedy et al., 1994; Kim et al., 2006b; Mehlen and Furne, 2005). Depending on cellular and developmental context and the concentration of cyclic nucleotide in the cell, these molecules can function as either long-range or short range cues that are either attractive or repulsive (de la Torre et al., 1997; reviewed in Mann et al., 2004). For example, netrin-1 is secreted by cells in the developing floor plate, creating a decreasing ventral-dorsal gradient that guides axons in embryonic spinal cord, attracting axons of commissural neurons via DCC signaling, and netrin or DCC function deficiency leads to a loss of ventral commissures and a loss of the corpus callosum connecting left and right brain hemispheres (Fazeli et al., 1997; Kennedy et al., 1994; Kennedy et al., 2006; Serafini et al., 1996). Interestingly however, this ventrodorsal netrin-1 gradient can also repel trochlear motor neuronal axons, and this chemorepulsion is mediated by Unc5C receptors (Burgess et al., 2006; Colamarino and Tessier-Lavigne, 1995). In retina, netrin-1 attracts RGC axons to the optic nerve via DCC receptor signaling (de la Torre et al., 1997; Deiner et al., 1997). However assessing these RGC axons at different stages along the pathway suggests that after passing into the optic nerve, RGC axons become insensitive to netrin, and RGC axons that cross the optic chiasm are in fact repelled by netrins (Shewan et al., 2002). This developmental switch from attraction to repulsion may be mediated by a decrease in cytosolic cAMP (Corset et al., 2000). In addition to axon guidance, Frazzled /DCC and netrins also mediate dendritic orientation in *Drosophila* (Furrer et al., 2003).

Signaling

Netrin-1 binding to DCC leads to homodimerization of DCC initiating several signaling cascades that converge onto increasing Rac1 and Cdc42, and induce lamellipodial and filopodial extension, axonal growth or attractive turning (reviewed in Bradford et al., 2009). In

contrast, netrin-1 binding to DCC associated with Unc-5 or Unc-5 alone mediates repulsive signaling (Hong et al., 1999; Keleman and Dickson, 2001). Signaling downstream of Unc-5 activation has been poorly characterized, but seems to involve second messengers (ratio of cAMP to cGMP) and various kinases (FAK, Src, Shp2) which ultimately increase RhoA activity, leading to growth cone collapse or repulsive turning. Interestingly, in embryonic *Xenopus* spinal axons, activation of the slit receptor Robo silences netrin-1 mediated attraction by direct binding of the Robo cytoplasmic domain to the DCC intracellular region, and this hierarchical organization of guidance cue receptors prevent a tug of war between Robo mediated repulsive versus DCC mediated attractive signaling (Stein and Tessier-Lavigne, 2001).

1.4.2.2.4 Semaphorins and Plexins/Neuropilins

Molecular structure

The first semaphorin (Semaphorin-1a or Sema-1a, previously called fasciclin IV) was discovered as a molecule expressed in pioneer axonal growth cones of the grasshopper embryo, and soon afterwards several families of Semaphorins were cloned in *Drosophila*, human, and virus (Kolodkin et al., 1993; Kolodkin et al., 1992). To date, twenty-seven semaphorin proteins, categorized into eight classes (Sema 1-7 and viral Sema V) based on amino acid and structural similarities, have been identified (reviewed in Pasterkamp, 2012). Structurally, semaphorins are secreted (Sema-2, Sema-3, and SemaV families), transmembrane (Sema-1, Sema-4, and Sema-5 families), or GPI-anchored (Sema-7). Of these, Sema-1 and Sema-2 family members have been identified exclusively in invertebrates, Sema-3,4,6,7 have been identified only in vertebrates, and SemaV is viral only. All Semaphorins have a conserved N-terminal signal sequence and a semaphorin domain as well as other conserved domains (C-terminal basic domain, thrombospondin repeats, or a GPI anchor) based on the

semaphorin family (reviewed in de Wit and Verhaagen, 2003). While most Semaphorins signal through plexin receptors, Sema-3 also requires neuropilins as coreceptors to plexins, and Sema-7A can bind integrins to promote axonal outgrowth(reviewed in Pasterkamp, 2012). Four classes of plexins (plexinA-D), including two invertebrate and nine vertebrate plexins, have been identified.

Function

Semaphorins are a group of diverse and multifunctional molecules that not only function as repulsive axon guidance molecules in nervous system development, but are also involved in a myriad of other organ systems, including cardiovascular, hepatic, immune, and reproductive among others (Yazdani and Terman, 2006). A general theme that has emerged in Semaphorin signaling is its ability to reorganize actin and microtubule network to reorganize different aspects of the cytoskeleton. Of particular interest to the study of dendrite growth and guidance is Polleux and colleagues' demonstration that Semaphorin 3A serves as a chemoattractant for apical dendrites of mouse cortical pyramidal neurons (Polleux et al., 2000), but as a chemorepellant in the axons of the same neurons, an effect that is mediated by differential concentration of cGMP in axons versus dendrites.

Signaling

A large number of molecules have been implicated in signaling downstream of plexin activation, including kinases, cyclic nucleotides, and actin-modifying molecules, which rapidly reorganizes the actin cytoskeleton. Not surprisingly, the particular signaling cascade and the type of axonal response are determined by the type of plexin and combination of cofactors involved (reviewed in Pasterkamp, 2012). For example, Sema3A binds neuropilin-1 coreceptor, which forms a complex with plexin-A, and initiates downstream plexin signaling that causes cofilin mediated depolarization of F-actin, leading to growth cone collapse (reviewed in

Nakamura et al., 2000; Nakamura et al., 1998; Takahashi et al., 1999). In contrast, Sema-5A induces growth cone attraction when co-expressed with HSPGs, but causes repulsion if expressed with CSPGs (Kantor et al., 2004).

1.4.3 Cell-adhesion molecules

Cell adhesion molecules (CAMs) comprise a group of molecules, typically transmembrane proteins, that functions to attach cells to other cells or to the extracellular matrix. In neurons, CAMs have been studied for their role in synapse formation, maturation, specification, differentiation, and dendritic spine formation, with more recent focus on their roles in dendrite growth (reviewed in Dalva et al., 2007, Chen et al., 2010). Both ephrin-A/EphA and ephrin-B/EphB, in addition to their roles as short-range guidance cues, also serve as CAMs. EphB activation via application of clustered ephrin-B-Fc proteins induces dendritic spine formation and clustering of AMPARs and NMDARs (Dalva et al., 2000; Henkemeyer et al., 2003; Kayser et al., 2006). Strikingly, cultured hippocampal neurons from EphB1-3 triple knockout mice are almost completely devoid of dendritic spines (Henkemeyer et al., 2003). Moreover, in immature neurons, dynamic imaging in cultured cortical neurons revealed that EphB2 is required for dendritic filopodial motility (Kayser et al., 2008). Recently, β-neurexin and neuroligin, another set of CAMs expressed in axons and dendrites respectively, have also been shown to modulate dendritic filopodial motility and long-term overall dendrite growth (Chen et al., 2010). Interfering with β-neurexin binding to neuroligin decreases filopodial stability, increases motility of a subset of filopodia, and decreases synapse number in *Xenopus* tectal neurons. Another CAM that regulates synapse formation and synaptic plasticity (reviewed in Brigidi and Bamji, 2011), N-Cadherin, has recently been implicated in activity-dependent dendrite growth of cultured hippocampal neurons (Tan et al., 2010).

1.4.4 Regulators of cytoskeleton

The underlying dendritic cytoskeleton, including actin and microtubules, as well as regulatory molecules involved in assembling, dissembling, and reorganizing actin and microtubules, are integral to the growth, retraction, branching, and turning behavior of dendrites. Neuronal dendrites are composed of three core structural features, including the dendritic shaft (dendrite branch), dendritic filopodia, and dendritic growth cones (Hossain et al., 2012).

Cytoskeletal architecture of dendrites

Dendritic shafts, the most stable regions of a dendritic tree, are often branched or studded with dendritic filopodia, and are composed of an inner core of microtubules surrounded by a cortex made of filamentous actin (reviewed in Scott and Luo, 2001). Several cytoskeleton associated molecules, including microtubule-associated protein 2 (MAP2) and CHO1/MKLP1, are present in dendrites but not in axons, whereas tau is present in axons but not in dendrites (Kosik and Finch, 1987; Matus et al., 1981; Tytell et al., 1984). Another striking cytoskeletal difference between dendrites and axons consists of microtubule polarity orientation. In axons, microtubules are uniformly arranged in a plus-end distal orientation, but in dendrites, microtubules exist in both plus-end distal and minus-end distal orientations (Baas et al., 1988).

Dendritic filopodia are thin and unbranched protrusions, typically less than 10 µm in length, that protrude from the dendritic shaft or from dendritic growth cones (Mattila and Lappalainen, 2008). Much of our knowledge regarding the structural composition of filopodia comes from motile non-neuronal cells such as macrophages and epithelial cells. In non-neuronal cells, filopodial cytoskeleton is composed of several actin filaments bound together by an actin-bundling molecules such as fascin. These actin filaments elongate via actin polymerization from one end, termed the ‘barbed end’ and shorten via retrograde flow involving release of actin subunits on the other end, called the ‘pointed end’, and the balance of this

extension and retraction regulates filopodial length and motility. Recent evidence indicates that the structural composition of neuronal and non-neuronal filopodia differ in several respects. In contrast to the linear actin bundles in non-neuronal cells, in neuronal filopodia, actin is organized in a network of both branch and linear actin (Korobova and Svitkina, 2010). In addition, neuronal filopodia are devoid of fascin and contain Arp2/3 complex, a protein oligomeric complex involved in actin branching that are normally absent in non-neuronal filopodia.

Dendritic growth cones (DGCs) are dynamic structures present at dendritic branchtips, which have been shown to be present specifically in immature neurons. (Dailey and Smith, 1996; Hossain et al., 2012; Vaughn et al., 1974). DGCs are difficult to visualize *in vivo*, and thus have received far less attention than dendritic filopodia and dendritic branches. Although axonal growth cones have been studied in detail, role of DGCs in neuronal development has been illuminated very recently (Hossain et al., 2012). Knowledge regarding DGC cytoskeleton come from sparse studies conducted using electromicrographs (EM), and thus lack characterization of dynamic motility (Jhaveri et al., 2004). In contrast to the looped microtubules in the central region of axonal growth cones, EM of spinal motor neuronal DGCs indicate that the center region of DGCs, at least in this neuronal population, lacks this looped microtubule structure (reviewed in Conde and Caceres, 2009; Sabry et al., 1991; Vaughn et al., 1974). Although it is possible that DGC dynamics is regulated in the same manner as in axonal growth cones, direct *in vivo* evidence for this, as with all aspects of DGCs, is lacking.

Rho GTPases

Given the central structural role of actin and microtubules in cellular architecture, cells have a multitude of molecules devoted to the regulation of these cytoskeletal elements. Among these regulators, several studies have implicated Rho GTPases in actin remodeling, and

specifically three Rho GTPases, Rho, Rac, and Cdc42, have been shown to participate in dendritogenesis (reviewed in Jaffe and Hall, 2005; Sin et al., 2002). In general, Rho, Rac, and Cdc42 are involved in contractile actin-myosin filament assembly, lamellipodia formation, and protrusive filopodia formation, respectively. Rho GTPases cycle between two states, GTP bound active state, and GDP bound in active state (reviewed in Jaffe and Hall, 2005). When active, these GTPases interact with their downstream effector proteins, many of which are involved in actin regulation. Rho GTPases are activated by guanine nucleotide exchange factors (GEFs), which stimulate exchange of GTP for GDP, and are deactivated by GTPase activating proteins (GAPs).

Studies of Rho GTPase involvement in dendritogenesis have generally shown that RhoA decreases, whereas Rac and Cdc42 increase dendrite growth (reviewed in Negishi and Katoh, 2005). As discussed above, dendrite growth proceeds through several stages, including dendritic initiation, growth, branching, and in a subset of neurons, dendritic spine formation. Dominant-negative Rac1 and Cdc42 decrease number of primary dendrites in developing rat cortical neurons, suggesting that Rac and Cdc42 are involved in dendrite initiation (Threadgill et al., 1997). These two Rho GTPases have also been shown to participate in dendritic branching in *Xenopus* RGCs, where expression of dominant-negative Rac1 or Cdc42 decreases number of dendritic branches (Ruchhoeft et al., 1999). In contrast, in *Drosophila*, neurons lacking RhoA overextend their dendrites, and in both *Drosophila* and rat hippocampal pyramidal neurons, increased RhoA activity reduces dendritic complexity (Lee et al., 2000; Nakayama et al., 2000). In *Xenopus* tectal neurons, Rac and Cdc42 activation increases branch turnover, and RhoA activation decreases pre-existing branch length without affecting branch turnover, suggesting that these molecules are differentially involved in new branch initiation or pre-existing branch growth (Li et al., 2000). Interestingly, in this same model, decreased RhoA activity and increased Rac and Cdc42 activity are required for visual stimulation activity driven

dendritogenesis (Sin et al., 2002). Notably however, not all results are consistent with a role of RhoA in decreased dendritogenesis; in immature rat cortical neurons, constitutively active RhoA decreases number of primary basal dendrites (Threadgill et al., 1997).

Guidance cues mediate signaling to the cytoskeleton

Many of the guidance cues discussed above have been shown to induce intracellular signaling that converge on cytoskeletal molecules, although whether or not these same signaling pathways are involved in guidance cue mediated dendritogenesis remains largely unknown (reviewed in Dent et al 2011, Aizawa et al., 2001; Bashaw et al., 2000; Chang et al., 2006; Forsthoefel et al., 2005; Gitai et al., 2003; Marsick et al., 2010; Piper et al., 2006; Strasser et al., 2004; Wills et al., 2002). Semaphorin 3A signaling in dorsal root ganglion neurons induces phosphorylation of cofilin, a molecule involved in depolymerizing actin, leading to growth cone collapse (Aizawa et al., 2001). Genetic and biochemical studies have suggested that Abelson (Abl) tyrosine kinase and Enabled (Ena), two proteins intimately involved in actin remodeling, are effectors in Robo and Frazzled (Netrin receptor in *Drosophila*) signaling (Bashaw et al., 2000; Bear and Gertler, 2009; Forsthoefel et al., 2005). In *Drosophila*, Robo mediated repulsion of midline crossing neurons requires decreased DRac1 and DCdc42 (Rac and Cdc42 homologs in *Drosophila*) activity, and increased Rho activity (Fritz and VanBerkum, 2002).

1.4.5 Neuronal activity

The developing brain is structurally plastic with remarkable ability to undergo morphological changes based on experience (Wong and Ghosh, 2002). A growing body of science suggests that the general framework of dendritic morphology is intrinsically determined and can form even in the absence of activity (Banker and Cowan, 1979; Bartlett and Banker, 1984a; Bray, 1973). However, this crude framework must then undergo activity-mediated

refinement in order to give rise to functionally accurate neuronal circuitry. For experimental purposes, neural activity can be manipulated by a number of means, including culturing neurons in an environment that enhances or depresses activity from afferent inputs, pharmacological modulation of activity, electrical modulation of activity, and altering sensory stimuli.

1.4.5.1 Pharmacological modulation

Common methods of using drugs to alter neuronal activity in developing dendrites include manipulation of sodium channels, glutamatergic receptors, calcium channels, and potassium channels. In cultured neurons, global blockade of action potentials can be induced by using tetrodotoxin (TTX) to block sodium channels. Although TTX does block all sodium channels and abrogate action potentials, it does not block spontaneous glutamate release. In acute slices of developing mouse cortex, TTX application or using calcium depleted media to decrease neuronal activity leads to increased density and length of interstitial filopodia. In this system, blocking NMDA receptors using APV or MK801 or blocking non-NMDA receptors using CNQX decreases density and turnover of interstitial filopodia, whereas focal application of glutamate increases length of a subset of interstitial filopodia (Portera-Cailliau et al., 2003). Importantly, none of these manipulations in this system affect branchtip filopodia. Excitatory glutamatergic transmission in immature neurons in the CNS are predominately NMDA receptor mediated (Rajan and Cline, 1998; Wu et al., 1996). As neurons mature, the ratio of AMPA receptor mediated transmission to NMDA receptor mediated transmission increases. Requirement for NMDA, but not AMPA, receptor activity in dendritogenesis *in vivo* in immature neurons (with <200 µm dendritic branch length) has been demonstrated in *Xenopus* tadpole tectal neurons. NMDA receptor blockade over 24 hours inhibits addition of new branches and elongation of existing branches, but AMPA receptor blockade has no effect (Rajan and Cline, 1998). Interestingly, in more mature neurons (with >200 µm dendritic branch length), both

NMDA and AMPA receptor activity decreases dendritic arbor growth. Moreover, whereas decreased NMDA receptor activity increases axonal arbor turnover (branch additions and retractions), the same condition leads to decreased dendritic branch turnover (Rajan et al., 1999). Mechanisms underlying neuronal activity mediated dendrite growth include increased intracellular calcium concentration delivered by activation of NMDA receptors, voltage sensitive calcium channels (VSCC), or intracellular calcium release (reviewed in Konur and Ghosh, 2005). Local or global changes in intracellular calcium concentration is involved in a number of intracellular signaling cascades, including calcium/calmodulin-dependent protein kinase (CAMK) activation, mitogen-activated kinases (MAPK), and calcium-dependent transcription. In dissociated embryonic rat cortical neurons, blocking calcium entry through VSCCs with Nifedipine, decreases total dendritic branch length via CREB mediated transcription, but NMDA receptor blockade has no effect (Redmond et al., 2002).

1.4.5.2 Genetic manipulation

In addition pharmacological agents, activity can be altered by genetic manipulation. Reducing AMPA receptor transmission by cell-autonomous expression of peptides corresponding to the intracellular c-terminal regions of AMPA receptors in *Xenopus* tectal neurons decreases branch stability and reduces branch complexity (Haas et al., 2006a). Another means of depressing neural activity, by reducing membrane excitability through misexpression of potassium channels, increases branch number and length of each branch leading to overall increased size of dendritic arbors in *Xenopus* immature RGCs (Hocking et al., 2012).

1.4.5.3 Electrical stimulation

Focal tetanic electrical stimulation on neuronal dendrites of developing rat hippocampal slices leads to localized rapid increase in filopodial density at regions close to the stimulated site, an effect that can be blocked by NMDA receptor blockade (Maletic-Savatic et al., 1999).

1.4.5.4 Afferent sensory stimuli

In its native environment, a sensory stimulus provides input to sensory neurons, as well as to other neurons through indirect synaptic transmission relayed through activated sensory neurons. One of the most meaningful ways to understand how activity affects dendrite growth is to change sensory stimulation and to observe how it affects dendrite growth of target neurons. The onset of afferent input to the rat cerebellar cortex and synapse formation in the *Xenopus* tectum occur concurrently with dendritogenesis of cerebellar and tectal neurons respectively, thus suggesting a temporal correlation between synaptogenesis and dendritogenesis (Miller, 1981; Miller and Peters, 1981). Monocular visual deprivation decreases dendritic fields of some, but not all, classes of neurons observed in the lateral geniculate nucleus in postnatal cat, and decreasing unilateral auditory activity by monaural ear plugging in increases length of low-frequency and decreases length of high-frequency dendritic regions in developing chick nucleus laminaris (Friedlander et al., 1982; Smith et al., 1983). Remarkably, in chick *nucleus laminaris*, dendritic arbors within individual neurons are selectively retracted, such that only dendritic regions from which inputs are eliminated retract whereas other regions remain intact (Benes et al., 1977; Deitch and Rubel, 1984). Moreover, rats raised in enriched environments have increased dendritic branch complexity of pyramidal neurons in visual cortex compared to those reared under control conditions (Greenough and Volkmar, 1973; Volkmar and Greenough, 1972). In contrast, visual deprivation by dark rearing does not alter branch length or complexity of basal dendritic fields of layer 3 pyramidal neurons (Tieman et al., 1995). Interestingly,

inhibition of neural activity often has the paradoxical effect of increasing dendrite growth. For example, in young macaques, both monocular and binocular eyelid suturing leads to increased dendrite growth of layer 4 stellate neurons. (Lund et al., 1991). Whereas these studies observed changes in dendritogenesis or dendritic maintenance after the animal was sacrificed, more recently, visual stimulation has been shown to increase *in vivo* activity-dependent dendrite growth in a manner that requires NMDA receptors and Rho GTPases (Sin et al., 2002). These studies indicate that although neural activity is a critical component of dendritic growth, maintenance, and remodeling, the exact nature of its effect varies among different types of neurons, system under study, developmental stage, and type of sensory input.

Synaptotropic hypothesis

Mounting data suggests that synapse formation drives dendrite growth, corroborating evidence for the "synaptotropic hypothesis", which posits that synapse formation confers morphological stabilization to growth dendritic arbors, leading to dendritic arbor expansion and maintenance in synapse rich regions (Niell et al., 2004; Vaughn et al., 1974). In several systems, dendritic branching directly correlates with amount of presynaptic inputs. For example, rabbit ciliary ganglion neuronal dendritic branch complexity is directly proportional to the number of presynaptic axonal inputs received by (Purves and Hume, 1981). Similarly, in mutant 'weaver' mice in which granule cells, the excitatory presynaptic partners of Purkinje neurons die, Purkinje neuronal dendrites are significantly smaller than wild type mice (Rakic, 1975; Sotelo, 1975). A more striking and direct evidence of synapse-driven dendrite growth comes from studies of zebrafish tectal neurons. Using time-lapse two-photon imaging of a growing tectal neuron, Niell and colleagues have demonstrated that increased intensity or nascent formation of PSD95 puncta, an indicator of excitatory synapses, directly correlates with new dendritic branch formation and branch stabilization, whereas PSD95 puncta disappearance precedes branch retraction (Niell et al., 2004).

1.5 The albino *Xenopus laevis* tadpole as an animal model to study vertebrate brain development

Xenopus laevis, or the African clawed frog, is a species indigenous to South Africa that serves as a classical animal model system in several different aspects of developmental neurobiological studies. In the late 1800's to early 1900's, biologists were investigating how an embryo develops using species such as newt *Triturus*, axolotl *Amblystoma*, and *Xenopus laevis*. For example, Hans Spemann showed that certain 'organizers' in the developing embryo can direct the development of other parts of the embryo. However, the inconvenience of having to catch animals in the wild or waiting for them to reproduce in order conduct projects hampered these experiments. This issue was soon resolved by a fortuitous finding, when in the 1930's it was discovered that urine from pregnant women induces ovulation of female *Xenopus laevis*, and this species became a favorite as a lab animal model. Interestingly, some hospitals kept these frogs as pregnancy tests (reviewed in Gurdon and Hopwood, 2000). Normally, these frogs lay several hundred eggs at a time, and using hormone preparations from other animals or urine from pregnant females, scientists could acquire a multitude of experimental models in a timely, controlled manner. Moreover, this species is relatively hardy and easy to maintain in terms of both housing and feeding, and has a relatively fast life cycle which makes it ideal for developmental studies. Later, physiologists began to use the organism not only because of these advantages, but also because *Xenopus laevis* frog eggs were relatively large and ideal for investigating ion channel conductance. Biochemists and molecular biologists jumped on as well, thus giving rise to a wealth of standard protocols and knowledge specific to this animal model. Due to this prominence of *Xenopus laevis* in labs during this period, developmental neurobiology research pursued in the mid to late twentieth century, including some guidance cue studies, heavily utilized this animal. For axonal guidance studies, *in vitro Xenopus laevis* explants were used to directly manipulate developing axons in a dish by applying purified

guidance cues.

Hollis Cline's lab, along with several other labs have taken advantage of the albino *Xenopus laevis* tadpoles, which lacks pigmentation, to study developing dendrites *in vivo* (Cline and Haas, 2008). Numerous advantages made these tadpoles suitable for dendritic development studies. Tadpoles develop *ex utero*, which provides a much easier access to the developing brain as compared to other commonly used model animals such as mice. The advent of single-cell electroporation allows introduction of a variety of macromolecules, including fluorescent dyes, plasmids, and peptides, into single cells (Haas et al., 2002; Haas et al., 2001). This technique, combined with two-photon microscopy, which allows visualization of fluorescent molecules in deep tissue while limiting photo-toxicity (reviewed in Denk et al., 1990), allows imaging dendrites of fluorescently tagged neurons in the intact and awake (unanesthetized) animal. The lack of pigmentation of albino tadpoles makes the skin transparent, thus eliminating the need for surgical manipulation.

In vivo dendrite development to date has largely focused on neurons of the visual system, particularly RGCs and tectal neurons. Tectal neurons undergo dendritic maturation over a protracted time period (5-6 days) which allows convenient experimental schedules. My work has benefitted tremendously from the knowledge gained in the area of axon guidance, expression patterns of guidance cue molecules, and dendrite development, conducted not only in *Xenopus laevis*, but also in other animal models (i.e. chick, mouse, grasshopper, and fruit fly). For these reasons, I have utilized this animal model for all the experiments conducted in this thesis.

1.6 Dendrite growth analysis software

Imaging techniques have evolved, generating rich datasets with high spatiotemporal

resolutions, giving rise to increasing requirement to bring tracing and analysis tools up to speed with prevailing imaging techniques (Al-Kofahi et al., 2002; Choromanska et al., 2012; Lu et al., 2009; Meijering et al., 2004; Peng et al., 2010). However, development of image analysis tools with sufficient analytical capabilities have met with limited success, and thus, dendritic tracing and analysis has emerged as a bottleneck in neuroscience research (reviewed in Meijering, 2010). This lack of sufficiently user-friendly and adaptable neural tracing softwares is emphasized by the organization of competitions, such as the Digital Reconstruction of Axonal and Dendritic Morphology (DIADEM) challenge held in 2009-2010, to provide incentive to create these tools (Ascoli et al., 2009; Brown et al., 2011; Gillette et al., 2011).

1.6.1 History of neural tracing and analysis

In the early 1900's Ramon y Cajal pioneered research involving neural reconstruction with his manual drawings of intricate dendritic processes. Attempts to automate neuron tracing dates back to at least as early as 1965, with the development of a microscope connected to a computer used to calculate crude 'straight line' dendritic lengths from manually indicated coordinates obtained from microscopic observations (Glaser and Vanderloos, 1965). For decades, manual tracings of dendrites using 'camera lucida', an optical system composed of lenses and mirrors used to superimpose the subject to be drawn (i.e. images from a microscope or a computer screen), on a drawing medium such as a paper or wax paper, have been used to reconstruct neurons . However, this method is tedious, time-consuming, error-prone, and limits the number of analysis that can be done. To address this issue, a myriad of dendritic drawing software, using various tracing algorithms, analysis toolkits, and different levels of automation with the goal of generating digitized neural tracings, have generated a small community of research dedicated to solving this problem (reviewed in Myatt et al., 2012).

Commercially available software

Commercially available software provide solutions to generic neuron tracing problems and are usually user friendly with attractive “front-end” displays. These tools tend to have easy setup and have readily available technical support provided by the companies, and some have limited automated or semi-automated tracing options. However, these software are often prohibitively expensive and are often licensed for a specified number of computers. Also, given that images of dendritic trees are complex and heterogeneous, and scientists continually update experimental questions, capabilities of these tools lag behind the most recent, cutting-edge questions (Chen et al., 2010; Hossain et al., 2012). Furthermore, the source codes for these tools are proprietary, making it impractical to add user-defined increased functionalities based on current research. Examples of current commercially available neuron tracing software include Neurolucida (MBF Bioscience), Amira (Visualization Sciences Group), Imaris (Bitplane), and Meta-Morph (Molecular Devices).

Open-source software

Largely due to the high cost, lack of adaptability, and insufficient capabilities to address the heterogeneous nature of neuron tracing problems in neuroscience, a number of open-source software (i.e. ImageJ plugins NeuronJ and Neuron_Morpho, Neuron_Studio, Vaa3D-Neuron) have been developed. A few of these programs were submitted as responses to neuron tracing competitions.

1.6.2 Stages of neural tracing and analysis

Image acquisition

Proper image acquisition is critical to acquire accurate morphometric data from neurons,

since this primary dataset limits analyzable dendritic components. Images of neurons used for dendrite growth studies are acquired by a variety of means, including light microscopy, confocal fluorescence microscopy, or two-photon fluorescence microscopy. Furthermore, these image files can be a single 2D image, a stack of 2D images at different focal planes that represent the neuron in 3D (z-stacks), and files comprising 2D or 3D images acquired at different time-points. Images with low signal-to-noise ratio comprises one of the primary difficulties in neural tracing, which decreases ability to discern features of dendrites (i.e. dendritic spines, dendritic filopodia, or DGCs), and creates ambiguity between background noise and dendritic components, thus making it difficult for both automated and manual tracing. Creating a balance between acquiring images with high signal-to-noise ratio while preventing phototoxic effects, maintaining cellular health or inducing photobleaching, is often an art as much as science.

Image adjustments

Based on the capabilities and limitations of the software and user, images may need to be modified prior to tracing. These modifications may include image alignment across time to account for drift in time-lapse imaging and image adjustments to increase signal-to-noise ratio (i.e. thresholding or removing back ground noise).

Tracing

The general theory behind tracing programs is fairly simple. The computer program displays images or image stacks (for 3D neuronal representations) on the screen, and the user, or the computer for automated tracing, traces over the objects of interest (dendrites, axons, filopodia, etc.), creating a digitized representation of the object, which can then be used for analysis. In the case of dendrites, the actual tracing process, especially for complex dendritic arbors, is often laborious and sometimes confusing. For example, in 3D image stacks, it is sometimes difficult to differentiate between dendritic branching and overlap of two separate

dendrites. To increase efficiency and objectivity, several automated and semi-automated tracing programs have been developed. However, although at first glance, many computer scientists deem the issue of automated neural tracing to be entirely solvable, none of the algorithms developed thus far have been able to provide a satisfactory solution (Ascoli et al., 2009; Myatt et al., 2012).

Analysis

The traced dendrite generates a set of xy or xyz coordinates, which are used to analyze various aspects of the dendritic tree. Some common analyses include, total branch length, number of branch points, complexity of dendrites at various distances from the soma (termed Sholl analysis (Sholl, 1953)), filopodial additions/retractions, filopodial or branch motility, among many others. As imaging technologies have evolved, with increasing emphasis on time-lapse data, we can now extract more information through improved analysis of imaging data. However, limited by analytical functions available in current software tools, few labs take advantage of the plethora of analytical capabilities of these rich datasets. In this respect, some of the most comprehensive and detailed dendrite analysis studies, particularly in the area of *in vivo* dendritogenesis, have emerged from studies in *Xenopus laevis* tectal neurons, with novel dynamic morphometric analyses of rapid time-lapse data (Chen et al., 2012; Chen et al., 2010; Hossain et al., 2012). For example, using novel analysis to differentiate between lifetime and motility of filopodial populations based on when they emerge has given novel insight into whether these filopodia contribute solely to cell-adhesion or participate in synapse formation (Chen et al., 2010); and analyzing frequency of lamellipodia versus filopodial frequency on DGCs has contributed to the understanding of DGC characteristics at different neuronal maturational stages and how DGCs contribute to overall dendrite growth and behavior (Hossain et al., 2012). However, novel detailed analysis with existing software tools are tedious, often engaging the user in tasks that can be better automated, giving rise to the need for not only

better tracing algorithms, but also for automated novel quantitative morphometric methods, and integration of convenient user-defined analyses that biologists can add as their analysis evolves.

1.7 Rationale and hypotheses

One of the most pressing questions in developmental neurobiology is how neurons transform from simple spherical cells when newly formed to cells with large and complex dendritic and axonal arborizations required for constructing intricate neural networks. Dendrite growth is a highly dynamic process with extension, retraction, stabilization, and destabilization of different components of dendrites during development, which ultimately gives rise to the mature dendritic architecture, setting the groundwork for the physical neural connectivity of the functional brain. A common theme that has emerged from cumulative studies of different aspects of both axonogenesis and dendritogenesis is that, in general, unrefined overall arbor growth is activity independent (dependent on neurotrophic factors, guidance cues etc.) whereas refinement (i.e. spinogenesis in mature animals, or axonal pruning) occurs through neuronal activity. The effect of guidance cues on filopodia has been studied in non-neuronal cells and in axonal growth cones, however whether guidance cues affect interstitial and/or DGC filopodia is unknown. In this dissertation, one of my goals was to understand how dendritogenesis occurs *in vivo* in the unanesthetized brain by carefully examining various features and behaviors of growing dendrites as they mature through different phases of growth. Also, during the course of this research, I found that the current tools available were insufficient to analyze dynamic dendritogenesis growth patterns; thus, I sought to develop the necessary technology. Finally, another goal of this work was to determine whether dendrite growth occurs in a biased orientation toward their target *in vivo*, and if so, to explore the potential role of guidance cue molecules in guided dendritogenesis.

Chapter 2: Dynamic morphometrics reveals contribution of dendritic growth cones and filopodia to dendritogenesis

2.1 Introduction

The structural development of brain circuits is one of the most complex processes in early life critical to future brain function and is susceptible to errors that may give rise to neurodevelopmental disorders. Brain neurons must grow elaborate dendritic and axonal arbors and form precise inter-neuronal synaptic connections to create the physical structure necessary for functional neural circuits. Establishing correct dendritic arbor morphologies is required to contact appropriate axons, to provide surface area for synaptic inputs, and to influence electrical properties underlying the integration, processing, and plasticity of synaptic currents (Hausser et al., 2000). The mechanisms regulating neuronal dendritic arbor growth are beginning to emerge, and involve a combination of intrinsic genetic programming to establish basic neuron-type specific patterning and extrinsic cues that underlie individual neuronal variations, as well as extensive activity-dependent remodeling (Grueber et al., 2003; Haas et al., 2006a; Jan and Jan, 2010; Jinushi-Nakao et al., 2007; McAllister et al., 1997; Nedivi et al., 1998; Polleux et al., 2000; Rajan and Cline, 1998; Sin et al., 2002; Wu et al., 1999).

Our understanding of mechanisms underlying dendritogenesis has been greatly advanced by the recent development of technologies allowing direct imaging of neuronal growth within intact developing brains. *In vivo* rapid time-lapse imaging of individual growing brain neurons in transparent embryos of albino *Xenopus laevis* tadpoles and zebrafish has provided new insights to how growing dendritic arbors achieve their mature shapes (Chen et al., 2010; Liu et al., 2009; Mumm et al., 2006; Niell et al., 2004; Wu et al., 1999). Sampling entire growing dendritic arbors at intervals of minutes, over periods of hours, reveals an exceptional amount of

motility and turnover of both short filopodia and longer branches, which could not be predicted from imaging at longer intervals. Another feature of growth readily apparent from rapid time-lapse imaging is the high incidence of DGCs at the tips of branches, which are often not evident in single time point images because of their highly variable morphologies with sparse expression of lamellipodia. High interstitial filopodial turnover and the presence of dynamic DGCs suggest mechanisms by which extrinsic factors, such as presynaptic input, growth factors and guidance cues may influence dendritic arbor patterning.

While interstitial dendritic filopodia are largely associated with spine formation in neurons with established dendritic arbors, it has been postulated that in immature growing neurons, they are precursors of longer branches (Dailey and Smith, 1996; Niell et al., 2004; Scott and Luo, 2001; Wu et al., 1999). Imaging individual brain neurons expressing the fluorescently tagged postsynaptic marker PSD-95 supports a synaptotropic model of dendritogenesis in which synapse formation stabilizes filopodia, allowing further extension and branch formation (Chen et al., 2010; Niell et al., 2004; Vaughn et al., 1988). Therefore, contact with appropriate presynaptic terminals and activity-dependent synapse formation may direct dendritic branch formation and growth. Lacking from this model, however, is a comprehensive quantification of interstitial filopodial growth dynamics and their relationship to branch formation *in vivo*.

While growth cones on leading tips of axons have been extensively characterized for their roles in guidance and their morphological changes associated with axonal growth behaviors, reports on the existence of DGCs in intact brain tissues are scant (Dailey and Smith, 1996; Furrer et al., 2003; Gascon et al., 2006; McMullen et al., 1988; Polleux et al., 2000; Tamamaki, 1999; Vaughn et al., 1974; Wu et al., 1999). However, neurons typically orient their dendrites in a characteristic manner, and several axonal guidance cues, including Semaphorin 3A, netrin-A and -B, and slit, have been shown to direct orientation of dendritic growth (Furrer et al., 2003; Godenschwege et al., 2002; Komiyama et al., 2007; Polleux et al., 2000).

In order to further understand the roles of dendritic filopodia and DGCs in dendritogenesis within native environments, we have undertaken a comprehensive study of rapid dendritic arbor growth of newly differentiated projection neurons within the optic tectum of the intact and unanesthetized *X. laevis* tadpole. By tracking and measuring all dendritic processes in three dimensions from rapid and long-interval time-lapse imaging, we achieve sensitive measures of “dynamic morphometrics” that characterize the contributions of rapid growth behavior to the mature arbor structure. We find that all growing dendritic branches express DGCs, with morphologies correlating to distinct growth behaviors. Further we demonstrate that interstitial filopodia are precursors of longer and persistent dendritic branches.

2.2 Materials and methods

2.2.1 Animals

Freely swimming albino *X. laevis* tadpoles were housed at 22°C in 10% Steinberg's solution (1× Steinberg's: 10 mM HEPES, 60 mM NaCl, 0.67 mM KCl, 0.34 mM $(CaNO_3)_2$, 0.83 mM $MgSO_4$, pH 7.4) and maintained on a 12-h light/dark cycle. Experiments were conducted on Stage 47 tadpoles (Nieuwkoop and Faber, 1994) and were performed within guidelines set by the Canadian Council on Animal Care following protocols approved by the Animal Care Committee of the Faculty of Medicine at the University of British Columbia.

2.2.2 Single-cell electroporation

Individual projection neurons within the mediocaudal optic tectum of the intact tadpole brain were fluorescently labeled using single-cell electroporation (SCE) (Haas et al., 2001;

Hewapathirane et al., 2008). Tadpoles were briefly anesthetized with 0.02% 3-aminobenzoic acid ethyl ester (MS222, Sigma). A sharp glass pipette (~0.6 μm tip diameter) loaded with a solution of plasmid DNA encoding farnesylated Green Fluorescent Protein (pEGFP-F, Clontech; 2 μg/μL in dH2O) was inserted into the proliferative zone in the mediocaudal region of the optic tectum, to transfect individual newly differentiated neurons using an Axoporator 800A (Molecular Devices, Sunnyvale, CA; stimulus parameters: pulse intensity = 1 μA; pulse duration = 1 msec; pulse frequency = 300 Hz; train duration 300 msec).

2.2.3 *In vivo* time-lapse two-photon imaging in the unanesthetized brain

In order to image dynamic neuronal growth *in vivo* without the confounding effects of activity blockade from anesthetics, awake tadpoles were immobilized with the reversible paralytic pancuronium dibromide (PCD, 3 mM, Tocris) and mounted on a custom-built imaging chamber, embedded under a thin layer of agarose (1%) and continuously perfused with oxygenated 10% Steinberg's solution. Images of fluorescently labeled neurons were acquired using a custom-built two-photon microscope consisting of a modified Olympus FluoView 300V confocal scan box mounted on an Olympus BX50WI microscope coupled to a Chameleon Ti:Sapphire laser (Coherent, Santa Clara, CA). Three-dimensional stacks of images of the entire dendritic arbor were captured using a LUMPlanFI_IF 60×, 1.1 NA, water immersion objective (Olympus) and FluoView software (Olympus). Optical sections were acquired using 1.5 μm *z*-axis intervals, and stacks of images encompassing entire dendritic arbors were taken at 5 min intervals for 1 h each day for 5 consecutive days, at 5 min intervals for 5 h, or at 2 h intervals for 10 h. Following imaging, tadpoles were returned to rearing solution where they rapidly recovered from the paralytic.

2.2.4 Selection criteria for neurons

Since interneurons and projection neurons have different patterns of dendrite growth in this system, I excluded any neuron with no discernible projecting axon such that only projection neurons were included for all experiments (Wu and Cline, 2003; Wu et al., 1999).

2.2.5 Analysis of dendritic arbor growth

Tectal neuron dendritic arbor morphology and growth were measured using custom written software to identify, track, and measure all dendritic branches and filopodia across all time points (software created by Dr. Jamie Boyd and Kaspar Podgorski, University of British Columbia). In all cases, all processes on the entire dendritic arbors were measured in three dimensions. Filopodia were defined as short, <10 μm, processes of uniform width and lacking protrusions. Due to differences in growth behaviors, including rates of addition, retraction, and lifetimes, filopodia were classified as either “interstitial,” emerging from a dendritic shaft, or “branchtip,” emerging within 5 μm of the branch ending. DGCs were defined as elaborations at the ends of processes, characterized by lamellipodial swellings with a width at least 1.5 times the width of the process shank, or the presence of a high density of filopodia over time. Filopodia and branch motility were measured by taking the sum of the absolute value of extensions and retractions over time. Proportions were analyzed using χ^2 tests followed by pair-wise *post hoc* comparisons (Chien et al., 1993) and Sholl analysis of branch length between successive spheres of increasing radii centered on the soma was conducted using two-way ANOVA followed by Bonferroni post tests. Differences between Day 1-2 neurons and Day 4-5 neurons and between interstitial filopodia and branchtip filopodia dynamics were analyzed using unpaired Student's *t*-tests. Multiple comparisons were done using one-way ANOVA followed by *post hoc* analysis by Tukey's multiple comparison test.

2.3 Results

2.3.1 Tectal neurons progress through 3 phases of dendritic arbor growth

As demonstrated previously (Haas et al., 2006a; Liu et al., 2009; Wu et al., 1999), we find that *Xenopus* tectal neurons elaborate dendritic arbors over the course of 4 to 5 days after differentiation (Figure 4). Newly differentiated neurons first extend an axon without substantial dendritic branch formation or elongation over 24 h. As shown by Sholl analysis, the majority of dendritic arbor complexity is restricted proximal to the soma (Figure 4). During this period, a high rate of dendritic filopodial turnover occurs without branch extension. Over the next 2 days, a growth spurt is driven by new branch addition and elongation. By the fourth day, dendritic arbor growth subsides and a stable state is reached with little net change in total dendritic branch length (TDBL), total dendritic branch number (TDBN), or three-dimensional arbor complexity. These results are in accordance with previous characterization of three phases of vertebrate dendritogenesis (Wu et al., 1999). In Phase 1, newly differentiated neurons exhibit axonal growth while the dendritic arbor is restricted to short and unstable protrusions. In Phase 2, over 24 to 48 hours dramatic branch addition and elongation establishes the dendritic arbor. In Phase 3, this dramatic growth ceases and the dendritic arbor achieves a mature and stable conformation.

2.3.2 Dynamic daily imaging

To characterize dynamic dendritic growth behavior we employed rapid time-lapse imaging to capture the entire dendritic arbor every 5 min over 1 h. To measure growth behavior throughout distinct stages of maturation, dynamic imaging was conducted on the same neurons at 24 h intervals over 5 days. Importantly, all imaging was conducted on immobilized tadpoles

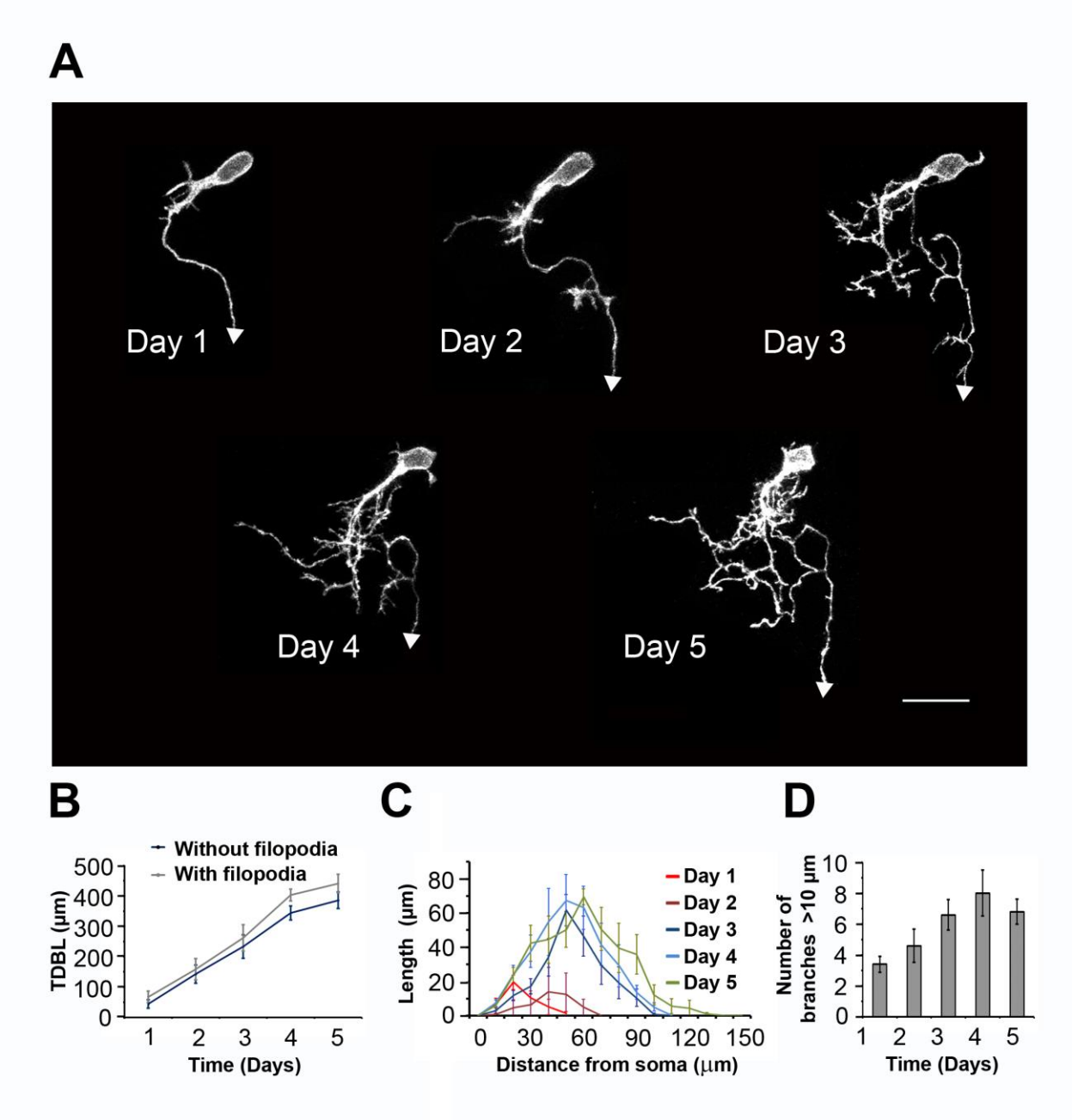

Figure 4. Maturation of tectal neurons *in vivo*.
(A) Two-photon images of an individual neuron imaged at daily intervals for 5 days. The arrowhead depicts the axon, which projects out of the tectum. Scale bar = 20 µm. (B) Total dendritic branch length including and excluding all filopodia. (C) Three-dimensional Sholl analysis of changes in dendritic arbor complexity over 5 days. (D) Total number of dendritic branches >10 µm over 5 days. N = 5 neurons. Error bars denote SEM.

without anesthesia, since neuronal transmission has been shown to regulate tectal dendrite growth (Chen et al., 2010; Ewald et al., 2008; Haas et al., 2006a; Rajan and Cline, 1998; Rajan et al., 1999; Sin et al., 2002). Further, growth of all branches and filopodia on entire arbors were measured in three dimensions across all time points. We find that rapid time-lapse imaging reveals maturation-dependent dynamic growth behaviors undetectable from long-interval, "snap-shot" imaging (Figure 5). As shown in Figure 5B, although DGCs are not visible at all time-points, they are clearly visible from time-lapse imaging (see branchtips in overlays, Figure 5B). Moreover, dendritogenesis involves a remarkable amount of turnover of filopodia and branches, transitions of filopodia into branches, and varied dendritic growth cone behaviors.

2.3.3 Dynamic daily imaging: dendritic branches

While we see little overall change in net dendrite growth over 1 h at any maturational state, dynamic growth behavior of dendritic branches changes over 5 days of neuronal development (Figure 5). Dendritic branches were characterized as processes >10 μm, or shorter processes exhibiting filopodial or branch protrusions, or any processes expressing lamellipodia. Branch motility significantly decreases over maturation, with 2.00 ± 0.12 μm/5 min on Day 1 to 2 to 1.22 ± 0.07 μm/5 min on Day 4 to 5 (all values presented as mean ± SEM; Figure 5C). Similarly, we find a maturational decrease in dynamic range, the difference between the longest and shortest length of each branch over 1 h (Figure 5E), and a maturational increase in dendritic pausing behaviors as compared to extension and retraction behaviors which further corroborates evidence for increased dendritic stability with maturation (Figure 5F). Longer interval imaging, 2 h intervals over 10 h, was employed on Day 2 neurons to determine the lifetime of new branches (Figure 7C). Approximately half of new branches rapidly retracted within 2 h of initial detection, with 52.63% persisting for >2 h, and only 10.53% persisting for

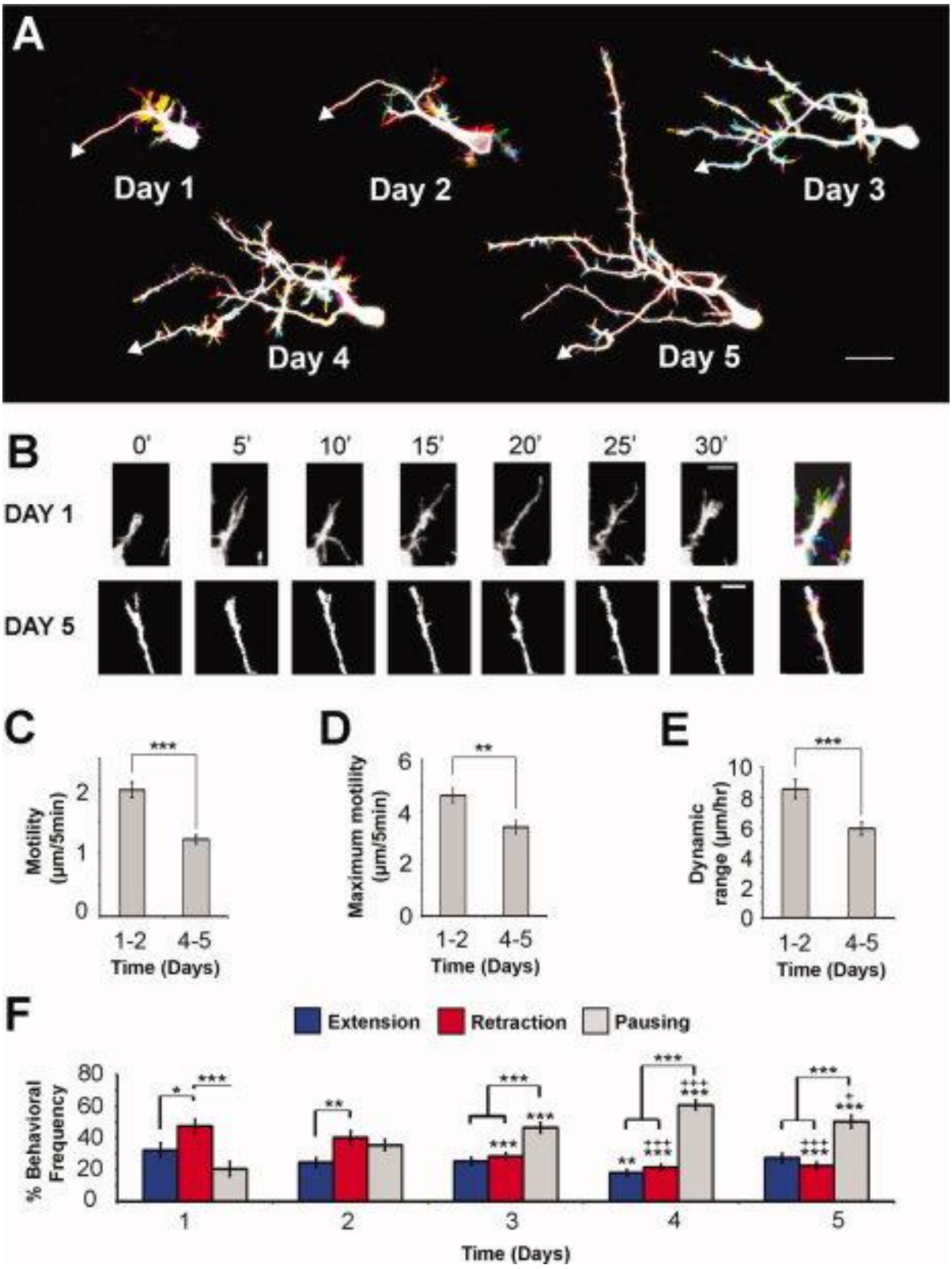
A
Day 1
Day 2
Day 3
Day 4
Day 5
B
0'
5'
10'
15'
20'
25'
30'
DAY 1
DAY 5
C
Motility (µm/5min)
1-2
4-5
Time (Days)
D
Maximum motility (µm/5min)
1-2
4-5
Time (Days)
E
Dynamic range (µm/hr)
1-2
4-5
Time (Days)
F
Extension
Retraction
Pausing
% Behavioral Frequency
Time (Days)

Figure 5. Maturation-dependent dynamic dendritic morphology.
(A) Superimposed images of seven successive time points at 10 min intervals of a single neuron imaged daily for 5 days. Each time point within an overlay is a different color (red, green, blue, cyan, magenta, yellow, and orange; mixed colors and white = overlap). Arrowhead depicts the axon. Scale bar = 20 μm. (B) Images of a branchtip from a Day 1 neuron (top) and a Day 5 neuron (bottom) at 5 min intervals showing reduced motility and lamellipodia with maturation, followed by a superimposed image of all the time points in different colors (colors: red, green, blue, cyan, magenta, yellow, and orange; mixed colors and white = overlap; Scale bar = 5 μm). Note that for time point 20′ for the Day 1 neuron and 25′ for the Day 5 neuron the DGC is not discernible from a single image. (C) Motility, (D) maximum motility, defined as the maximum absolute value of extensions and retractions reached by each branch/5 min, and (E) dynamic range, defined as the absolute value of the maximum distance traveled by each branch/h, grouped by Day 1 to 2 neurons and Day 4 to 5 neurons (N = 5 neurons, n = 62 branches for Day 1–2 neurons and n = 82 branches for Day 4–5 neurons). (F) Percentage of the observed time points each branch undergoes extension, retraction, or pausing behaviors over 5 days of dynamic imaging. "*" denotes comparison with Day 1 and "+" denotes comparison with Day 2. Error bars denote SEM; *$p < 0.05$; **$p < 0.01$; ***$p < 0.001$.

>8h. Thus, branches on developing neurons are labile and susceptible to a high degree of turnover during morphological refinement.

2.3.4 Dendritic filopodia

Dendritic filopodia are short (<10 μm) and highly motile dendritic processes of uniform thin width expressed on branches throughout the growing dendritic arbor. Based on distinct growth behaviors, we have separated dendritic filopodia as "branchtip" if within 5 μm of a branch ending, and all others as "interstitial" (Portera-Cailliau et al., 2003). Branchtip filopodia typically exhibited shorter lifetimes, higher density, and higher addition and retraction rates compared with interstitial filopodia (Figure 6). Extrapolating from measures of filopodial addition rates from 5 min interval imaging over 1 h, every day for 5 days, we estimate that each tectal neuron produces approximately 3628 interstitial and 2402 branchtip filopodia over 5 days of dendritic arbor maturation. By imaging Day 2 neurons at 5 min intervals over 5 h and tracking every

filopodia, we find that filopodia exhibited an average lifetime of 16.01 ± 1.89 min for interstitial and 10.57 ± 1.89 min for branchtip filopodia. Furthermore, we find a developmental shift in filopodial growth behavior. Immature Day 1 to 2 neurons exhibit higher filopodial motility and increased length as compared with more mature neurons (Figure 6E,F). Interstitial filopodia exhibit an increase in lifetime with maturation, with approximately 6.7 min for Day 1 neurons and 21.3 min for Day 5 neurons (Figure 6G).

2.3.5 Dendritic filopodia emerging during dendritogenesis are precursors of longer branches

The function of dendritic filopodia has been an area of debate, which has largely focused on their relation to dendritic spines (reviewed in Jontes and Smith, 2000). Here, by tracking filopodia across 5 min intervals over 5 h, we find that interstitial dendritic filopodia can transition into branches during periods of arbor elaboration (Figure 7). Filopodia-to-branch transitions were defined as filopodia that extend to lengths greater than 10 μm, and/or elaborate lamellipodia at their endings, and/or extend additional processes. Of 1347 filopodia tracked across 5 min interval imaging over 5 h on complete arbors of 5 Day 2 neurons, 4.68% transformed into dendritic branches, and of these, 13.4% attained a length >10 μm. A breakdown of the three types of transitions reveal that most of these filopodia-to-branch transitions occurred by extending additional processes (48.48%) or by a combination of developing lamellipodia, branching, or attaining a length >10 μm over the 5 h imaging period Figure 7D. While a low percentage (6.06%) of filopodia transitioned by developing only lamellipodia, none transitioned solely by increasing in length to >10 μm. From dynamic imaging over 5 days, we find that the percentage of filopodia that transition into branches decreases over neuronal maturation (Figure 7B). Although newly formed branches are unstable and exhibit

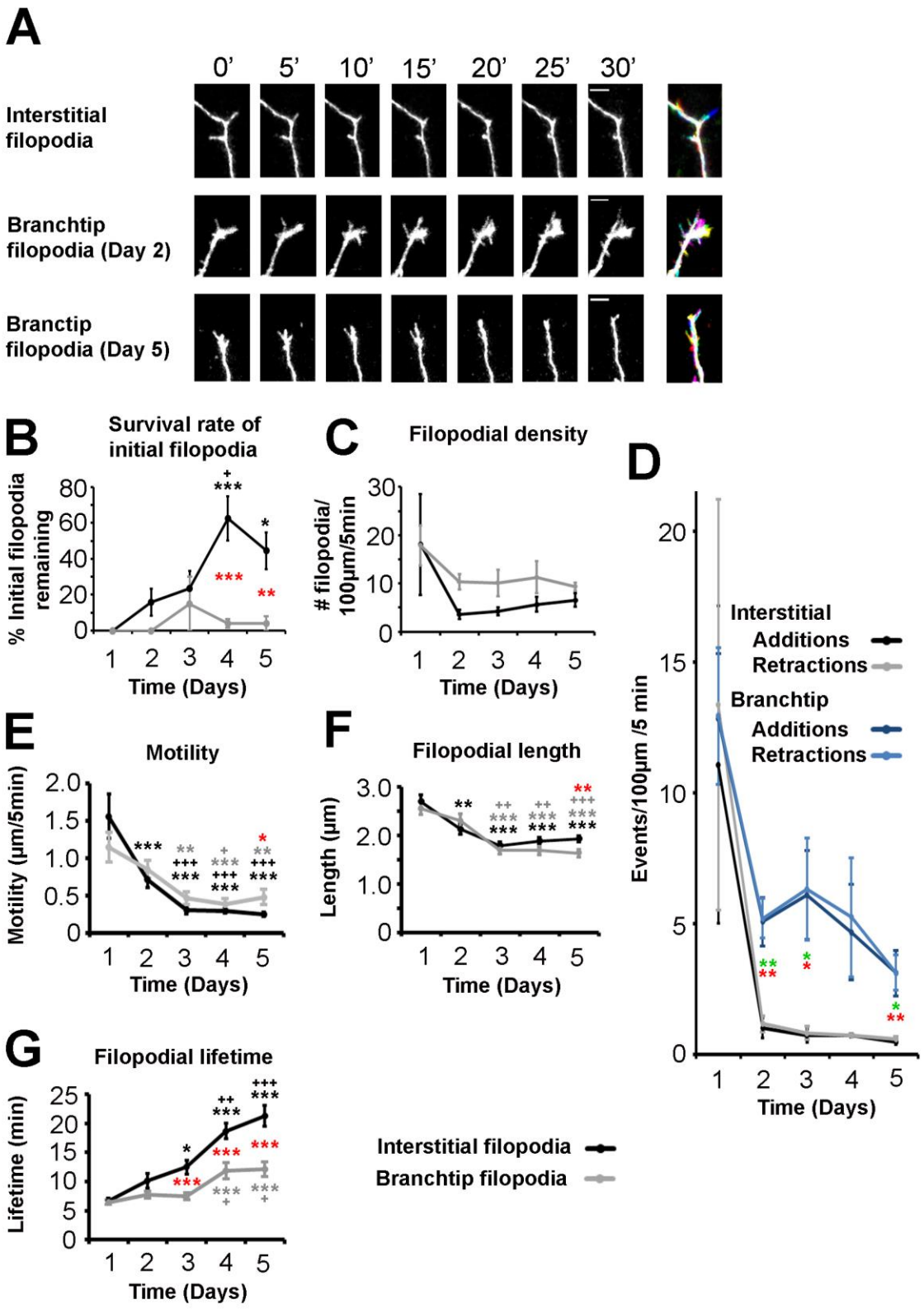
A
0'
5'
10'
15'
20'
25'
30'
Interstitial filopodia
Branchtip filopodia (Day 2)
Branctip filopodia (Day 5)
B
Survival rate of initial filopodia
% Initial filopodia remaining
Time (Days)
C
Filopodial density
filopodia/ 100µm/5min
Time (Days)
D
Events/100µm /5 min
Interstitial
Additions
Retractions
Branchtip
Additions
Retractions
Time (Days)
E
Motility
Motility (µm/5min)
Time (Days)
F
Filopodial length
Length (µm)
Time (Days)
G
Filopodial lifetime
Lifetime (min)
Time (Days)
Interstitial filopodia
Branchtip filopodia

Figure 6. Branchtip versus interstitial filopodial dynamics over neuronal maturation. (A) Rapid time-lapse images of interstitial filopodia from a Day 5 neuron (top), branchtip filopodia from a Day 2 neuron (middle), and branchtip filopodia from a Day 5 neuron (bottom), followed by an overlay of all time points shown (right) (colors used were red, green, blue, cyan, magenta, yellow, and orange; mixed colors and white = overlap; scale bars = 5 μm). (B) Percent of pre-existing branchtip and interstitial filopodia that survived until the end of the 1 h imaging period for Days 1 to 5. (C) Filopodial density, (D) additions and retractions, (E) motility, (F) length, and (G) lifetime for both branchtip and interstitial filopodia for Days 1 to 5. $N = 5$ neurons; $n = 26$, 30, 36, 48, and 44 branchtip filopodia and $n = 24$, 50, 85, 167, and 173 interstitial filopodia for Days 1 to 5, respectively. For significance on (B, E, F, and G), "*" denotes comparison with Day 1 and "+" denotes comparison with Day 2, gray for branchtip and black for interstitial filopodia. Red "*" denotes comparison between interstitial and branchtip filopodia. For (D), green and red "*" signify comparison of additions and retractions respectively between interstitial and branchtip filopodia. Error bars denote SEM; *, $+p < 0.05$; **, $++p < 0.01$; ***, $+++p < 0.001$.

a high rate of retraction, some nascent branches arising from interstitial filopodia were observed to persist for hours until the end of imaging (Figure 7C). The lifetime and average length of processes that underwent filopodia-to-branch transitions were significantly greater than for filopodia that did not transition to branches (Figure 7E,F). Therefore, during dendritogenesis, dendritic filopodia can function as precursors of longer and persistent branches, and expression of DGC appears to be a requirement for branch formation.

2.3.6 Dendritic growth cones (DGCs)

Rapid imaging reveals that dendritic endings exhibit dynamically changing morphologies with intermittent display of lamellipodia and/or a high density of branchtip filopodia, characteristics of growth cones (Figure 5A,B). A lamellipodium was defined morphologically as a dendritic ending with a width greater than 1.5 times the width of the adjacent dendritic shaft. In order to determine the expression pattern of DGCs throughout neuronal maturation and their relationship to dendritic growth, we examined all branch endings in all rapid time-lapse imaging

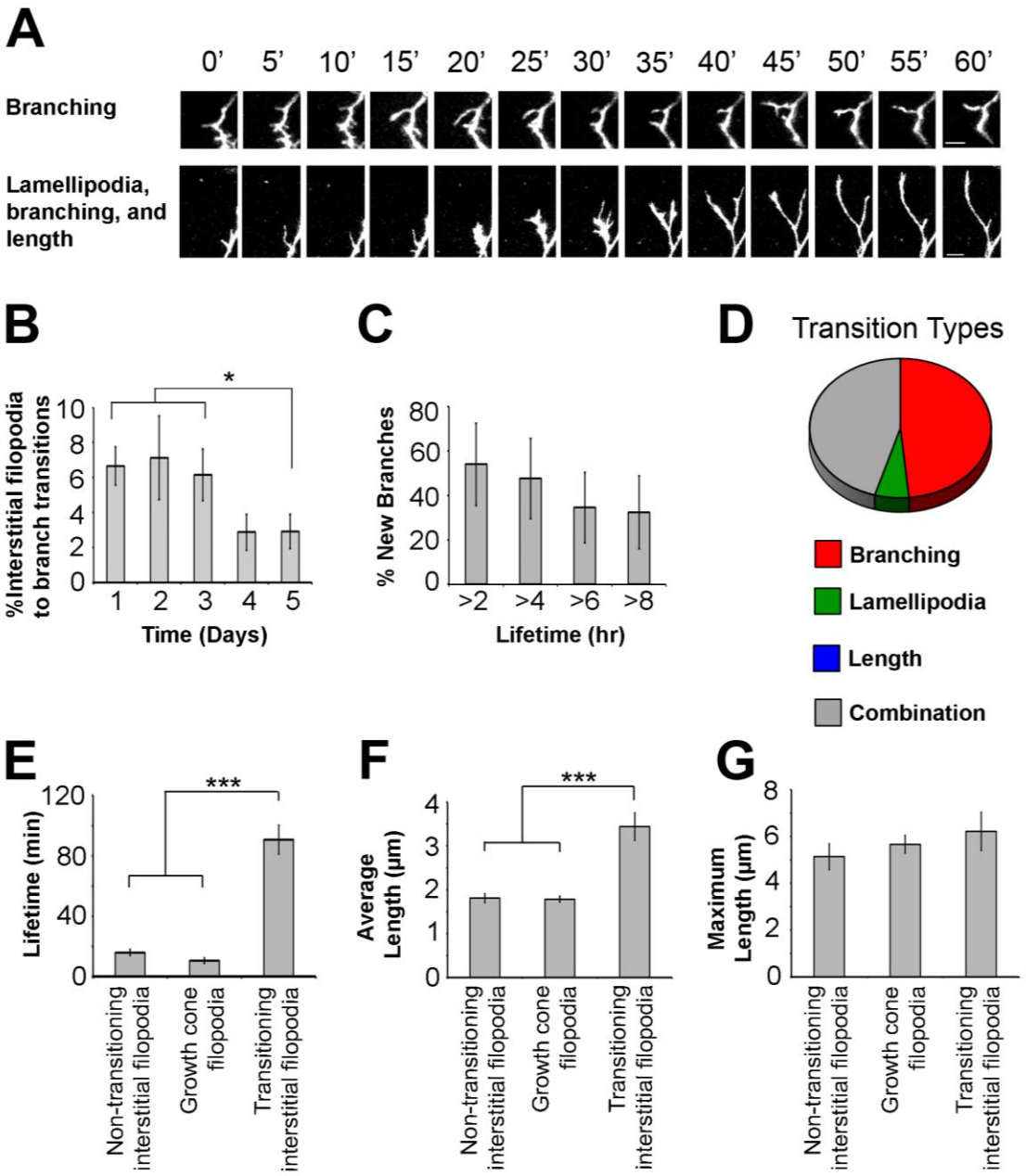
A
0’ 5’ 10’ 15’ 20’ 25’ 30’ 35’ 40’ 45’ 50’ 55’ 60’
Branching
Lamellipodia, branching, and length
B
%Interstitial filopodia to branch transitions
Time (Days)
C
% New Branches
Lifetime (hr)
>2 >4 >6 >8
D
Transition Types
Branching
Lamellipodia
Length
Combination
E
Lifetime (min)
F
Average Length (µm)
G
Maximum Length (µm)
Non-transitioning interstitial filopodia
Growth cone filopodia
Transitioning interstitial filopodia

Figure 7. Interstitial filopodia transition to persistent dendritic branches.
(A) Rapid time-lapse images of filopodia transitioning to a branch by branching (top, see t = 45 min), and by expressing lamellipodia, branching and increasing length to >10 μm (bottom). Scale bar = 5 μm. (B) Percent of interstitial filopodia that transition to branches within 1 h over Days 1 to 5. *N* = 5 neurons. (C) Lifetime of newly emerged branches obtained from imaging each neuron at 2 h intervals for 10 h. *N* = 5 neurons. (D) Percentage of each type of observed filopodia-to-branch transitions from imaging at 5 min intervals for 5 h. *N* = 5 neurons, *n* = 66 filopodia-to-branch transition events. (E) Lifetime, (F) average length, and (G) maximum length of "non-transitioning interstitial filopodia," "growth cone filopodia," and "transitioning interstitial filopodia" from imaging at 5 min intervals for 5 h. *N* = 5 neurons for (D–E). Error bars denote SEM; *, +$p < 0.05$; **, ++$p < 0.01$; ***, +++$p < 0.001$.

experiments. Remarkably, given the paucity of published reports on DGCs, we find that all growing branches (>5 μm net growth/h) expressed DGCs identifiable by the presence of lamellipodia and/or a high density and turnover of branchtip filopodia (Figure 6A). DGCs are not readily apparent from single images because characteristic lamellipodia are observed in only 10% to 30% of images captured at 5 min intervals (Figure 5B). DGC morphology fluctuates dramatically within minutes from structures containing lamellipodia, both lamellipodia and filopodia, only filopodia, or none of these structures. The presence of DGCs on all growing branches suggests a central role in dendrite growth.

2.3.7 DGC maturation involves increases in lamellipodia and decreases in filopodia

To determine whether DGC morphology changes over dendritic arbor maturation we examined morphologies of all branch endings throughout 5 min/1 h dynamic imaging over 5 days of arbor growth. Branch endings were classified into categories based on presence or absence of lamellipodia or filopodia. Across all 5 days, the dominating branch morphologies were bare endings, or with only filopodia, with lower frequencies of expression of lamellipodia (Figure 8E). These results underscore the difficulty in identifying DGCs from single-image data.

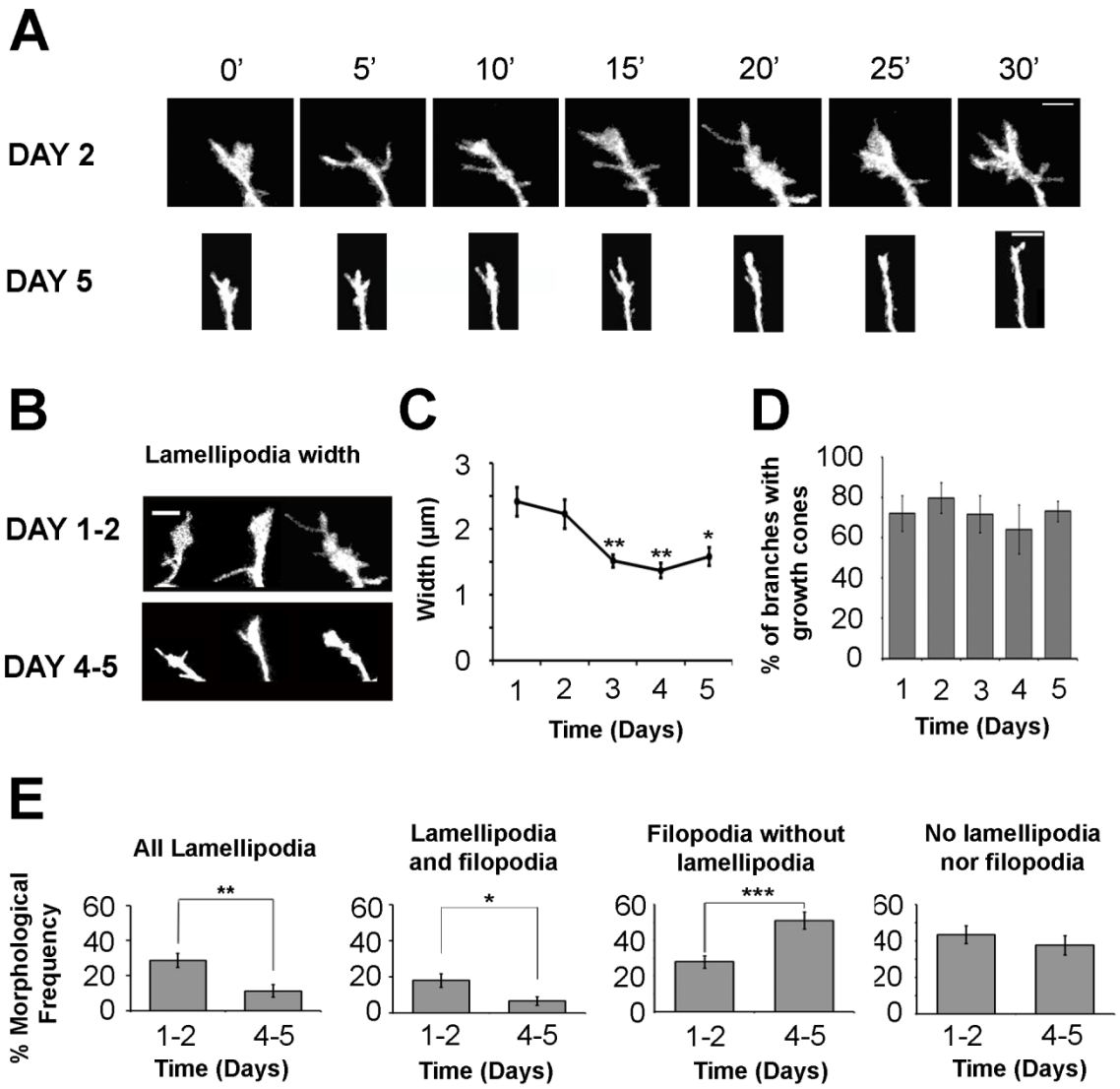

Figure 8. Morphological maturation of DGCs.
DGC morphologies of the same set of five neurons were tracked over 5 days. (A) Images of three DGC exhibiting lamellipodia from Day 1 to 2 neurons (top) and from Day 4 to 5 neurons (bottom). Scale bar = 5 µm. (B) Maximum width of DGC lamellipodia over 5 days. N = 5 neurons, and n = 18, 10, 13, 7, 11 lamellipodia for Days 1, 2, 3, 4, and 5 respectively. (C) Percent of all branches with DGCs as indicated by the presence of lamellipodia or high filopodial density. N = 5 neurons. (D) Percentage of time points DGCs exhibited different morphologies for Days 1 to 2 neurons versus Day 4 to 5 neurons. "All Lamellipodia" includes DGC morphologies with lamellipodia alone or lamellipodia with filopodia. N = 5 neurons, and n = 35 DGCs for Days 1 to 2 and n = 32 DGCs for Days 4 to 5. Error bars denote SEM; *p < 0.05; **p < 0.01; ***p < 0.001.

Maturational changes in DGC morphology were evident as a decrease in the expression of lamellipodia, which were significantly more prevalent on Day 1 to 2 neurons than Day 4 to 5 neurons (Figure 8E). In contrast, the frequency of DGCs with only filopodia was lower for Day 1 to 2 neurons as compared with Day 4 to 5 neurons. Furthermore, the average lamellipodial width of DGCs was significantly reduced from 2.42 ± 0.22 μm on Day 1 to 1.6 ± 0.14 μm on Day 5 (Figure 8B,C). These results suggest a progression of DGC morphologies from lamellipodial to filopodial structures over neuronal maturation.

2.3.8 DGC morphology correlates with extension, retraction, and pausing behaviors

Given evidence for an association between axonal growth cone morphology with axonal growth behavior (Mason and Wang, 1997), we examined the relationship of DGC morphology to extension, retraction, and pausing behavior of dendrites. Axonal growth cones exhibit streamlined morphologies during periods of rapid growth and more complex lamellipodial morphologies while pausing. We find that all branches exhibiting greater than 5 μm/h net extension expressed DGCs (Figure 9A,C). Of all the paused dendritic branches, defined as exhibiting less than 1 μm/h net change in length, 63.4 ± 9.4% expressed DGCs, while only 26.7 ± 7.3% of retracting branches (greater than 5 μm/h net retraction) expressed DGCs (Figure 9C). Furthermore, binning net branch extension and retraction by 1 μm/h intervals shows a clear trend of increasing percent of branches with growth cones with increasing net extension and a decreasing presentation of growth cones with increasing net retraction. To analyze this relationship between branch morphology and behavior in more detail, we compared DGC morphology immediately before the branch growth behavior for each 5 min interval of rapid time-lapse imaging. For this analysis, over each 5 min interval, greater than 1 μm of branch elongation was defined as “extension,” greater than 1 μm of branch shortening as “retraction,” and <1 μm movement as “pausing”. We find that lamellipodia are associated with extensions

(26.12%) and to a lesser extent pausing, and not retractions (6.88%) (Figure 9B). In contrast, morphologies lacking lamellipodia and filopodia are associated to a larger extent with retractions (56.13%) then extensions (34.83%). Furthermore, average motility of branches expressing both lamellipodia and filopodia (1.40 ± 0.22 μm/5 min) were significantly greater than the average motility of branches without lamellipodia or filopodia (−0.46 ± 0.07 μm/5 min). These results indicate that growth cones on dendrites of developing brain neurons are associated with both pausing and active extension, whereas retracting dendrites tend to express a collapsed morphology.

2.4 Discussion

Using a combination of short- and long-interval time-lapse imaging of growing dendrites in the intact and unanesthetized developing brain, we address fundamental questions regarding the function and behaviors of key components of the developing dendritic arbor, including dendritic filopodia and growth cones. By employing powerful custom-built software to track and measure all processes on entire dendritic arbors in three dimensions over short intervals for long periods, we characterize the contributions of these structures to neuronal morphological maturation. This comprehensive quantification and novel analysis offers unprecedented detail of dynamic growth behaviors and their changes across different stages of dendritic arbor development.

Our identification of DGCs at the ends of all extending branches is in contrast to the limited description and study of these complex cellular specializations in published literature (Dailey and Smith, 1996; Furrer et al., 2003; Gascon et al., 2006; McMullen et al., 1988; Polleux et al., 2000; Tamamaki, 1999; Vaughn et al., 1974; Wu et al., 1999). Lack of attention to DGCs

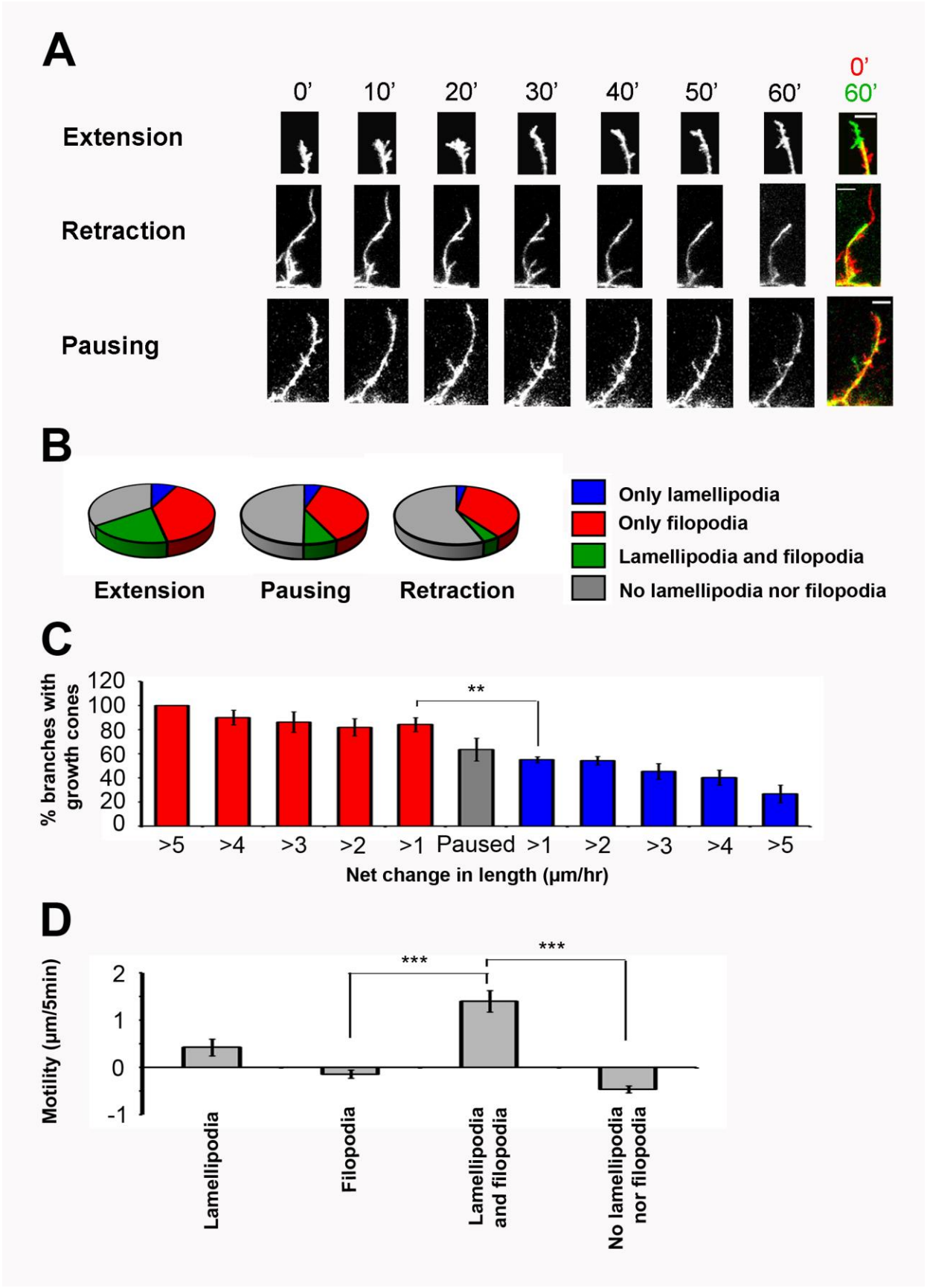
A
0'
10'
20'
30'
40'
50'
60'
0'
60'
Extension
Retraction
Pausing
B
Extension
Pausing
Retraction
Only lamellipodia
Only filopodia
Lamellipodia and filopodia
No lamellipodia nor filopodia
C
% branches with growth cones
120
100
80
60
40
20
0
**
>5
>4
>3
>2
>1
Paused
>1
>2
>3
>4
>5
Net change in length (µm/hr)
D
Motility (µm/5min)
2
1
0
-1
***
***
Lamellipodia
Filopodia
Lamellipodia and filopodia
No lamellipodia nor filopodia

Figure 9. DGC morphology correlates with dendrite growth behavior.
(A) Rapid time-lapse images of the branchtips of an extending dendrite from a Day 5 neuron (top), a retracting branch from a Day 2 neuron (middle), and a paused branch from a Day 4 neuron (bottom), shown at 10 min intervals, followed by an overlay of the first (red) and last (green) time points (right). Scale bar = 5 μm. (B) Percentage of each branch growth behavior, including extension, pausing, and retraction, exhibiting specific branchtip morphologies. (C) Dendrite growth over 1 h binned by the amount of net change in length and plotted with respect to the presence or absence of DGCs on each branch. Red bars denote extension, gray bars denote pausing, and blue bars denote retraction. N = 5 neurons. (D) Average branch motility for four different branchtip structures, including "lamellipodia," "filopodia," both "lamellipodia and filopodia," and "no lamellipodia nor filopodia." N = 5 neurons, n = 85, 621, 146, and 791 behaviors for "lamellipodia," "filopodia," "both lamellipodia and filopodia," and "no lamellipodia nor filopodia," respectively. Error bars denote SEM; *$p < 0.05$; **$p < 0.01$; ***$p < 0.001$.

in vivo is most likely due to technical limitations in conducting rapid time-lapse imaging of dendrite development. Our results demonstrate that since DGCs typically exhibit temporally varying and relatively small lamellipodia compared with axonal growth cones, these structures are often not apparent in single time point images. Also, we find that although DGCs are associated with a higher density of branchtip filopodia over time than at interstitial regions, this difference is most evident from examining multiple time points.

Previous studies have described two major categories of axonal growth cone functions: facilitating process elongation and providing orientation (reviewed in Lowery and Van Vactor, 2009). However, the relevance of DGCs *in vivo*, and specifically to what extent they share functions with their axonal counterparts remain largely unexplored. Previous studies in fixed tissue and in acute slices provide evidence supporting DGC involvement in both dendritic orientation (Furrer et al., 2003; Godenschwege et al., 2002; Komiyama et al., 2007; Polleux et al., 2000) and extension mediated by increased microtubule stabilization (Gascon et al., 2006). Our findings suggest DGCs are essential for dendritic growth *in vivo* in the developing central nervous system since they occur on all actively extending branches, and are rapidly expressed by filopodia transitioning into branches. Axonal growth cone morphology correlates with

extension and pausing behaviors, such that in rapid growth phases, axonal growth cones exhibit streamlined appearance, while during pausing at choice points, they exhibit broad fan-like lamellipodia and filopodia (Bovolenta and Mason, 1987; Mason and Erskine, 2000; Mason and Wang, 1997). In contrast, we find that lamellipodia on DGCs are relatively small and are primarily expressed on extending branches, and to a lesser extent on pausing branches. Dendritic growth occurs by intermittent extension, retraction, and pausing behaviors within minutes, which over a longer period results in slow net rate of elongation of approximately 5 μm/h. In contrast, extending axons advance with a consistent and much higher growth rate of approximately 55 μm/h (Mason and Erskine, 2000). The display of lamellipodia during pausing behavior in axons, yet during both extension and pausing behaviors in dendrites may reflect distinct growth patterns corresponding to requirements for axons to extend across long distances through uniform tissue, while dendrites need to orient across shorter domains as they form and test synapses.

This study is the first to characterize developmental changes in DGC morphology *in vivo*. We find that as neurons mature, DGC morphology shifts to reduce the size and frequency of lamellipodia, and to increase the frequency of branchtip filopodia. Lamellipodia are largest at initial stages of primary branch extension, potentially suggesting a critical decision point to detect external cues for initial orientation of branch growth. Further, lamellipodia have been shown to be necessary for stabilization of new branches in immature neurons (Gascon et al., 2006). At stages when activity-dependent CaMKII-mediated synaptogenesis is not available to promote dendritic stabilization (Wu and Cline, 1998; Zou and Cline, 1999), lamellipodia may play an important role to prevent process retraction. As branches elongate and mature, lamellipodia become smaller and less frequent, and branch endings shift to expression of highly dynamic filopodia. This transition may be due to branches reaching appropriate termination zones within neuropil, and an altered role from orientation to identification of synaptic contacts.

We find that interstitial dendritic filopodia are precursors of longer and more persistent branches. Our results demonstrate there are distinct classes of dendritic filopodia on immature neurons during dendritogenesis that give rise to dendrites or are associated with DGCs. The origin of new dendritic branches has been debated, with lamellipodial splitting reported to be the dominant mechanism of dendritic branching in cultured neurons (Bray, 1973; Scott and Luo, 2001). In contrast, filopodia transitioning to branches has been demonstrated in brain slices and *in vivo* (Dailey and Smith, 1996; Niell et al., 2004). The low rate of filopodial transitions to branches we observed here suggests a high threshold for morphological stabilization, likely induced by synapse formation (Chen et al., 2010; Niell et al., 2004; Vaughn et al., 1988). However, given the relatively small number of branches comprising the mature and stable arbor, each transition event leading to a persistent branch contributes significantly to the computational capabilities of the neuron on which it resides.

This study of developing projection neurons within Stage 47 *Xenopus* tadpoles examines dendritic growth into a functional visual circuit undergoing activity-dependent refinement. Relevance of these finding to other vertebrate systems is supported by observations of dendritic growth cone guidance (Polleux et al., 2000) and activity-dependent dendritogenesis in rodent cortex (Espinosa et al., 2009). Our results employing rapid and long interval time-lapse imaging and comprehensive morphological quantification reveal multiple mechanisms of directed dendritic arbor growth including maturation dependent expression of DGCs potentially providing orientation, and high interstitial filopodial and branch turnover suggesting extensive sampling of local environments for appropriate presynaptic contacts. Together, these growth programs allow external cues and intercellular interactions to contribute to dendritic arbor patterning.

Chapter 3: Dynamic morphometrics: advances in imaging and analysis of rapid dendrite growth

3.1 Introduction

Information processing within single neurons and overall brain connectivity are intimately connected to neuronal morphology. Structure of neuronal dendritic arbors, including length, width and branching patterns, lays the physical foundation for receiving spatially specific presynaptic inputs and governs how these inputs are integrated, thus ultimately dictating neuronal encoding properties. Dendritic morphology is not constant, but undergoes time-varying dynamic changes associated with experience-dependent plasticity and developmental maturation, such that observing dendrites at one point in time often occludes relevant dynamic information (Hossain et al., 2012).

Still images can be used to provide measures of length, number and density of processes, and overall complexity and shape of dendritic arbors. However, a major limitation of single time point or long-interval imaging of dendritic arbor changes is that the growth events producing the imaged morphology remain unknown, and an infinite number of paths are possible. Each distinct potential path would be directed by a unique set of underlying molecular mechanisms. Therefore, in order to create realistic models of dendritogenesis, it is essential to conduct rapid time-lapse imaging with intervals that capture all, or the majority of morphological changes. Such imaging provides accurate measures of parameters including motility (distance moved per time), lifetime, and turnover rate of processes (Hossain et al., 2012). Long-term sampling of rapid time-lapse imaging allows establishing models of how rapid morphological changes, over time, culminate to produce persistent arbor patterning over time.

Observations of dynamic dendrite growth are also essential for characterizing the effects

of experimental manipulations to identify basic molecular mechanisms directing dendritic arbor patterning. Such manipulations include altered gene expression and function, controlled sensory stimuli, and application of exogenous molecules, including growth factors, guidance cues and pharmacological drugs (Chen et al., 2010; Dunfield and Haas, 2009). Critically, all manipulations resulting in changes to larger arbor patterning are the consequence of the accumulation of their effects on small-scale dynamic growth events.

Major errors in models of dendritogenesis have arisen from the reliance on single-time point, or long-interval imaging. For example, static observations of growing dendritic arbors using electromicrographs or Golgi stain (Cano et al., 1989; Mathers, 1977) initially led to the misconception that dendrite growth occurs only by the constant addition and elongation of branches, a theory which was later disproved as time-lapse imaging showed the vacillating nature of dendritogenesis encompassing continuous extension and retraction of processes (Wu et al., 1999). A second example of a major error in field of dendritogenesis has been the failure to recognize dendritic growth cones (DGCs) as major components of dendrites with significant influence on arbor patterning. The limited attention to DGCs is likely due to their lack of large lamellipodia in single time point images, which do not yield large fan-like structures similar to some axonal growth cones. However, the highly dynamic nature of DGC, makes them readily apparent in movies or multiple time point overlays of rapid time-lapse imaging (Hossain et al., 2012). Thus, still images provide limited information, leading to misinterpretations and incorrect models of growth.

3.1.1 Morphometrics

Characterizing dendritic arbor morphology is particularly challenging given their complexity and wide variation in shape, process number, length, orientation, density, and complexity among many other variables. Morphometric analysis of dendrite growth involves

tracing neuronal images to accurately reconstruct neuronal morphology in a manner amenable to detailed analyses (Meijering, 2010). Typically, imaging datasets are acquired from fluorescence imaging using confocal or two-photon microscopy to produce 2D images or 3D image stacks. Neurons may be traced by either manual or automated methods . Depending on the tracing software used, this tracing converts dendritic images into skeletons (connected lines), or volume-filled geometric approximations of dendritic segments (i.e. circles, cylinders).

To accomplish neuronal reconstruction, a small niche of tracing software tools has been developed. These tools are continually evolving to keep pace with improving imaging technologies and enhanced analyses requirements. Due to the complexity of most dendritic arbors, neuronal tracing is often an arduous and time-consuming task, and much effort has been directed toward increasing the speed and ease of tracing. For example, the DIADEM challenge, was established to incentivize accurate and automated 3D neuronal tracing (Ascoli et al., 2009).

3.1.2 Dynamic morphometrics

Dynamic morphometrics refers to the quantification and analysis of changes in dendritic arbor morphology over time. Rapid time-lapse imaging has emerged as a powerful tool to study dynamic dendritic arborization. Time-lapse imaging adds layers of complexities for both experimentation and morphometric software design. Time-lapse data sets can be collected using confocal or two-photon fluorescence imaging to produce 2D or 3D image stacks at multiple time points. The extra temporal dimension when using 3D imaging is results as ‘4D imaging’. Currently, there is limited available software to analyze 4D image data sets (Table 1, Table 2).

3.1.2.1 Experimental advances underlying dynamic morphometrics

Two-photon microscopy for dynamic morphometrics

One of the major advances contributing to 4D imaging of dendritogenesis *in vivo* has been the development of two-photon microscopy. Two-photon microscopy employs a high-energy, pulsed laser that produces sufficiently high concentrations of photons at the objective focal point that individual fluorophore molecules are able to absorb 2 photons simultaneously. The energy of the two photons must sum to the energy levels of single-photon absorbance. This effect has numerous advantages over confocal microscopy. Since the two-photon absorption only occurs at the focal point of the objective fluorophore no out-of-focal point fluorescence occurs. This allows capturing all emitted light and assigning it to the focal point voxel. Without extra-focal place fluorescence, a confocal pinhole is not required, leading to less loss of excitation light. The use of long wavelength, lower energy light has the advantage of producing less thermal damage and deeper penetration into brain tissue than the shorter, higher energy wavelengths required for single-photon absorption. Critically, photo-bleaching and photo-toxicity are reduced overall since out-of-focal point fluorescence does not occur. All together, these features make two-photon microscopy the leading method for attaining high-resolution 4D images of dendritogenesis *in vivo*.

Advances to counter drift during 4D imaging

One of the greatest challenges to capturing high-resolution 4D images of entire dendritic arbor growth is sample drift since living, whole-animal preparations are difficult to stabilize. To counter this problem when conducting 4D imaging of growing tectal neurons in *Xenopus laevis* tadpoles, we use the reversible paralytic pancuronium dibromide to inhibit voluntary muscle

movements. A brief, 5 minute, exposure paralyzes tadpoles for up to 5 hours, after which they recover normal motor function. In addition, we have dedicated significant efforts to the development of *in vivo* imaging chambers to hold tadpoles in a manner that maximized health, while restricting movement. These chambers have a circular opening precisely fitted to the head of stage 47 or 49-50 tadpoles, which hold the head firmly in place. Small agar 'pillows' are placed under the tadpole head, which can be adjusted in size for specific tadpoles. A coverslip is placed on top of the head and held in place with clamps to exert sufficient pressure to prevent movement, but not distorting the tadpole in a manner to produce damage. The tadpole tail extends into a wide-open space, which is continuously perfused with oxygenated tadpole bath solution. The transparency of the albino tadpole allows direct visualization of heart rate and blood flow, which are monitored as sensitive measures of tadpole health. Our design and construction of these chambers were critical for achieving stable *in vivo* 4D images of single brain neuron growth.

A rapid sample rate of full 3D dendritic arbor structure is also a critical component of dynamic morphometrics. In addition to capturing all process additions, subtractions and providing accurate measures of motility (rates of process extension and retraction), rapid imaging prevents gaps in morphological changes which lead to ambiguity of how these changes occurred, or confusion of the identity of processes in successive image stacks. The speed of imaging is limited by the imaging technology. Laser-scanning two-photon microscopy has allowed rapid imaging over long periods by reducing photo-toxicity and fluorophore photo-bleaching. High sensitivity photo-multiplier tube (PMT) photon detectors allow short dwell times on each voxel to sufficiently sample fluorophore concentration. While scan mirror-based laser scanning microscopy is not the fastest technology currently available, we have found that it is sufficient to sample a complete 3D dendritic arbor of a tadpole tectal neuron in less than 5 minutes, an interval we have found to be sufficient to capture all, or the majority of dendritic

process turnover. The combination of stabilization using a reversible paralytic and custom imaging chambers, along with low-damage two-photon rapid time-lapse imaging has allowed the capture of 4D data sets for dynamic morphometrics.

3.1.2.2 Challenges in developing dynamic morphometric software

Time-lapse imaging data sets present particular challenges for neuronal tracing to capture 4D morphological changes over time. The tool used must recognize all morphological components from one time point to the next, taking into account and measuring all changes associated with growth. Additionally, while drift can be mitigated with paralytics and stabilizing chambers, some drift will occur due to uncontrolled movement of microscope components, the tadpole, as well as intrinsic changes in the tissue due to an ever changing cellular environment, including migration, growth and movement of surrounding cells. Neuronal tracing software converts images of dendritic arbors into digitized 3D structures made up of XYZ axis coordinates. Due to drift and internal movement the neuronal traces of successive time points, even with short interval time-lapse imaging, will result in the same morphological feature to have different XYZ coordinates. Since a critical component of dynamic morphometric analyses is the tracking changes of all dendritic processes over time, it is necessary to properly align neuronal traces across successive time points and to accurately assign consistent identity to each process over time. This problem has been the major hurdle blocking development of effective 4D analysis software.

To overcome challenges of misalignment of xyz coordinates across successive time-points, some tracing software programs prompt the user to delineate “landmarks”, or features that are constant over time-points, such as major branch intersections. Landmarks allow the software to calculate and align coordinates for image alignment. One way to accomplish this is

by simply calculating the distance between landmarks in consecutive images and adding or subtracting this distance, based on direction of image shift, to all traced points. While this method is sufficient for addressing drift along one axis, it fails when the image undergoes rotation over time.

Applications of Dynamic Morphometrics

Dynamic morphometrics has revolutionized the study of neuronal morphogenesis by providing detailed quantification of rapid growth dynamics. Recently, dynamic morphometrics has been used to characterize basal brain neuronal dendritogenesis, the effects of altered gene expression, and role of sensory experience on brain neuronal growth. For example, Chen and colleagues have used rapid *in vivo* time-lapse imaging and comprehensive quantification of dendritic growth dynamics to demonstrate the role of synapse formation and cell adhesion molecules in directing dendritic arbor growth (Chen et al., 2010).

During dendritogenesis neurons extend short and thin processes called filopodia, which are typically less than 10 µm in length and 1 µm in width. The cytoskeleton within filopodia is comprised of actin filaments, which confer high extension and retraction motility. Dendritic filopodia exhibit a high rate of turnover due to frequent new extensions from dendritic shafts and complete retraction over periods of minutes. While dendritic filopodia have been associated with dendritic spine formation in some classes of mature neurons (Yoshihara et al., 2009), their role during early dendritogenesis is unclear. Early electron microscopy (EM) studies identified synapses on dendritic filopodia in developing brain (Vaughn, 1989). To understand the morphological effect of synapse formation on filopodia, Niell and colleagues used *in vivo* time-lapse imaging of growing tectal neurons in developing zebrafish to track synapse formation during dendritogenesis (Niell et al., 2004). In this study, a space-filling fluorophore and a second

fluorophore linked to the postsynaptic protein PSD-95 were co-expressed. Stable PSD-95 puncta have been previously used as a marker for potential postsynaptic sites. In 2004, Niell and Smith found that as dendritic arbor grow, the number of PSD-95 puncta increase at the same rate as total dendritic branch length. They found that following extension of a new filopodia, PSD-95 puncta typically occur within 30 minutes. As filopodia extend and retract, retraction is limited to the site of the puncta, and before filopodia completely retract the PSD-95 puncta must first be removed. Both Niell and colleagues and Chen and colleagues (Chen et al., 2010) found that filopodia expressing PSD-95 puncta are most stable than those lacking puncta. All together, these results support a synaptotropic model of dendritogenesis in which synapse formation confers morphological stabilization to nascent dendritic filopodia.

In order to further investigate the molecular mechanisms underlying synaptotropic dendritogenesis, Chen *et al.* tested the role of the cell adhesion molecules Neurexin (NRXN) and Neuroligin (NLGN) in dendritic arbor growth using dynamic morphometrics (Chen et al., 2010). Chen *et al.* conduced rapid time-lapse *in vivo* two-photon imaging of individually labeled growing neurons within the optic tectum of the transparent albino *Xenopus* tectal tadpole. They found that disruption of trans-synaptic interactions between NRXN and NLGN decreases filopodial lifetime and density and increases filopodial motility and elimination rate. Conversely, overexpression of NLGN1 leads to hyperstabilization of dendritic filopodia, leading to increased filopodial density and lifetime and decreased elimination rate. Furthermore, these stabilization effects required NMDA receptor activity, suggesting downstream activity-dependent mechanisms. Remarkably, they found that enhancing trans-synaptic NRXN-NLGN interactions, but blocking NLGN-mediated postsynaptic synapse formation partially increased lifetimes without altering motility. These results demonstrate the sensitivity of dynamic morphometrics to discriminate growth effects of cell adhesion junction formation, which induces increased lifetimes without decreasing motility, from synapse formation, which induces longer lifetimes and

decreases motility.

Dynamic morphometrics has also been applied to characterizing the effects of environmental experience on brain neuronal structural development (Chen et al., 2012; Chen et al., 2010). Chen and colleagues have demonstrated that a visual stimulation protocol that induces functional plasticity of tectal neurons in the tadpole optic tectum (Dunfield and Haas, 2009) also impact structural growth. Using *in vivo* two-photon calcium imaging, the Haas Lab has characterized short, 25 minute, visual stimulation paradigms that induce lasting changes in the amplitude of visual evoked responses. High-frequency OFF visual stimuli presented in a spaced format (termed “spaced-training”) induces long-lasting potentiation of tectal firing to brief OFF stimuli. In contrast, presenting an invariant ON stimulation for 25 minutes (“invariant” training”), induces long-lasting depression of firing in response to OFF pulses. Chen and colleagues have demonstrated that in addition to functional plasticity, spaced training also leads to morphological plasticity of dendritic filopodia, which can be observed as increased morphological stability, including increased lifetime and decreased motility of filopodia that emerge within the hour prior to the training protocol (Chen et al., 2012). Invariant training leads to destabilization of filopodia that emerges prior to the training protocol. Furthermore, Chen et al. find that activity-dependent changes in synapses on filopodia likely underlie the observed experience-driven structural plasticity of dendritic filopodia. These applications of dynamic morphometrics powerfully demonstrate its ability to identify fundamental mechanisms directing dendritic arbor growth.

While a few studies have applied dynamic morphometrics to dendritic filopodia and dendritic spines (Trachtenberg et al., 2002), its application to the study of the dynamic behavior of entire dendritic arbors in 4D is rare (Hossain et al., 2012; Libersat and Duch, 2002). Full arbor analyses allow study of growth behavior with respect to location on dendritic arbors. For example, two distinct populations of filopodia are found on developing dendrites: ‘interstitial

filopodia', which emerge from dendritic shafts, and 'branchtip filopodia', which are localized within 5 to 10 microns from the ends of dendritic branches (Portera-Cailliau et al., 2003). While interstitial filopodia in mature neurons give rise to dendritic spines, those in developing neurons participate in synapse formation and are precursors of longer branches (Hossain et al., 2012; Niell et al., 2004; Ziv and Smith, 1996). Branchtip filopodia are less stable than interstitial filopodia, and whereas interstitial filopodial dynamics change in response to pharmacological blockers of glutamate receptor and calcium channels, branchtip filopodial dynamics does not (Hossain et al., 2012; Portera-Cailliau et al., 2003). The role of branchtip filopodia in developing neurons has not been elucidated, although it is possible that like in axonal growth cones, they participate in dendritic guidance. The study of entire dendritic arbors *in vivo* in 4D is also critical for studies of how arbor patterns emerge during maturation. For example, *in situ* observation of the dendritic arbor of an identified motorneuron (MN5) in *Manduca sexta* (tobacco hornworm), followed by 3D reconstruction and analysis using a commercial software (Neurolucida), has revealed how dendritic arbor complexity changes as this insect proceeds from larval to pupal, and adult stages (Libersat and Duch, 2002). Acquisition of images of entire arbors of developing dendrites *in vivo,* however, is challenging particularly in mammals and vertebrates given current limitations to imaging brain *in utero* and early postnatal stages. *Xenopus* tadpoles and zebrafish larvae, on the other hand, offer transparent vertebrate model systems in which developing dendrites can be observed without any surgical manipulations (Chen et al., 2012; Haas et al., 2002; Haas et al., 2001; Hossain et al., 2012; Niell et al., 2004; Sin et al., 2002; Wu et al., 1999). For this reason, I have directed my dynamic morphometric analyses of dendritogenesis towards *in vivo* studies of brain neurons in the *Xenopus laevis* tadpole optic tectum.

While great recent advances in imaging, including *in vivo* two-photon rapid time-lapse imaging provides high-resolution 4D images of growth within the intact and awake developing brain, software to quantify and analyze these 4D data sets have lagged. The absence of

software to quickly analyze 3D morphological changes across short intervals over long periods has created a bottleneck at the level of dendritic arbor morphological data analysis. Although the development of a few software programs has made some progress to rectify this issue, the problem remains far from resolved (Longair et al., 2011; Meijering et al., 2004; Myatt et al., 2012; Peng et al., 2010). The major goals of these tools are to allow efficient and accurate neuronal reconstruction in an easy-to-use environment, to provide detailed and comprehensive quantitative analysis, and to allow convenient customization to keep up with the need for novel analyses. Commercial image analysis software is available, but suffers from prohibitively high cost, poor modifiability to changing research conditions and questions due to proprietary source codes. Open-source software present an attractive alternative; however, many of these assume that given the availability of the source codes, users will be able to write the necessary analysis tools, without accounting for the limited programming experience of most biologists. Here, we have developed a novel MATLAB-based software, called *Dynamo* to analyze dynamic dendrite growth, which is both easy to use and conducive to incorporating novel user-defined analysis tools.

3.1.3 Neuronal reconstruction methods

Neuronal reconstruction methods are broadly classified into four categories, including “manual”, “semi-manual”, “semi-automatic”, and “fully-automatic”, based on the amount of required user input (Myatt et al., 2012). Manual reconstruction involves using prisms to overlay the microscopic image onto a piece of paper and tracing the neuron by hand (i.e. camera lucida drawings). Semi-manual reconstruction refers to using a computer program to manually trace neuronal segments. In semi-automatic reconstruction, the user selects branch source and terminations, allowing the program to fill in the branch paths. Finally, in fully automatic reconstruction, essentially the entire neuron is reconstructed by the program.

Although in theory, automatic 3D reconstruction of neurons appears feasible, in practice, such systems are error-prone and require care and time-consuming proofreading, erasing the time saved from more manual approaches. While “semi-manual” reconstructions, in which the user manually adds individual components of the neuron using a computer program (Myatt et al., 2012; Peng et al., 2011), requires added time and continuous human-based decision making, they yield lower error rates compared to automated approaches. For these reasons, while the scientific community eagerly awaits an accurate automatic neuronal reconstruction program, most tracings are still conducted semi-manually. Our new software Dynamo currently utilizes a semi-manual tracing algorithm, which requires the user to trace the complete neuron. The great strength of Dynamo comes from its rapid analysis of multiple time point data sets. For 4D data, Dynamo employs rapid 3D alignment and automated fitting of the initial time point reconstruction to subsequent time point image stacks.

3.1.4 Comparison of neuronal reconstruction software

Neuronal reconstruction software are either commercially available, requiring a license to be purchased, or open-source, which are freely available online. A list of common neuronal reconstruction software, both open-source and commercial, and their capabilities and drawbacks, are provided in Table 1 and Table 2. As shown in Table 1, most available image analysis software do not have 3D time-lapse capabilities. Also, with the exception of commonly used Sholl analysis, most have limited post-rendering analytic tools.

3.2 Dynamo

In order to address the need for rapid and accurate analysis of 4D image datasets of dendritogenesis, we have developed novel software called *Dynamo*. Design and development

		Author	Reference	Platform	Automation
OPEN-SOURCE	**Dynamo**	Sharmin Hossain; Kasper Podgorski; Steffen Kaiser	This thesis. http://haaslab.github.io/dynamo/installation.html.	Cross platform	Semi-manual
	Migor	Jamie Boyd; Shay Neufeld; Sharmin Hossain; Sesath Hewapathirane	Not published.	Cross platform	Semi-manual
	Vaa3D-Neuron	Hanchuan Peng	(1) Peng et al. (2010) Nature Biotechnology. (2) Peng et al. (2010) Bioinformatics.	Cross platform	Fully automatic (version 2.0)
	NeuronJ (ImageJ plugin)	Erik Meijering	Meijering et al. (2004). Cytometry Part A.	Cross platform	Semi-automatic
	Fiji-Simple neurite tracer (ImageJ plugin)	Mark Longair	Longair et al. (2011). Bioinformatics.	Cross platform	Semi-automatic
	Neuron_Studio	Alfredo Rodriguez	Rodriguez et al. (2003). Methods.	Cross platform	Semi-manual, Semi-automatic, Fully automatic
	Neuromantic	Darren R. Myatt	Myatt et al. Front Neuroinform. (2012).	Cross platform	Semi-manual/Semi-automatic
	Neuron_Morpho (ImageJ plugin)	Kerry M. Brown	Brown et al. Neuroinformatics. (2005)	Cross platform	Semi-manual
	FARSIGHT (Open-curve snake tracing system)	Yu Wang; Arunachalam Narayanaswamy; Chia-Ling Tsai; Badrinath Roysam	Wang et al. (2011). Neuroinformatics.	Cross platform	Fully automatic
COMMERCIAL	**Neurolucida**	MBF Bioscience, Vermont	www.mbfbioscience.com/neurolucida	Windows 7 or Windows 8	Semi-manual, but can be fully automatic with "AutoNeuron" addon.
	Amira (Skeletonization option)	Visualization sciences group	http://www.vsg3d.com/amira/skeletonization	Cross platform	Semi-automatic
	Imaris-Filament Tracer (formerly NeuronTracer)	Andor Technology, Belfast, Northern Ireland	www.bitplane.com	Windows and Mac OS	Semi-manual, Semi-automatic-Fully-automatic
	Meta-Morph (Neurite outgrowth application module)	Molecular Devices, Sunnydale, CA	http://www.moleculardevices.com/systems/metamorph-research-imaging/metamorph-microscopy-automation-and-image-analysis-software	Windows XP, Windows 7, Windows 8	Semi-manual

Table 1. Availability of open-source and commercial neuronal reconstruction tools.

		Spatial information over time	Advanced dynamic morphometrics	Custom analysis	Development environment	2D/3D/time-lapse
OPEN-SOURCE	**Dynamo**	Yes	Yes	Yes	Matlab (open-source code; available online)	All
	Migor	No	No	Yes	Igor	All
	Vaa3D-Neuron	No	No	Yes	Qt and C++	2D/3D
	NeuronJ (ImageJ plugin)	No	No	Yes	Java and ImageJ	2D only
	Fiji-Simple neurite tracer (ImageJ plugin)	No	No	Yes	Java and ImageJ	2D/3D
	Neuron_Studio	No	No	Yes	Windows	2D/3D
	Neuromantic	No	No	Yes	Borland C++ builder	2D/3D
	Neuron_Morpho (ImageJ plugin)	No	No	Yes	Java and ImageJ	3D
	FARSIGHT (Open-curve snake tracing system)	No	No	Yes		3D
COMMERCIAL	**Neurolucida**	Sholl, angular information	No	No	Proprietary	2D/3D; No time-lapse
	Amira (Skeletonization option)	Sholl only	No	Yes	Extensible via C++ compilers.	2D/3D
	Imaris(Filament tracer)	Yes	No	Yes	Extensible via MATLAB based Imarris XTensions	All
	Meta-Morph (Neurite outgrowth application module)	No	No	No	Proprietary	2D/3D

Table 2. Features of open-source and commercial neuronal reconstruction tools.

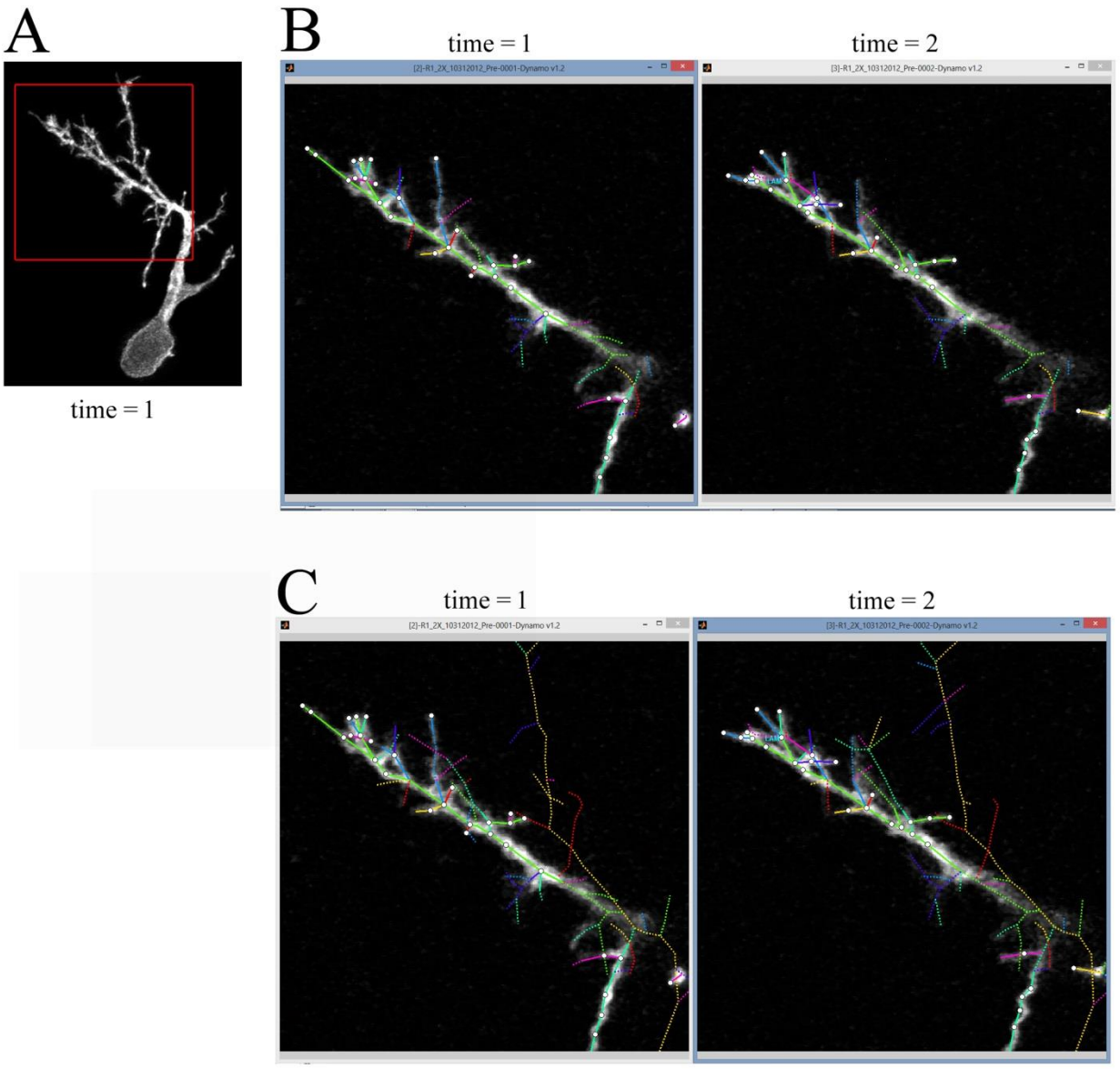

Figure 10. Dynamo screenshot
(A) Image of a tectal neuron. (B) Two different time-points of the inset of the neuron in A, on top of which the Dynamo tracing of the neuron is superimposed. In these two images, only the tracing on a single plane is shown. (C) The same neuronal images in B, on top of which neuronal tracing of all z-planes are superimposed.

of Dynamo comprised a significant part of my Ph.D. thesis project. Dynamo is a powerful tool for dynamic morphometric analysis, which makes significant contribution to the field of dendritogenesis. This tool is specifically designed to allow rapid tracing of large numbers of time-lapse 3D image stacks, and to handle challenges with drift and neuronal rotation through use of a robust landmarking tool by associating relationships between morphological features, such as distances between branch points, rather than relying solely on XYZ coordinates. This provides recognition and tracking of branch features across time points even if the coordinates do not match precisely.

To use Dynamo, 4D data sets (multiple 3D image stacks or successive time points) are opened in order and aligned based on landmarked demarcated by the user. Next, the neuron is traced manually in 3D, usually starting from where the primary dendrite joins the soma. Keyboard shortcuts and neuron tracing commands are described in the Appendix (Table 4). Once the neuron tracing is complete, the user has access to several dynamic morphometrics analyses using built-in functions in Dynamo; in addition, custom functions can be written and saved in the Dynamo analysis toolbox.

3.2.1 Morphometric analysis using Dynamo

Dynamo comes preloaded with basic dendrite analysis as well as advanced “dynamic morphometrics” tools designed specifically for analyzing the dynamics of neuronal processes using data acquired from rapid time-lapse imaging. Traditional dendritic analysis includes calculation of “total dendritic branch length”, filopodial density, filopodial/branch turnover, filopodial/branch length, filopodial/branch lifetime, Sholl analysis (a quantitative measure of branch length or branch intersections at different radial distances from the soma), and orientation of primary dendrites (specific to dendrite guidance studies). Recently, a few studies

have employed a much more rigorous analysis of detailed morphometric analysis by classifying dendritic filopodia into subpopulations based on either their time of appearance or their location on branches to observe, for example, the motility and lifetime of pre-existing versus newly emerged filopodia or the behavior of branchtip versus interstitial filopodia (Chen et al., 2010; Hossain et al., 2012).These studies demonstrate the practical power of these novel analyses, since many of the conclusions, such as unraveling the role of cell-adhesion molecules in different stages of synapse formation, were obscured when distinct populations are analyzed together, which is common practice (Chen et al., 2010). Unfortunately, most current dendritic tracing and analysis software do not include these analyses, resulting in cumbersome strategies to separate data during the analysis stage.

Dynamo possesses a wide range of built-in analytical tools including standard dendritic analysis functions, but also “dynamic morphometrics” tools for 4D data sets and tools for measuring dynamic changes in dendritic orientation, motility and lifetime at different distances from the soma (similar to Sholl for length and branch intersection analysis), and motility, lifetime, and turnover of interstitial versus branchtip filopodia. All of these functions are accessible by using the Dynamo Analysis GUI, a graphical user interface that analyzes dendritic tracings generated by methods described in the previous section.

Highlights of novel analyses incorporated in Dynamo:

1. Differentiate between filopodia and branch based on morphological parameters (i.e. length, presence of lamellipodia, secondary-branching), and use this criteria to analyze dynamic behaviors. The default definition of a branch in Dynamo is a process that meets at least one of the following criteria: >10 µm in length, has lamellipodia at the branchtip, or has secondary branching. All other processes are defined as filopodia. This definition was formed based on observations of dendritic process behavior in *Xenopus* tectal

neurons. However, neuronal branching patterns can vary based on neuronal type, and the user may want to change these parameters based on their individual use cases.

2. Differentiate between “branchtip” and “interstitial” filopodia based on location of filopodia from the dendritic branchtip. This analysis has been effective in determining differential filopodial response to neuronal activity as well as differential filopodial behavior based on neuronal maturation (Hossain et al., 2012).
3. Differentiate filopodial behavior based on when the emerged (Chen et al., 2010)
4. Determine whether filopodia or branch behavior change based on process location (radial or angular distance from the soma) or process orientation (vector orientation with respect to a reference branch such as the primary dendrite). Branch behavior with respect to process orientation has been used to analyze branch behavior with response to various guidance cues in chapter 4 of this thesis (Figure 16).

3.2.2 User-defined functions

While Dynamo comes pre-configured with advanced dynamic morphometric capabilities for rapid time-lapse imaging of motile dendritic structures such as immature filopodia, growth cones, and rapidly growing branches, some users may wish to add custom functions. To incorporate user-defined functions, it is useful to understand how the neuronal tracing datasets are stored in Dynamo and how to access them. It is important to note that while the use of built-in functions does not require prior programming knowledge, in order to write new functions in Dynamo or to modify previously built-in functions, the user must be somewhat familiar with basic MATLAB programming. For novices, sufficient level of programming may be achieved through freely available online MATLAB tutorials as well as looking through the Dynamo source codes for built-in functions to serve as templates. Also, some analyses require understanding of basic linear algebra. For example, neuronal tracings are essentially an accumulation of points in 3D

space. So, to calculate distances or orientations between points in 3D requires vector calculation. All analysis functions utilize the saved neuronal tracing files, called ‘savedata’ files, which contain information on each of the points on the neuronal tracing (Figure 19). A description of this file and its components, and examples of how to use it to write user-defined functions are proved in the Appendix section of this dissertation.

3.3 Dynamo project workflow

Project design in the development of Dynamo involved two major aspects, including implementation of ‘Neuron tracing’ and ‘assembly of Analysis’ features (Figure 11). As shown in Figure 11, for each of these two parts, the project plan involved program design and specification, user-interface design, algorithm design, and coding, in this order. After features were coded, they were sent through a process of validation via significant testing by different users. At this stage, if errors occurred, these steps were repeated until they were resolved. Finally features were documented for ease of use.

3.4 Discussion

High resolution *in vivo* 3D imaging of dendritic arbor morphology to follow structural changes over time combined with digitized computer-assisted rendering allows accurate quantification and analysis of growth. Dynamo provides a novel tool that can be utilized to generate accurate neuronal reconstructions, with particular emphasis on reconstructing highly dynamic neurons imaged with a rapid time-lapse protocol. In contrast to most other open-source software, which assume a certain degree of programming ability of the user to use dynamic morphometrics, Dynamo comes preloaded with both traditional as well as novel dynamic morphometric analyses, many of which were successfully utilized to study dendrite growth in

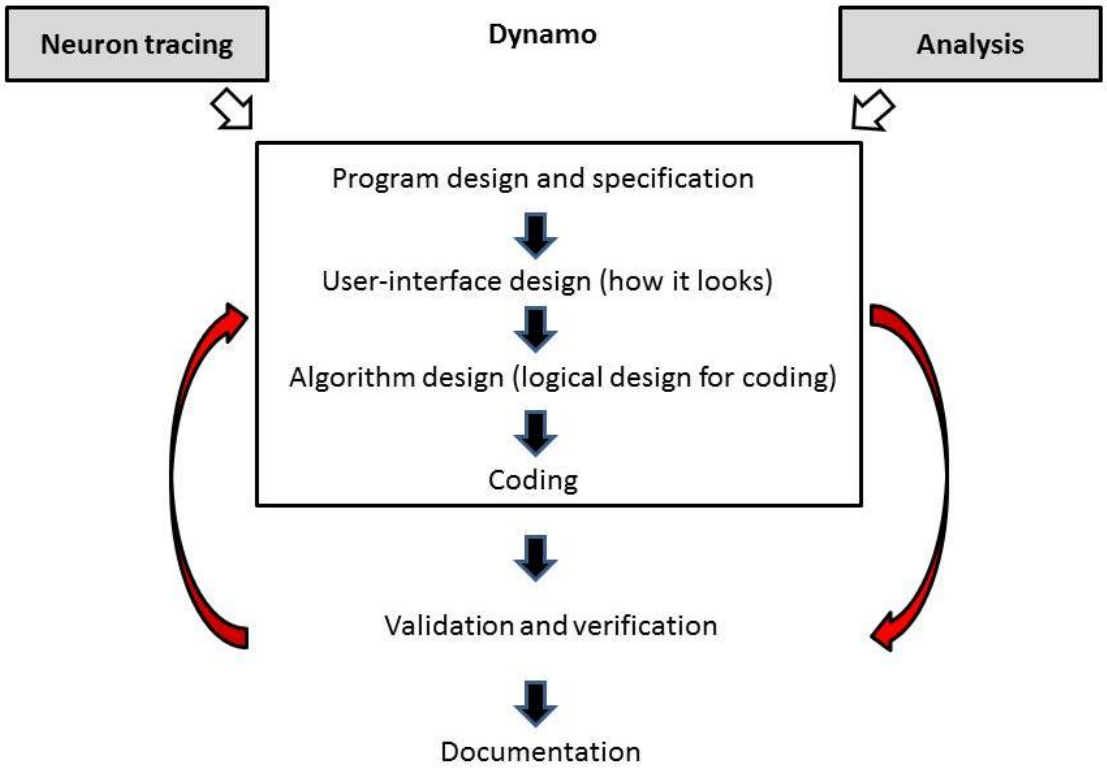

Figure 11. Dynamo project workflow.
Black arrows denote sequence of steps followed in the development of Dynamo. Red arrows indicate that the 4 steps within the box can recur depending on results from 'validation/verification'.

previous studies (Chen et al., 2010; Hewapathirane et al., 2008; Hossain et al., 2012; Liu et al., 2009). This analysis package is, to my knowledge, the most extensive set of tools available for 4D data analysis. In addition to these tools, Dynamo also has to option to incorporate user-defined analysis functions. Although writing custom analysis does assume basic MATLAB programming experience, for anyone willing to put in the effort, MATLAB environment is one of the most robust environments for self-learning, with extensive online support and existing code to use as template.

Reconstructing dynamic neuronal images from time-lapse imaging, particularly of 3D images of neurons, presents unique challenges since it requires tracking each process over time despite its changing morphology. The landmarking feature of Dynamo allows selecting reference points in 3D, allowing the program to use these points and interpolate the identity of all other points on the neuron. Thus, this tool can determine neuronal morphological changes even in the face of minor shifting or rotation of the neuron (i.e. due to image drifting, rotation, or biological movement such as gradual neuronal migration).

Understanding how the dendritic framework is created provides a critical first step toward determining how neural networks generate higher brain functions, identifying origins of neurodevelopmental disorders when these mechanisms go awry, and for reverse engineering the wiring and function of the developing brain (Peng et al., 2010). To more fully utilize the power of neuronal morphometric data, recently, a repository of digitally reconstructed neurons has been initiated (i.e. NeuroMorpho.org), which provides detailed morphological characterization of neurons from various species, brain regions, and pathological conditions, with the goal to ultimately provide a rich reference for neuronal morphology to aid in understanding neuronal circuitry (Ascoli et al., 2007).

Due to the high cost of commercial neuronal reconstruction software, increasing availability of usable open-source software, and the convenience of an increasing online community contributing to novel analytical tools, a growing number of labs are shifting from using commercial programs to open-source tools. Currently, the evolution of these tools is largely focused on automating neuronal tracing problem, with minimal emphasis on incorporating easy to use advance analysis tools. This is largely because programmers often overestimate the programming capabilities of biologists, assuming that analyses can be easily incorporated as needed. In Dynamo, we have made an effort to place focus on analysis and overall usability as well as on neuronal tracing, with built-in analysis tools that are more

advanced than most open-source, as well as most commercially available, software that are currently available.

Chapter 4: Slit/Robo mediates directed dendritogenesis in tectal neurons

4.1 Introduction

To form appropriate synaptic connections, spatial proximity of dendrites and their correct target axons are of critical importance. Evidence from numerous experimental systems indicates that dendrites orient toward brain regions containing their presynaptic partners (Niell et al., 2004; Vaughn et al., 1988). Thus far, two mechanisms of dendritic targeting have been identified: synaptotropic dendrite growth and guidance cue mediated dendrite targeting. Synaptotropic dendrite growth involves synapse formation guiding dendritogenesis. In this process, synapse formation leads to selective stabilization of dendrites or retraction of branches from areas of synaptic destabilization, thus leading dendrites to preferentially arborize in brain regions containing their presynaptic partners. Synaptotropic dendrite growth has been observed in zebrafish and *Xenopus laevis* tectal neurons (Liu et al., 2009; Niell et al., 2004). Alternatively, dendrites may extend in the appropriate direction by sensing and responding to guidance cues present in the extracellular environment. While guidance cue molecules were initially of interest due to their participation in guiding axons, they have recently been shown to guide and sculpt dendritic arbors as well (Furrer et al., 2003; Furrer et al., 2007; Kayser et al., 2008; Polleux et al., 2000; Xiao et al., 2011). Experiments in this chapter explore potential role of guidance cues in orienting dendrites of *Xenopus* tectal neurons.

In *Xenopus laevis* tectum, neurogenesis occurs within a proliferative zone at the caudomedial region lining the ventricle (Lazar, 1973). The continuous addition of new neurons at the caudomedial proliferative zone shifts more mature cells rostrolaterally, creating a gradient of neuronal maturational along to caudomedial-to-rostrolateral axis. Tectal neurons project their dendrites laterally into the tectal neuropil, which is the termination zone of RGC axons. The universal orientation of tectal neuron dendritic arbors toward lateral neuropil suggests an active

mechanism directing dendritogenesis in the *Xenopus* tectum. However, to date, evidence for oriented dendritogenesis of tectal neurons has not been established.

To determine whether long-term dendritogenesis in tectal neurons involves oriented growth toward the neuropil, single-cell electroporation was used to label immature tectal neurons located in the caudal tectum, and two-photon microscopy was used to obtain images at 24h intervals over 5 days. This imaging protocol captures the entire process of dendritogenesis from initial extension of primary branches, elaboration of higher order branches, and maturation to a stable arbor structure. Analysis of long-term growth behavior is required to determine how arbor orientation is established. Rapid time-lapse imaging is required to determine how fast dynamic growth events culminate to produce long-term orientation. To investigate acute effects of guidance cue molecules on short-term changes in oriented dendritogenesis, tectal neurons were imaged at 5 min intervals over 1hr to establish a morphological baseline, followed by tectal infusion of candidate guidance cue molecules and subsequent imaging of the same neuron at 5 min intervals over 2 hours. Infusion of potential cues is expected to saturate any local gradients of these proteins to disrupt their use in orientation.

The objectives of Chapter 4 are:

1. To determine whether caudally located tectal neurons display anterior bias in short- and long-term dendritic arbor growth to reach the neuropil.
2. If anterior arbor bias is seen, to test candidate guidance cues for acute effects on dynamic morphometric parameters of dendritic growth.
3. If a candidate guidance cue displays acute dendritic effects, to determine whether its receptor mediates long-term dendrite growth.

4.2 Materials and methods

Fluorescent labeling of neurons using single-cell electroporation and rapid interval *in vivo* two-photon imaging were conducted as described in Chapter 2. In the tadpole tectum, there is a maturational gradient of neurons with immature neurons located in the caudomedial region and more mature neurons located in the anterolateral regions. To selectively label immature neurons, electroporation was targeted to the caudomedial tectum. In *Xenopus laevis*, the tectum is structured such that medial tectum is higher (more dorsal) compared to lateral regions. As such, “medial” and “dorsal” are often used interchangeably, whereas “lateral” and “ventral” refer to the same orientation.

4.2.1 Reagents

Recombinant proteins used for the following experiments are as follows: ephrin-A1-Fc (R&D systems), ephrin-B1-Fc (R&D systems), slit-2-Fc (R&D systems), and anti IgG-Fc antibody (R&D systems). The dominant-negative Robo3 construct (dnxRobo3) was a generous gift from Dr. Sarah McFarlane. This construct codes for *Xenopus laevis* Robo3, but lacks the c-terminal domain, and has been previously used as a dominant-negative Robo3 in *Xenopus* (Hocking et al., 2010). Recombinant proteins for injection was prepared in phosphate buffered saline (PBS), consisting of 137 mM NaCl, 2.7 mM KCl, 10mM Na2HPO4, and 1.8 mM KH2PO4 with pH adjusted to 7.4. Recombinant protein dilutions were prepared as follows: ephrin-A1-Fc (5µg/µL), ephrin-B1-Fc (500ng/µL), and slit-2-Fc (80ng/µL) (Lim et al., 2008a; Mambetisaeva et al., 2005; Tanaka et al., 2004). Previous experiments have shown that ephrin-B clustering is required for EphB receptor activation (Lim et al., 2008a). Thus, prior to application, ephrin-B1-Fc was pre-clustered with Fc conjugated anti-IgG antibody at 1:2 ratio of antibody to ligand by incubating together in sterile PBS at 4 degree Celsius for 1 hour. PBS alone was used as vehicle control for tectal injection. Alexa 594 (Invitrogen, USA) was used at 0.6 mM

concentration for tectal injection. For co-electrporation of dnxRobo3 constructs, dnxRobo3 plasmids were mixed with plasmid encoding fGFP (pfGFP) at 1:10 dilution (2µg/µL total DNA concentration). This low dnxRobo3 concentration compared to pfGFP was used because at 1:1 ratio of dnxRobo3 to pfGFP, the number of electroporated neurons and neuron survival over 5 days was dramatically reduced.

4.2.2 Tectal injection

Tectal injection of *Xenopus laevis* tadpoles was described previously (Liu et al., 2009). Briefly, for this protocol, the tadpole was removed from the imaging chamber and anesthetized in 0.02% 3-aminobenzoic acid ethyl ester (MS-222). A glass electrode (tip diameter of ~0.6 µm) was filled with the recombinant guidance cue solution, as described in the reagents section, or with PBS. A sharp needle was used to create a small incision on the skin adjacent to the lateral tectum, and the micropipette was gently inserted into the lateral tectum through this incision. The micropipette was attached to a Picospritzer (General Valve) and ~200 nL of the solution was pressure injected into the optic tectum. Tectal injection of Alexa 594 to visualize neuroanatomy was performed in the same manner as with recombinant proteins.

4.2.3 Exclusion criteria

Previous experiments have determined that among tectal neurons, projection neurons, which project their axons out of the tectum, demonstrate different dendritic growth patterns than interneurons, whose axons innervate within the tectum (Wu and Cline, 2003; Wu et al., 1999). Therefore, for this study, similar to Chapter 2, we chose to include only projection neurons. In addition, previous work has shown that some guidance cues, such as sema3A, affect basal dendrites as compared to apical dendrites in a contrasting manner (Polleux et al., 2000). In

tectal neurons, apical dendrites typically branch off from a single major primary dendrite, whereas basal dendrites project from the soma rather than from the major primary dendrite. In tectal neurons, apical dendrites are more numerous than basal dendrites, and generally apical dendrites project toward the neuropil. Therefore, in this study, all analyses were restricted to apical dendrites.

4.2.4 Morphometric analysis using Dynamo

The complete dendritic arbor morphology of each neuron at all time-points was manually traced and analyzed using Dynamo (as described in Chapter 3).

Angular and radial Sholl Diagram

This analysis was used as a starting point for analysis and visualization of neurons that were imaged at daily intervals. Angular Sholl diagram consists of an overlay of the neuron on top of a graph consisting of angular bins or concentric radial bins (Figure 13B). Each bin is shaded according to the net length of the dendritic arbor that falls within each bin, thus allowing visualization of how dendritic arbor length is distributed in terms of both angular orientation as well as radial distance with respect to the neuronal cell body.

Calculation of normalized net dendritic vector angle and length

To determine the net dendritic orientation for each neuron, each dendritic process was converted into a dendritic vector by translating all process origins onto a common point and calculating the vector between origin and endpoint for each dendrite, and then calculating the net vector angle for each neuron. Net vector length of dendrites was calculated by taking the vector sum of all dendritic vectors of the neuron. Net vector length was normalized to total dendritic branch length for each neuron to obtain a normalized net vector length for that neuron.

Since a dendrite that has a winding path would have the same vector length as one that takes a direct route to an end point, normalization to total dendritic branch length provides a measure of the proportion of total dendritic branch length for each neuron that contributes to oriented dendrite growth.

Calculation of normalized filopodial motility, length, lifetime, and turnover

Filopodial length is the distance from each filopodial intersection on the branch shaft to the filopodial tip. Filopodial motility was calculated by taking the absolute value of individual filopodial motility (filopodial length change/5 min). Filopodial lifetime was determined by tracking the presence of each filopodia at 5 min time-points over 1h. Filopodial turnover includes filopodial additions and retractions, and was calculated as the number of filopodia added/subtracted per μm of dendritic branch length for each 5 min interval over 1h. To compensate for between neuron variability, all of these parameters (motility, length, lifetime, and turnover) were normalized to the average value of the same parameter in the same neuron prior to treatment ("pre" period).

Calculation of normalized branch motility and lifetime

Branch motility was calculated by taking the absolute value of individual branch motility (branch length change/5 min). Branch lifetime was determined by tracking the presence of each branch over 1h. Both of these parameters normalized to the average prior to treatment for each neuron.

Calculation of normalized branch motility for branches with rostral and caudal orientation

Tectal neurons typically have a single primary dendrite extending from the soma in a lateral direction toward the neuropil. The orientation of the initial segment of this branch up to

the first major branch intersection was designated the ‘root branch’ and was used as a reference for the orientation of all other dendritic processes. ‘Rostral branches’ were defined as branches whose vector orientation lies within 0 to 135 degrees in the rostral direction with respect to the primary root branch angle; ‘caudal branches’ similarly refers to branches whose vector is oriented at 0 to -135 degrees in the caudal direction with respect to the root branch angle (Figure 12). Rostral and caudal directions are in reference to the anatomy of the tectum. Branches with motility values <0.5µm was assigned a value of 0.

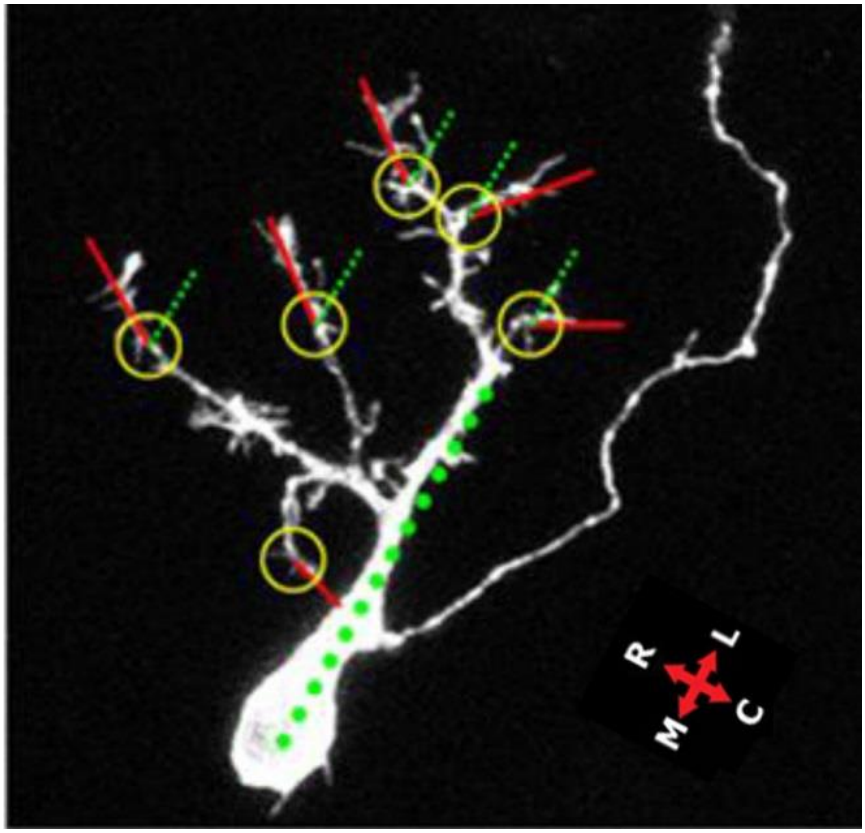

Figure 12. Analysis of vectoral orientation of dendritic branches.
Vectoral orientation of each dendritic branch was measured with respect to the neuron’s internal axis determined by the orientation of the primary dendritic shaft (denoted by green dotted line). Small red lines indicate the vectoral orientation of individual dendritic branches. Orientation is depicted by crossed red arrows and as follow: R (rostral), C (caudal), A (rostral), and P (caudal).

Statistics

Normalized branch motility between control and guidance cue effects was compared at two levels, between three time-points (pre-treatment, 1h post-treatment, and 2h post-treatment) and four groups (Control, slit-2 or ephrin-A1, or ephrin-B1) using two-way ANOVA followed by Dunn-Sidak *post hoc* test using MATLAB.

4.3 Results

4.3.1 Tectal neuronal dendrites grow in a biased orientation toward the neuropil

In vivo imaging reveals that tectal neurons in the caudomedial tectum project dendrites laterally toward the neuropil (Figure 13). Using rapid time-lapse imaging of growth dynamics and Dynamo analyses, dendritic vector lengths and orientations of all individual dendritic processes with respect to the orientation of the primary dendrite of each neuron were calculated for days 1, 3 and 5. To understand orientation of dendrites with respect to tectal anatomy, following completion of 5 day imaging, the tectum was visualized by filling the entire tectum with Alexa-594 as a contrast agent to demarcate cell body and neuropil domains (Figure 13D). As shown in Figure 13, for this representative neuron, the primary dendrite initially begins to arborize in a mediolateral orientation, but over days 3 and 5, is reoriented toward the neuropil. On day 5, a large portion of dendritic arbors are localized to the neuropil. The primary dendrite projects in a mediolateral orientation (Figure 13), such that either the primary branch has to be rerouted rostrally (as in Figure 13) or secondary branches have to project rostrally with respect to the primary dendrite (Figure 17, control neuron) to reach the neuropil. Vector addition of all dendritic vectors (excluding basal dendrites) was used to calculate the net dendritic length and angle for each neuron from a common origin (Figure 13C). Surprisingly, whereas on day 1, the net dendritic vector of a caudomedially located tectal neuron projects randomly with respect to the

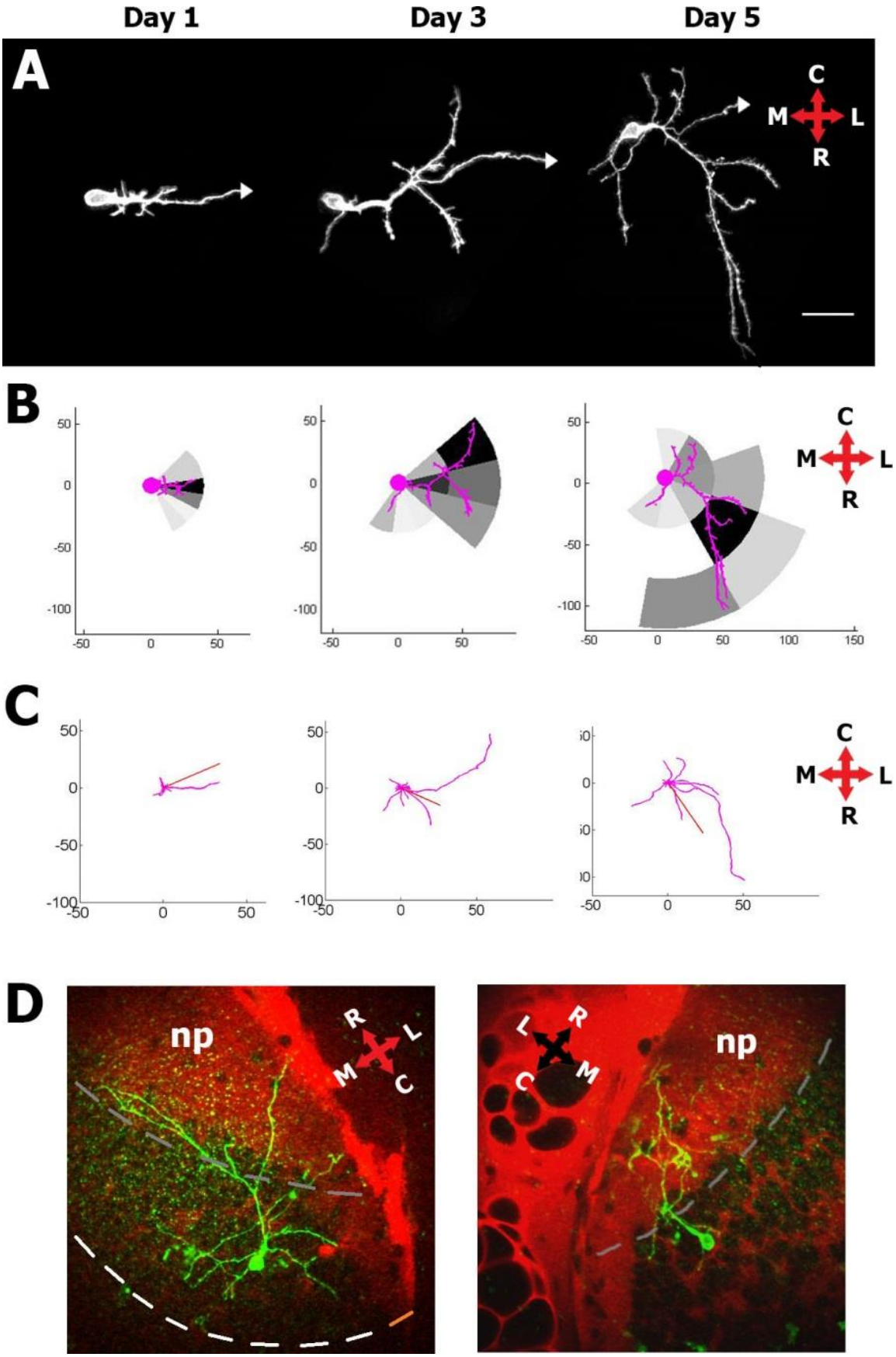
Day 1
Day 3
Day 5
A
C
M
L
R
B
C
M
L
R
C
C
M
L
R
D
np
R
L
M
C
L
R
C
M
np

Figure 13. Dendritic orientation changes over long-term dendritogenesis
(A) Images of a projection neuron located in the caudal tectum at 48h intervals over 5 days. Branches tipped by an arrowhead depict axons. Scale bar = 20 μm. (B) Angular Sholl diagram of the neuron in A (excluding basal dendrites). Greyscale intensity depicts dendritic branch length present in each angular and radial bin (A). Angular bins are determined by the angular dendritic span of each neuron, with 6 angular bins covering the entire angular range of dendrites in each neuron. Radial bins are at 40 μm intervals. (C) Angular Sholl diagram of dendrites in (A) with the origins of all dendritic arbors centered at the origin. Red line indicates the net dendritic vector calculated from all dendrites. (D) A tectal neuron (green) located in the tectum. The tectum was filled with Alexa-594 (red) to show morphological features. Left image and right image show a neuron in the right tectum and left tectum respectively. Neuropil (np). Dashed white line delineates border between ventricle and tectum (on left image only), and grey dashed line demarcates border between neuropil and cell body layer (on both images). Orientation is depicted by crossed red arrows and as follow: R (rostral), C (caudal), A (rostral), and P (caudal).

primary dendrite, on subsequent days, the net dendritic vector angle consistently project in a rostral orientation (Figure 13). Qualitative observation suggests two main modes of biased dendritic projection: bending of the primary dendrite (Figure 13A, D), and growth of subordinate collateral branches with rostral bias (Figure 17A). These experiments demonstrate that long-term dendritogenesis of caudomedially located tectal neurons involves rearrangement of dendritic arbors in a rostrolateral orientation (Figure 13D).

4.3.2 Candidate guidance cues selected based on literature

To understand whether guidance cue molecules regulate dendritogenesis in tectal neurons *in vivo*, I selected candidate guidance cue molecules based on their spatial localization in the *Xenopus* tectum and on evidence from previous experiments indicating potential involvement in dendrite growth (Table 3). These candidate molecules were then used to screen for their potential effect on short-term dendrite growth. In our initial screen, we exposed tectal neurons to these molecules for 2h. We focused our analyses on branchtip filopodia since it is possible that these processes may be involved in guiding dendrites (Hossain et al., 2012). We also analyzed behavior of individual dendritic branches following exposure to these molecules.

Ephrin-B and EphB

Ephrin-B and EphB are well known for their involvement in axonal guidance, synaptogenesis, synaptic plasticity, and dendritic filopodial motility (Contractor et al., 2002; Dalva et al., 2000; Kayser et al., 2008; Takasu et al., 2002). Given that several other axonal guidance molecules have also been implicated in dendrite guidance, it is possible that these molecules may also participate in dendrite targeting. However, whether EphB/ephrin-B participate in dendritic targeting remains unknown. Ephrin-B and EphB is present in the *Xenopus laevis* tectum at a stage when tectal neurons undergo dendritogenesis. In stage 48 *Xenopus* tectum, ephrin-B1 expression is low and constricted to dorsal midline (Higenell et al., 2011). At stages 45-48, EphB is expressed in a dorsoventral (mediolateral) gradient in *Xenopus* tectum; however, the gradient orientation is controversial (Higenell et al., 2011; Lim et al., 2008a). Whereas Lim *et al.* report high ventral (lateral) to low dorsal (medial) expression at stage 45, Higenell *et al.* find high caudomedial to low rostrolateral gradient at stage 48. In developing *Xenopus laevis* tadpole tectum, synaptic ephrin-B localizes primarily to presynaptic axons whereas synaptic EphB localizes primarily to postsynaptic dendrites, although a low percentage of extra-synaptic ephrin-B and EphB deviate from this pattern and instead localize to both dendrites and axons (Lim et al., 2008a). As a result of these experimental findings, we chose to include ephrin-B as a candidate guidance molecule for our screen. For our experiments, we used recombinant human ephrin-B1-Fc fusion proteins (R&D Systems), which has been previously shown to be effective in *Xenopus laevis* (Lim et al., 2008a).

Ephrin-A and EphA

Ephrin-A and EphA are also well known for their role in axonal guidance, although, little is known with regards to their role in developing dendrites. In adult brain, however, EphA4 has been implicated in dendritic spine retraction, and ephrin-A3 regulates dendritic spine morphology and long-term potentiation (LTP) (Carmona et al., 2009; Filosa et al., 2009; Fu et

al., 2007). In *Xenopus* tectum, ephrin-A and EphA are found in opposing anteroposterior

	Expression pattern	Reference
ephrin-A	Anteroposterior (High posterior)	Higenell et al., 2012
ephrin-B	Dorsal midline (stage 48), or uniform low expression (stage 45)	Lim et al., 2011; Higenell et al., 2012
slit-2	Dorsoventral (high dorsal, low ventral)	Hocking et al., 2010
EphA	Anteroposterior (High anterior)	Higenell et al., 2012
EphB	Dorsoventral (high dorsal)	Higenell et al., 2012
	Dorsoventral (high ventral)	Lim et al., 2011
Robo	Robo 1,3 Dorsoventral (high ventral)	Hocking et al., 2010

Table 3. Spatiotemporal patterns of candidate guidance cues and receptors in *Xenopus laevis* based on literature.
Cells shaded in blue indicate conflicting expression patterns reported in literature.

gradients; EphA is expressed highly in rostral tectum, whereas ephrin-A is expressed highly in the posterior tectum (Higenell et al., 2011). For our experiments, we used recombinant mouse ephrin-A1-Fc fusion proteins (R&D Systems), which has been shown to cause axonal growth cone collapse of *Xenopus laevis* RGCs (Woo et al., 2009).

Slit and Robo

Slit/Robo has been implicated not only in axon guidance, but also in dendrite guidance in *Drosophila* and zebrafish, and in dendrite branching in *Xenopus laevis* (Furrer et al., 2003; Xiao et al., 2011). Slit/Robo is responsible for guiding *Drosophila* motorneurons across the CNS midline and guiding zebrafish tectal neurons to appropriate lamina (Furrer et al., 2003; Furrer et al., 2007; Xiao et al., 2011). In addition to dendrite guidance, Slit/Robo interaction is also involved in dendrite branching (Furrer et al., 2007; Hocking et al., 2010; Whitford et al., 2002). In both pyramidal and nonpyramidal cultured cortical neurons from developing mouse cortex, slit-1 induces dendrite growth and branching, whereas dominant-negative Robo decreases branching (Whitford et al., 2002). In *Drosophila,* slit loss-of-function dramatically reduces dendrite number in aCC motorneurons, a type of identified neuron with stereotypical dendritic morphology (Furrer et al., 2007). However, in a different population of *Drosophila* neuron that normally has complex dendritic branching patterns, termed Class IV neurons, loss of slit or Robo increases branch length but decreases branch number (Dimitrova et al., 2008). Similarly, slit acts via Robo2 in *Xenopus laevis* RGC dendrites to increase dendrite branching, although it has no effect on RGC dendrite guidance (Hocking et al., 2010). In *Xenopus laevis* tectum, *in situ* hybridization reveals high levels of slit-1 in dorsal and low levels of slit-2 mRNA in ventral tectum (Hocking et al., 2010). Furthermore, all three Robo receptor mRNA were detected in the tectum. For this study, we used recombinant mouse slit-2-Fc fusion proteins (R&D Systems). Human slit-2 protein has been previously shown to induce *Xenopus* RGC dendritic branching *in vitro* (Hocking et al., 2010).

4.3.3 Acute effects of candidate guidance cues on branchtip filopodia and dendritic branches

To determine potential mechanisms of dendritic orientation, we tested three candidate

guidance cues, ephrin-A1, ephrin-B1, and slit-2 for their effect on short-term dendritogenesis. Tectal neurons were selected at the stage of rapid dendritogenesis (phase 2) as described in Chapter 2, prior to their transition into mature neurons with stabilized overall dendritic architecture. We used rapid time-lapse imaging to observe growth of tectal neurons before and after exposure to soluble guidance cue molecules. To investigate short-term effects of these molecules on dendrite growth, we employed dynamic morphometrics using our software, Dynamo, as described in Chapter 3.

4.3.3.1 Slit-2 increases branchtip filopodial motility and length

Axons utilize growth cone filopodia located at branchtips to sense guidance cues in the extracellular environment and to steer growth cones in appropriate directions. Since dendrites also have growth cones, we hypothesized that the observed oriented behavior of dendritic branches may arise from oriented extension mediated by dendritic growth cones. In mouse cortical pyramidal neurons, dendritic interstitial filopodial behavior changes in response to neuronal activity, but dendritic branchtip filopodial behavior does not, suggesting that these filopodia may not be involved in synaptotropic growth and rather function to detect guidance cues (Portera-Cailliau et al., 2003). Thus, we sought to test whether dendritic branchtip filopodial behavior changes in response to exposure to guidance cues.

To observe branchtip filopodial behavior, dynamic dendrite growth was examined using *in vivo* rapid time-lapse imaging followed by dynamic morphometric analysis. *Xenopus* tadpole tectal neurons were labeled with fEGFP imaged at 5 min intervals over 1h to establish a baseline prior to treatment. Subsequently, soluble slit-2-Fc recombinant protein, ephrin-A1-Fc, ephrin-B1-Fc, or PBS (as control) was injected into the tectum, and the same neurons were imaged at 5 min intervals for 2h following injection. We analyzed branchtip filopodial motility,

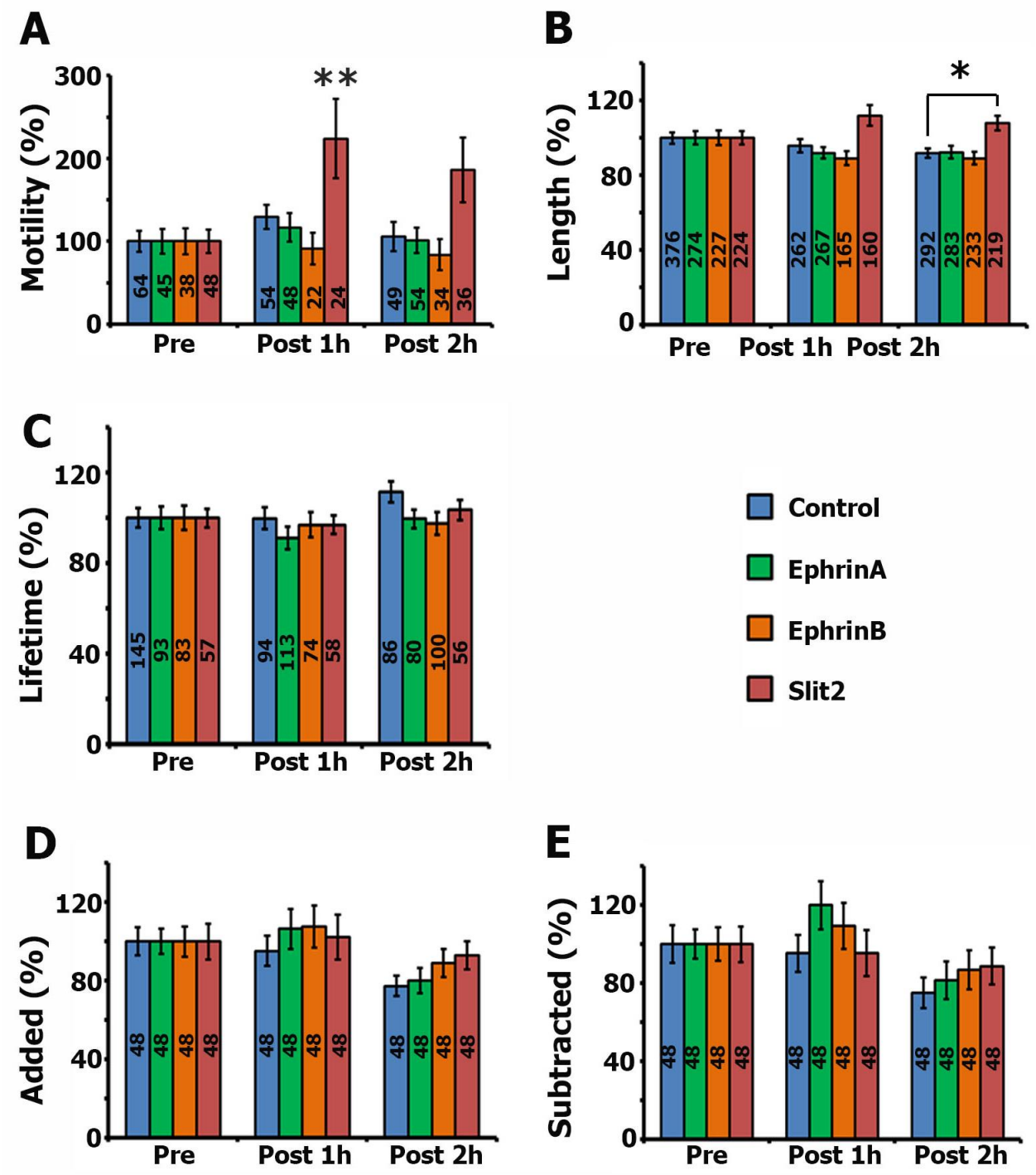
A
Motility (%)
300
200
100
0
**
64
45
38
48
54
48
22
24
49
54
34
36
Pre
Post 1h
Post 2h
B
Length (%)
120
80
40
0
*
376
274
227
224
262
267
165
160
292
283
233
219
Pre
Post 1h
Post 2h
C
Lifetime (%)
120
80
40
0
145
93
83
57
94
113
74
58
86
80
100
56
Pre
Post 1h
Post 2h
Control
EphrinA
EphrinB
Slit2
D
Added (%)
120
80
40
0
48
Pre
Post 1h
Post 2h
E
Subtracted (%)
120
80
40
0
48
Pre
Post 1h
Post 2h

Figure 14. Short-term effects of candidate guidance cues on branchtip filopodia. Behavior of branchtip filopodia before and after exposure to ephrin-A1, ephrin-B1, and slit-2, measured using dynamic morphometrics. “Pre” indicates before exposure to guidance cue, and “Post1h” and “Post2h” indicate 1h and 2h respectively after exposure. All figures are expressed as percentage change as compared to the “pre” treatment period. (A) Filopodial motility, (B) filopodial length, (C) filopodial lifetime, (D) filopodia added/5min, (E) filopodia retracted/5min, all of which are expressed as a percentage. N = 4 neurons per group; n = filopodial motility observation (A), length observation (B), number of filopodia (C), turnover observation (D, E) as indicated inside each bar on graph. Error bars denote SEM; * denotes $p < .05$; ** denotes $p < .01$.

length, lifetime, and turnover (additions and retractions). Interestingly, we find that slit-2 exposure significantly increases normalized branchtip filopodial motility at post1h (223.9 ± 48.1% for slit-2, 129.6 ± 14.7 % for Control, Figure 14A). slit-2 tectal injection also increases filopodial length as compared to Control treatment at 2h post treatment at post 2h (108.1 ± 4.00 % for slit-2, 91.9 ± 2.6 % for Control , Figure 14B). However, there was no slit-2 induced change in lifetime or turnover (Figure 14C, D, and E). Furthermore, we did not observe significant change in any parameters of branchtip filopodial behavior following ephrin-A1 or ephrin-B1 tectal injection.

4.3.3.2 Slit-2 and ephrin-A1 decreases branch motility

In addition to analyzing branchtip filopodial behavior, we also investigated dendritic branch behavior, including branch motility and lifetime, following tectal injection of the aforementioned guidance cues. Interestingly, we find that both slit-2 and ephrin-A1 decreases branch motility at 2h post treatment (84.9 ± 2.6 % for slit-2, 86.5 ± 2.4 % for ephrin-A1, and ± 98.7 ± 3.0 % for Control, Figure 15A). However, none of these guidance cues significantly altered lifetime of branches (Figure 15B).

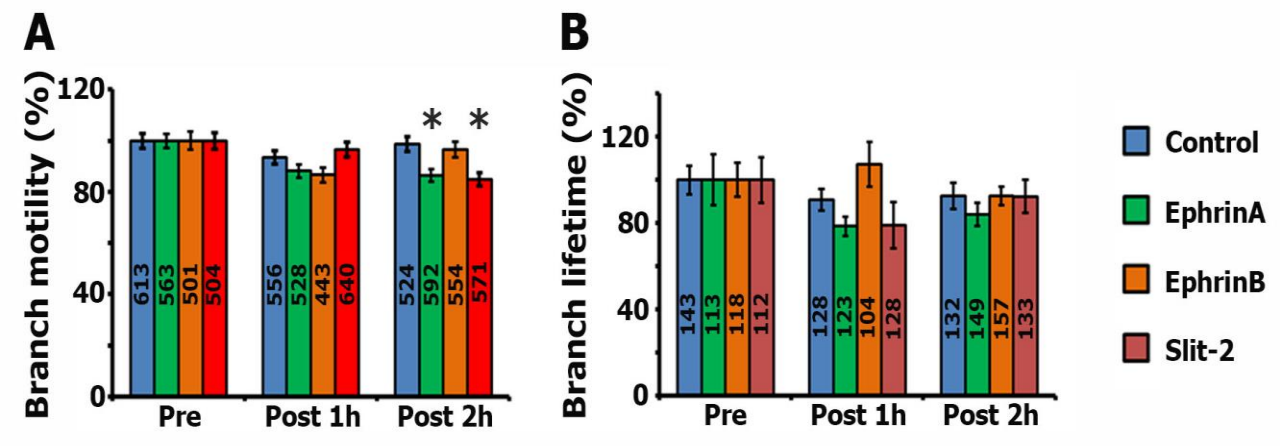

Figure 15. Short-term effects of candidate guidance cues on dendritic branches. Behavior of dendritic branches before and after exposure to ephrin-A1, ephrin-B1, and slit-2, measured using dynamic morphometrics. “Pre” indicates before exposure to guidance cue, and “Post1h” and “Post2h” indicate 1h and 2h respectively after exposure. All figures are expressed as percentage change as compared to the “pre” treatment period. (A) Branch motility, and (B) branch lifetime. N = 4 neurons per group; n = branch motility observation (A), and number of branches (B) as indicated inside each bar on graph. Error bars denote SEM; * denotes $p < .05$.

4.3.3.3 Motility effects on branches of various orientation

Since we find that slit-2 and ephrin-A1 decrease branch motility, we sought to determine whether any of these candidate guidance cue molecules differentially affect motility of branches that are oriented at specific directions. For this analysis, neuronal branches were separated into 4 different orientations, including “medial-rostral”, “lateral-rostral”, “medial-caudal”, and “lateral-caudal”, based on the orientation of individual branch vectors with respect to the primary apical branch (Figure 12, Figure 16). There appears to be a trend for decreased branch motility of ephrin-A1 and slit-2 on medial-anterior oriented branches as compared to control at 2h post treatment (Figure 16A); however, these differences are not significant (two-way ANOVA, $p = .08$)

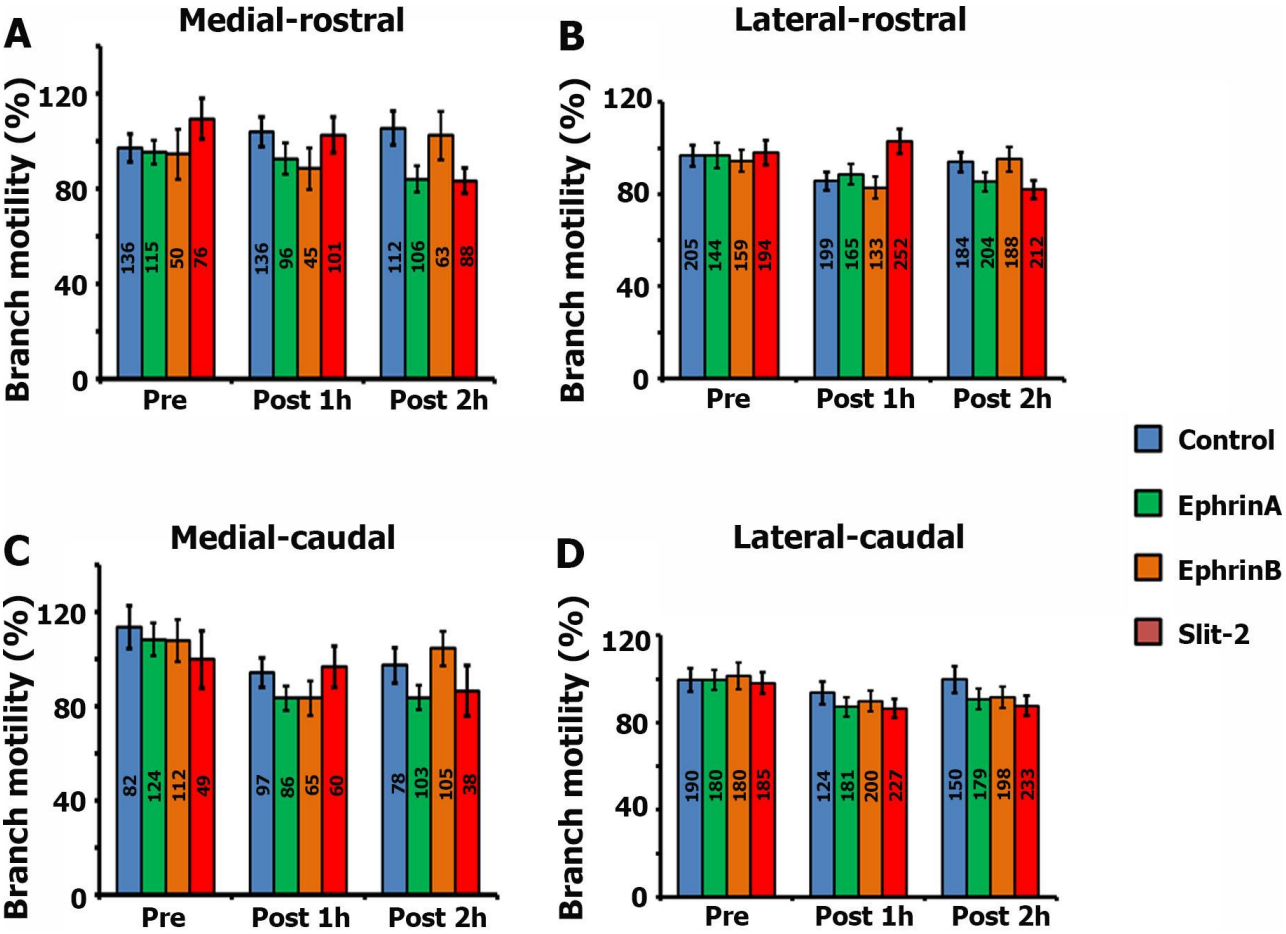

Figure 16. Effects of guidance cues based on branch orientation.
Motility of dendritic branches before and after exposure to ephrin-A1, ephrin-B1, and slit-2 with regards to dendritic orientation. “Pre” indicates before exposure to guidance cue, and “Post1h” and “Post2h” indicate 1h and 2h respectively after exposure. All figures are expressed as percentage change as compared to the “pre” treatment period. Branch motility of (A) medial-anterior, (B) lateral-anterior, (C) medial-posterior, and (D) lateral-posterior oriented branches. N = 4 neurons per group; n = branch motility observations. Error bars denote SEM.

4.3.4 Robo3 receptors potentially direct targeted dendritic elaboration

Given that the screen for guidance cue molecules directing dendrite growth showed that slit-2 affects both branchtip filopodia and dendritic branch behavior, we decided to explore whether decreasing activity of a receptor for slit-2 can lead to defects in the biased dendritic

orientation of caudomedially located tectal neurons. Previous work has shown that Robo3 is a receptor for slit-2 ((Chedotal, 2007)). To determine whether Robo3 mediates long-term dendrite growth, neurons were co-electroporated with plasmids encoding fGFP and dominant-negative Robo3 constructs (dnxRobo3). Labeled neurons were imaged at 24h intervals over 5 days. Dendritic vectors of all dendrites for each neuron was calculated from a common origin, and the 'net dendritic vector' was calculated for each neuron by taking the vector sum of all dendritic vectors. Compared to neurons labeled with only fGFP, in neurons expressing dnxRobo3, a significantly lower proportion of total dendritic branch length contributed to oriented dendrite growth toward a common angle in each neuron (85.1 ± 3.9% in controls vs 57.7 ± 5.7% in dnxRobo3 neurons) (Figure 17C). Normalized net dendritic vector length provides a measure of the extent to which individual dendrites contribute to a common neuronal dendritic vector, such that higher net dendritic vector length indicates that dendrites of a neuron are more "unified" in orientation.

4.4 Discussion

Here we find that dendritic arbors are oriented in a biased manner to compensate for location in the case of caudomedially located tectal neurons within the *Xenopus* tectum. This study provides the first evidence for oriented growth of dendritic arbors in the *Xenopus* tectum. We find that tectal neurons located in the caudomedial tectum *in vivo* project dendrites in a rostral orientation toward the tectal neuropil, the region where tectal neurons receive the majority of their presynaptic inputs from RGC axons. Our investigation of long-term growth of tectal neuronal arbors indicate that during earlier phases of dendritogenesis (days 1, 3 on Figure 13A), dendritic arbors are not biased, and that rostral bias develops concomitantly with neuronal maturation within the tectum. This dendritic bias is observed as either "bending" of the major dendrite or preferential growth of collateral branches in a rostral orientation.

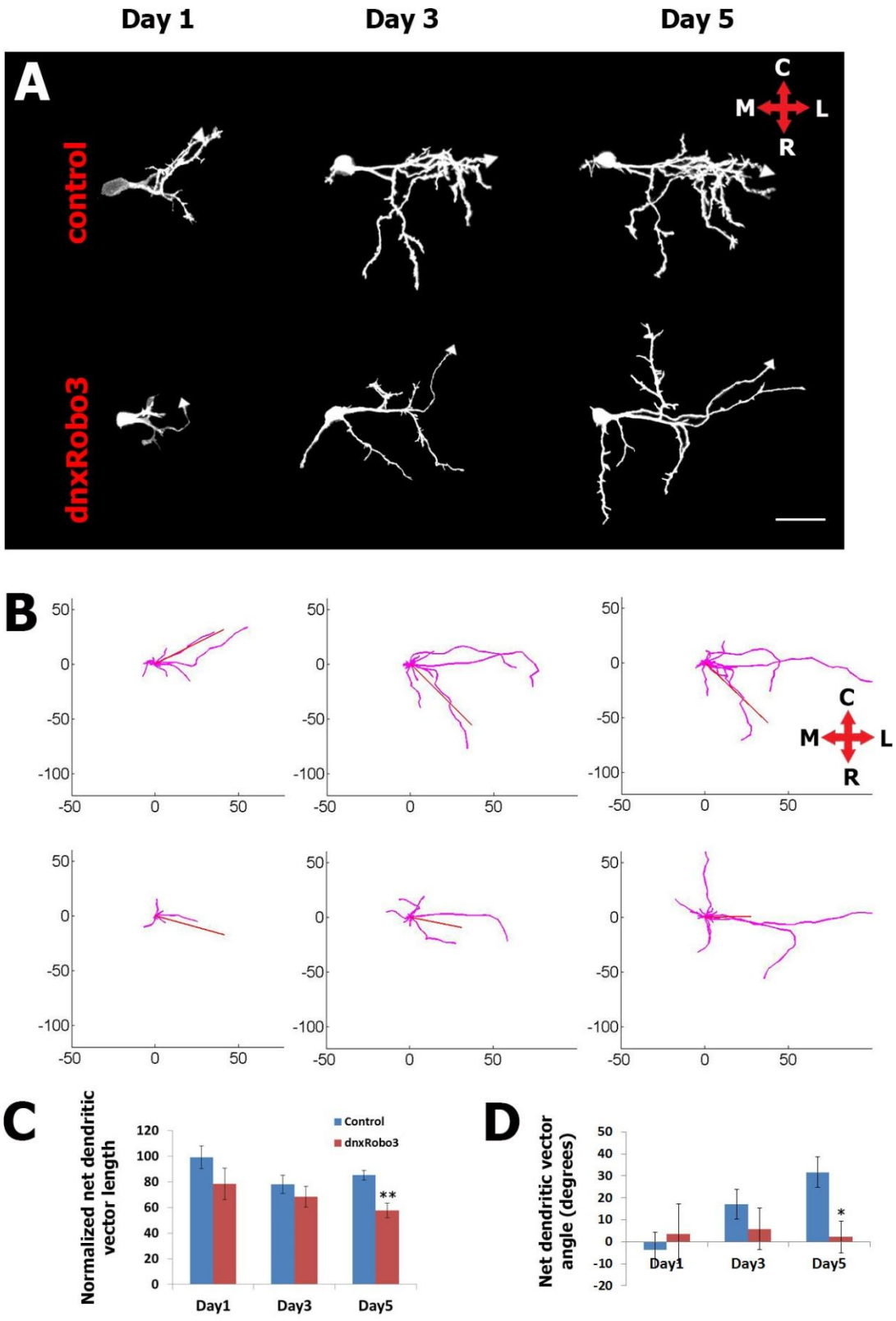
Day 1
Day 3
Day 5
A
C
M
L
R
control
dnxRobo3
B
C
M
L
R
C
Normalized net dendritic vector length
Control
dnxRobo3
**
Day1
Day3
Day5
D
Net dendritic vector angle (degrees)
*
Day1
Day3
Day5

Figure 17. Robo3 receptors direct dendritic orientation
(A) Images of a control neuron (top row) and a neuron electroporated with dominant-negative Robo3 (bottom) located in the caudal tectum at 48h intervals over 5 days. Branches tipped by an arrowhead depict axons. Scale bar = 20 μm. (B) Angular Sholl diagram of dendrites in (A) with the origins of all dendritic arbors (excluding basal dendrites) centered at the origin. Red line indicates the net dendritic vector calculated from all dendrites. (C) Net dendritic vector length of control neurons versus dnxRobo3 neurons as a percentage of total dendritic branch length. Orientation is depicted by crossed red arrows and as follows: R (rostral), C (caudal), A (rostral), and P (caudal). N = 4 neurons per group. Error bars denote SEM; **p < 0.01.

4.4.1 Slit2 effect on branchtip filopodia and dendritic branches

To investigate mechanisms underlying generation of biased dendritic arbors, we tested candidate guidance cues for their potential effects on dendritic arbors. We find that tectal infusion of slit-2 increases branchtip filopodial length and motility, whereas ephrin-A1 and ephrin-B1 tectal infusion has no effect on these two parameters of dendritogenesis. Most studies on dendritic filopodia do not differentiate between dendritic branchtip filopodia and interstitial filopodia, but rather combine them into one set of analyses. However, those studies that have studied these two populations separately underscore the difference in the behavior interstitial versus branchtip filopodial behavior (Hossain et al., 2012; Portera-Cailliau et al., 2003). Since we were particularly interested in guidance cues that may affect orientation of dendritic arbors, we chose to explore behavior of branchtip filopodia, components of dendritic growth cones in growing neurons. Increase in branchtip filopodial length and motility is used in this study as an indicator that slit-2 directs dendritogenesis. However, this result does not provide any indication as to whether slit-2 serves as an attractive or repulsive cue or whether it serves to increase or decrease dendrite growth in general. To differentiate among these functions requires further knowledge of the endogenous spatiotemporal localization of slit-2 in the tectum and observing how a dendritic growth cone behaves in response to acute exposure of this guidance cue. We further find that slit-2 decreases branch motility at 2h post injection.

Past studies on dendritogenesis have indicated that decreased branch motility is correlated with increased branch stabilization. Thus, we investigated whether increased branch stabilization of rostrally oriented branches in comparison with caudally oriented branches gives rise to the overall rostral bias of dendritic arbors. We find that there is a trend for decreased motility in branches that have a “medial-rostral” orientation in neurons exposed to ephrin-A1 or slit-2, suggesting that indeed preferential branch stabilization in appropriate regions mediated by either of these molecules may be involved in generating rostral dendritic bias. However, although there is a trend, these results are not significant ($p = 0.07$ using two-way ANOVA). It is very likely that the lack of significance when branches are grouped according to orientation is due to the n’s in each group (45-136 per group) and inherent variability, as compared to ungrouped statistics, where significant difference in branch motility was observed.

4.4.2 Robo3 involvement in generating dendritic bias of tectal neurons

Previous studies have shown that slit/Robo interaction is necessary for proper targeting of dendritic arbors to appropriate lamina within the zebrafish tectum, and Robo is required for preventing aberrant dendritic projection across the CNS midline in *Drosophila* (Furrer et al., 2003; Xiao et al., 2011). Our observation of long-term dendritogenesis with dominant-negative Robo3 strongly suggests that this receptor plays a role in generating dendritic bias, since interfering with endogenous Robo3 function caused tectal neuronal dendrites to grow more symmetrically, and not with a preference for rostral orientation. The dominant-negative constructs used in these experiments were designed specifically to interfere with *Xenopus* Robo3 function without affecting other Robo receptors (Hocking et al., 2010). Moreover, since we used single-cell electroporation for restricting expression of these constructs to individual tectal neurons, the effects observed with dominant-negative Robo3 in this study is cell autonomous. Thus it is highly unlikely that these effects are downstream of compromised axonal

growth in upstream RGCs.

However, it is important to point out that we cannot fully confirm a role for slit-2 and Robo3 proteins in generating dendritic arbor bias, since localization of these proteins within the tectum has not been yet confirmed. The presence of slit-2 and Robo3 mRNA has been confirmed in at stage 37/38 of *Xenopus laevis* tectum (Hocking et al., 2010). However, presence of slit-2 and Robo3 at the *Xenopus* stage used in our experiments (stage 48), remains unknown. Our initial attempts at using commercially available antibodies to detect endogenous slit-2 and Robo in the *Xenopus* tectum have not been successful. This is likely because currently, commercially available antibodies are targeted against mouse or human proteins, although it is also possible that this is due to the absence of these proteins in the tectum. The latter scenario is unlikely however, given the robust effect of using a dominant-negative Robo3 constructs. Further investigation with other antibodies or with *in situ* hybridization of these proteins are necessary to more conclusively establish the role of slit-2 and Robo3 in orienting dendrites in *Xenopus* tectum.

4.4.3 Methodological considerations

Effect of tectal injection: increased guidance cue or compromised guidance cue gradient

To screen for candidate guidance cue molecules that may affect dendritogenesis within the tectum, we used tectal infusion of ephrin-A, ephrin-B, and slit-2 soluble proteins to assess dendrite growth behavior before and after exposure to these molecules. It is important to point out that in addition to an increase in the infused guidance cue within the tectum, tectal infusion of exogenous proteins eliminates the endogenous gradients of these guidance cues. We know from axonal studies, that axonal guidance requires presence of a spatial gradient of guidance

cues, rather than simply a specific concentration of the protein. Thus, in future experiments, it would be interesting to explore whether effects seen on the branchtip filopodia and dendritic branches resulted from a lack of guidance cue gradients, or due to an increase in slit-2 protein.

4.4.4 Future directions

Observation of long-term dendrite growth over 5 days encompassing all phases of dendritogenesis (phase 1-3) suggests existence of two modes of generating dendritic bias: growth cone mediated guidance of major dendritic branches, and preferential growth or stabilization of rostral-oriented collateral branches (i.e. control neuron in Figure 17A). Mechanistically, dendritic growth can be further categorized into the following modes of growth: oriented extension (dendritic turning) of existing dendritic branches mediated by dendritic growth cones; emergence of more new collateral branches in rostral as compared to caudal orientation; disappearance of more collateral branches from caudal orientation; greater net growth in rostral as compared to caudal-oriented collateral branches; or higher stabilization of branches in rostral as compared to caudal-oriented branches. Using time-lapse imaging at appropriate intervals and utilizing dynamic morphometrics to observe branch lifetimes, new branch formation, and net extension of branches with respect to branch orientation, we can determine which of these mechanisms can account for oriented dendrite growth. Since we observed that majority of branches have lifetimes >2h (Chapter 2), the short-term imaging paradigms used in our experiments here are not adequate to answer these questions. On the other hand, since many major branches appear and disappear within 24h, the long-term daily imaging intervals used here is also insufficient to answer these questions.

Chapter 5: General Discussion

How dendrites develop *in vivo* in the intact immature brain remains poorly understood. To a large extent, this lack of understanding stems from two obstacles: technical challenges in acquiring images of developing dendrites *in vivo* in the developing brain, and the absence of analytical tools required for detecting subtle and varying changes in the dynamics of developing dendrites.

5.1 From seedlings to trees: novel insights into how dendritic arbors form

In Chapter 2 of this thesis, I performed an in-depth characterization of morphological aspects of dendrite development *in vivo* to understand how short-term behaviors of dendritic components contribute to persistent dendritic arbor morphological patterning. These experiments were conducted on the unanesthetized brains within intact vertebrates during early stages of brain formation. I combined rapid time-lapse with long-term imaging to quantify dynamic dendrite growth on the time scale of minutes, as well as how such dynamic changes culminate to influence larger arbor changes over 5 days. My contributions to the design of our Dynamo software allowed for tracking and measurement of all dendritic processes in 3D across brief interval image stacks for comprehensive quantification of growth dynamics. Furthermore, I established quantitative morphological criteria to differentiate various features of a developing dendrite *in vivo*, including interstitial and branchtip filopodia, DGCs, and dendritic branches.

Dendrites have growth cones too

This work provides clarification of the prevalence of DGCs *in vivo* and rectifies their gross underrepresentation in past studies, which was likely a result of eliciting data from static images. DGCs can be identified by a rapid turnover of branchtip filopodia; however, with infrequent demonstration of lamellipodia, they are easily overlooked in static images. I also find

that DGC morphology changes over neuronal maturation, with increasing presence of branchtip filopodia and decreasing presence of lamellipodia in mature neurons. Interestingly, in a time-lapse imaging study, Yuste and colleagues found that in acute slices of postnatal ages P2-P5 mouse pyramidal neurons, DGCs are composed of branchtip filopodia with no lamellipodia, and DGCs disappear after P7. It is possible that the lack of lamellipodia in Yuste's study is because the neurons studied were more mature compared to the immature neurons used in our experiments. In fact, comparison of my mature neurons with published images provided by Yuste et al. support this idea. However, it is also possible that the presence of lamellipodia-containing DGCs is dependent on the type of neuron. Further experiments in various experimental systems are needed to determine whether lamellipodia-containing DGCs are ubiquitious characteristics of immature dendrites. In this study, I have also identified a novel correlation between DGC morphology with branch behavior. I find that extending branches have DGCs whereas retracting branches are bereft of DGCs, suggesting that DGCs are a required component of actively extending dendritic branches and that all growing dendrites have DGCs.

Dendritic filopodia: location matters

In addition to DGCs, Chapter 2 further presents differences in the behavior of two different filopodial populations *in vivo*: interstitial filopodia and branchtip filopodia, and reports maturation-dependent modification of filopodial behavior. Both interstitial and branchtip filopodia undergo increased stabilization as neurons mature. However, compared to branchtip filopodia, stabilization is much more pronounced in interstitial filopodia, evidenced by longer lifetimes, decreased motility and a higher percentage of interstitial filopodia surviving over 1h of imaging. Furthermore, branchtip filopodia consistently exhibit a higher average turnover rate than interstitial filopodia except on very immature day 1 neurons. It is possible that this increased interstitial filopodial stability is because as neurons mature, there is increased participation of synapse formation by interstitial filopodia (Niell et al., 2004). Yuste *et al.* have reported a similar

increase in interstitial and branchtip filopodial stabilization over neuronal maturation, accompanied by decreased motility and increased lifetime *in vitro* in acute slices of postnatal ages P2-P5 mouse pyramidal neurons (Portera-Cailliau et al., 2003). Moreover, they have shown that whereas interstitial filopodia respond to activity-blockade, branchtip filopodia do not (Portera-Cailliau et al., 2003). This begs the question, if branchtip filopodia do not participate in synapse formation and do not respond to neuronal activity, what role do they play in dendrite development? Axonal growth cone filopodia sense extracellular guidance cues and orient axons in appropriate directions. In light of recent studies on dendritic guidance, which demonstrate that molecules initially known for their role in axon guidance, such as sema3A, slit, and netrin, can also guide dendrites, it is possible that dendritic branchtip filopodia play a similar role in sensing cues to orient dendrites (Furrer et al., 2003; Polleux et al., 2000). Effect of dendritic guidance molecules on behavior of branchtip filopodia *in vivo* was explored and is described in Chapter 4 of this thesis.

Growing new branches

Another noteworthy finding in Chapter 2 is the morphological basis for new branch formation *in vivo*. Whereas growth-cone splitting is the predominant mechanism for new branch formation in cultured neurons, new branches *in vivo* in zebrafish tectal neurons have been shown to arise by an iterative process whereby filopodia that forms synapses are stabilized and form new dendrites, whereas filopodia without synapses retract (Niell et al., 2004). We find that *in vivo*, interstitial filopodia transition into new branches via an additional mechanism; interstitial filopodia acquire lamellipodia-containing DGCs and transition into new dendritic branches. This mechanism has not been previously established *in vivo,* although it has been reported *in vitro* in developing hippocampal slices (Dailey and Smith, 1996). In our experiments, a very small percentage of interstitial filopodia transformed into new branches, indicating a high threshold for these transitions. Whether synaptogenesis, neuronal activity, or other factors determine which

filopodia will transition remains unknown. Furthermore, it remains to be seen whether distinct mechanisms are maturational stage dependent, vary across neuronal subtypes, or are influenced by *in vivo* versus *in vitro* conditions.

5.2 New frontiers in dendrite morphometrics

Research questions have far outpaced the analytics available in neurite tracing tools, and researchers have largely resorted to using manual methods for complex quantitative analysis. My efforts to quantify properties of neuronal dendrites highlighted major deficiencies in the availability of tools for some critical aspects of morphometric analysis, particularly with respect to time-lapse imaging. One such example is the inability to correlate behavior of motile dendritic processes (i.e. motility, lifetime) with a location or orientation (i.e. filopodial distance from the soma or vector orientation of a dendritic branch). For example, do filopodia located at a certain distance from the soma behave differently from filopodia located at other distances? Are there differences in the motility and stability of branches oriented at a particular orientation?

Recent publications have elegantly extrapolated information regarding cell-adhesion, synapse formation, morphological correlate to functional metaplasticity, and dendritogenesis using morphometric analysis of filopodial dynamics (Chen et al., 2012; Chen et al., 2010; Hossain et al., 2012; Kayser et al., 2008; Liu et al., 2009). Some advanced filopodial morphometrics used in these experiments include categorization of filopodia into “pre-existing” versus “new” filopodia, or “branchtip” versus “interstitial” filopodia. Similarly, from my research in Chapter 2, I realized the need for these tools to be able to differentiate among various components of a developing dendritic arbor, such as branches versus filopodia. Whereas in these experiments, manual methods were utilized to obtain information, Dynamo provides automated analysis. As more and more elegant methods of dendritic analysis emerge, it would

be prudent to keep a repository of these different forms of effective analysis for researchers to choose from and to make a repository of these tools that is easily accessible to researchers.

The overall structure of developing dendrites is highly dynamic, often characterized by major reconstruction over time. Thus tracing and analysis of developing dendrites presents unique challenges such as:

- Tracking dendritic branches over multiple time-points despite major dramatic morphological changes (i.e. branch turning, branch appearance/disappearance)
- Tracking filopodia that transition into branches
- Establishing criteria to define various dendritic components based solely on morphological criteria (note: this may be different based on neuronal types)

Accurate tracking of processes are of critical importance to when quantifying morphological changes of over time. A major challenge in quantifying dendrites is image rotation and translation, which result as a consequence of either inherent movement of neurons within developing brain tissue or as a result of specimen movement during imaging. To counter image drift and rotation, Dynamo dendritic processes are not tracked solely on the basis of pixel location, but rather on dendritic connectivity patterns, which allows identification of each dendritic component based on overall dendritic pattern of each arbor as well as landmarks rather than xyz coordinates only, thus allowing for more accurate process-tracking, especially when neurons undergo rotation in 3D.

Significant cost reduction and analytical flexibility in dendritic analysis

Undoubtedly, a major practical advantage in using open-source software is that it is free to use, and so can ameliorate some of the strain on lab resources. Commercially available neurite-tracing software is cost prohibitive for many labs, and are often restricted for use on a limited number of computers. Moreover, usually the source code for commercial software is

proprietary, which limits users implementing novel analysis. Seeing the need for adding user-defined functions, some companies such as Imaris, have designed platforms that allows integration of their own software with a third-party development environment to allow customers to develop customizable analysis. However, even though this initiative does allow flexibility in terms of types of analysis, the researcher must still purchase the imaging platform even to implement their own analysis.

Future directions

Dynamo delivers solutions to unique challenges associated with time-lapse image analysis of developing dendrites. However, the intent behind development of this tool is not for it to be an end-point in itself, but for it to serve as an adaptable repository of all analyses related to dynamic morphometrics. For example, the analysis developed for calculating branch angles was developed for neurons with a single primary dendrite. In future versions, we hope to incorporate this analysis to include morphometrics for bipolar neurons, or neurons with multiple branches emanating from the soma.

- Calculate branch angles for bipoloar, multipolar neurons
- Auto-detect lamellipodia based on thresholding
- Implement auto-tracing (although feasible theoretically, more research on previous work is needed prior to making this attempt)
- Utilize data mining algorithms to predict neuronal dendrite behavior based on multiple parameters
- Create an online repository of analyses written by users

With a flexible framework, this tool provides an avenue for asking exciting questions. For example, Dynamo has been recently applied to the tracking of dynamic axonal growth *in vivo* (Munz et al., 2014) and is currently being used to track mitochondrial movement within growing

neurons *in vivo*.

5.3 Slit/Robo in targeted dendrite growth

The role of slit and its receptor Robo in guiding dendrites to appropriate brain regions in *Drosophila* (Furrer et al., 2003), or to proper lamina in zebrafish tectum (Xiao et al., 2011), has been previously described. Our studies suggest yet another role of this guidance cue in directing dendrites to the tectal neuropil in *Xenopus laevis* tadpoles. In this study, we investigated neurons located in the caudomedial tectum and observed that their dendrites "bend" in rostral orientation biased towards the direction of the tectal neuropil. We also find that interfering with Robo3 function by using dominant-negative Robo3 constructs leads to a symmetrical and unbiased growth of dendrites. Previous studies of developing tectal neurons in *Xenopus* has shown that new neurons are generated in the caudomedial region, and as they mature, many of them are shifted in a rostrolateral orientation (Straznicky and Gaze, 1972). In this case, many of these neurons, once they mature will be located laterally, rather than caudolaterally with respect to the neuropil. As the end-point to our imaging experiments was day 5, we do not know whether the dendrites of these neurons would have to reorganize to project laterally, instead of rostrolaterally, to maintain connection with their respective presynaptic partners.

5.4 Overall significance

Whereas previous studies have largely looked at the static end product in dendritogenesis, such as the extent or length of dendritic arbors or total number of branch intersections, with response to treatment, using *in vivo* time-lapse imaging, my thesis makes a significant contribution by identifying what happens as dendrites undergo dynamic changes to

achieve that end state. A particular advantage of the work in this thesis is that all of the experiments were conducted *in vivo* in an unanesthetized vertebrate brain, and thus confounding factors such as effect of anesthesia or cell culture conditions are eliminated. This work is the first to characterize dynamics of dendritic growth cones *in vivo* and correlate dendritic growth cone morphology with behavior.

In this thesis, we have developed a powerful new tool – Dynamo, to more fully utilize the power afforded by time-lapse imaging of growing dendrites as well as axons. Development of dendritic analysis software is a nascent field that is gaining momentum in order to catch up to the data we can now generate with improved imaging systems (i.e. two-photon microscopy to visualize neurons *in vivo* in deeper tissue and time-lapse imaging). With particular emphasis on novel analyses, our contribution to this niche field is aimed at providing yet another advancement to overcome this challenge.

Clinical relevance

Abnormal dendrite growth has been implicated in several neurological disorders, such as mental retardation, including Down syndrome, Rett syndrome, and Fragile X (Kaufmann and Moser, 2000), as well as schizophrenia (Costa et al., 2001), and epilepsy (Hewapathirane et al., 2008). Some examples of these dendritic anomalies include reduced dendrite length, dendrite branching, and spine density in Down syndrome and Rett syndrome. It is my hope that with more in-depth knowledge of how dendritogenesis occurs under normal conditions, we will be better equipped to recognize anomalies and perhaps to find ways to counter them.

References

Aizawa, H., Wakatsuki, S., Ishii, A., Moriyama, K., Sasaki, Y., Ohashi, K., Sekine-Aizawa, Y., Sehara-Fujisawa, A., Mizuno, K., Goshima, Y., and Yahara, I. (2001). Phosphorylation of cofilin by LIM-kinase is necessary for semaphorin 3A-induced growth cone collapse. Nat Neurosci 4, 367-373.

Al-Kofahi, K.A., Lasek, S., Szarowski, D.H., Pace, C.J., Nagy, G., Turner, J.N., and Roysam, B. (2002). Rapid automated three-dimensional tracing of neurons from confocal image stacks. IEEE transactions on information technology in biomedicine : a publication of the IEEE Engineering in Medicine and Biology Society 6, 171-187.

Andersen, S.S., and Bi, G.Q. (2000). Axon formation: a molecular model for the generation of neuronal polarity. BioEssays : news and reviews in molecular, cellular and developmental biology 22, 172-179.

Andrews, W., Barber, M., Hernadez-Miranda, L.R., Xian, J., Rakic, S., Sundaresan, V., Rabbitts, T.H., Pannell, R., Rabbitts, P., Thompson, H.*, et al.* (2008). The role of Slit-Robo signaling in the generation, migration and morphological differentiation of cortical interneurons. Developmental biology 313, 648-658.

Aoto, J., Ting, P., Maghsoodi, B., Xu, N., Henkemeyer, M., and Chen, L. (2007). Postsynaptic ephrinB3 promotes shaft glutamatergic synapse formation. J Neurosci 27, 7508-7519.

Apps, R., and Garwicz, M. (2005). Anatomical and physiological foundations of cerebellar information processing. Nature reviews Neuroscience 6, 297-311.

Ascoli, G., Soboda, K., and Liu, Y. (2009). The DIADEM Challenge.

Ascoli, G.A., Donohue, D.E., and Halavi, M. (2007). NeuroMorpho.Org: A central resource for neuronal morphologies. Journal of Neuroscience 27, 9247-9251.

Baas, P.W., Deitch, J.S., Black, M.M., and Banker, G.A. (1988). Polarity orientation of microtubules in hippocampal neurons: uniformity in the axon and nonuniformity in the dendrite. Proc Natl Acad Sci U S A 85, 8335-8339.

Banker, G.A., and Cowan, W.M. (1979). Further observations on hippocampal neurons in dispersed cell culture. J Comp Neurol 187, 469-493.

Bartlett, W.P., and Banker, G.A. (1984a). An electron microscopic study of the development of axons and dendrites by hippocampal neurons in culture. I. Cells which develop without intercellular contacts. J Neurosci 4, 1944-1953.

Bartlett, W.P., and Banker, G.A. (1984b). An electron microscopic study of the development of axons and dendrites by hippocampal neurons in culture. II. Synaptic relationships. J Neurosci 4, 1954-1965.

Bashaw, G.J., Kidd, T., Murray, D., Pawson, T., and Goodman, C.S. (2000). Repulsive axon guidance: Abelson and Enabled play opposing roles downstream of the roundabout receptor. Cell 101, 703-715.

Bear, J.E., and Gertler, F.B. (2009). Ena/VASP: towards resolving a pointed controversy at the barbed end. Journal of cell science 122, 1947-1953.

Bedell, V.M., Yeo, S.Y., Park, K.W., Chung, J., Seth, P., Shivalingappa, V., Zhao, J., Obara, T., Sukhatme, V.P., Drummond, I.A.*, et al.* (2005). roundabout4 is essential for angiogenesis in vivo. Proc Natl Acad Sci U S A 102, 6373-6378.

Benes, F.M., Parks, T.N., and Rubel, E.W. (1977). Rapid dendritic atrophy following deafferentation: an EM morphometric analysis. Brain research 122, 1-13.

Bentley, D., and O'Connor, T.P. (1994). Cytoskeletal events in growth cone steering. Current opinion in neurobiology 4, 43-48.

Bonanomi, D., Chivatakarn, O., Bai, G., Abdesselem, H., Lettieri, K., Marquardt, T., Pierchala, B.A., and Pfaff, S.L. (2012). Ret is a multifunctional coreceptor that integrates diffusible- and contact-axon guidance signals. Cell 148, 568-582.

Bovolenta, P., and Mason, C. (1987). Growth cone morphology varies with position in the developing mouse visual pathway from retina to first targets. J Neurosci 7, 1447-1460.

Bradford, D., Cole, S.J., and Cooper, H.M. (2009). Netrin-1: diversity in development. The international journal of biochemistry & cell biology 41, 487-493.

Bradke, F., and Dotti, C.G. (2000). Establishment of neuronal polarity: lessons from cultured hippocampal neurons. Current opinion in neurobiology 10, 574-581.

Bray, D. (1973). Branching patterns of individual sympathetic neurons in culture. J Cell Biol 56, 702-712.

Brigidi, G.S., and Bamji, S.X. (2011). Cadherin-catenin adhesion complexes at the synapse. Current opinion in neurobiology 21, 208-214.

Brown, K.M., Barrionuevo, G., Canty, A.J., De Paola, V., Hirsch, J.A., Jefferis, G.S., Lu, J., Snippe, M., Sugihara, I., and Ascoli, G.A. (2011). The DIADEM data sets: representative light microscopy images of neuronal morphology to advance automation of digital reconstructions. Neuroinformatics 9, 143-157.

Burgess, R.W., Jucius, T.J., and Ackerman, S.L. (2006). Motor axon guidance of the mammalian trochlear and phrenic nerves: dependence on the netrin receptor Unc5c and modifier loci. J Neurosci 26, 5756-5766.

Camurri, L., Mambetisaeva, E., Davies, D., Parnavelas, J., Sundaresan, V., and Andrews, W. (2005). Evidence for the existence of two Robo3 isoforms with divergent biochemical properties. Molecular and cellular neurosciences 30, 485-493.

Cano, J., Pasik, P., and Pasik, T. (1989). Early postnatal development of the monkey globus pallidus: a Golgi and electron microscopic study. J Comp Neurol 279, 353-367.

Carmona, M.A., Murai, K.K., Wang, L., Roberts, A.J., and Pasquale, E.B. (2009). Glial ephrin-A3 regulates hippocampal dendritic spine morphology and glutamate transport. Proc Natl Acad Sci U S A 106, 12524-12529.

Chang, C., Adler, C.E., Krause, M., Clark, S.G., Gertler, F.B., Tessier-Lavigne, M., and Bargmann, C.I. (2006). MIG-10/lamellipodin and AGE-1/PI3K promote axon guidance and outgrowth in response to slit and netrin. Current biology : CB 16, 854-862.

Chedotal, A. (2007). Slits and their receptors. Advances in experimental medicine and biology 621, 65-80.

Chen, S.X., Cherry, A., Tari, P.K., Podgorski, K., Kwong, Y.K., and Haas, K. (2012). The transcription factor MEF2 directs developmental visually driven functional and structural metaplasticity. Cell 151, 41-55.

Chen, S.X., Tari, P.K., She, K., and Haas, K. (2010). Neurexin-neuroligin cell adhesion complexes contribute to synaptotropic dendritogenesis via growth stabilization mechanisms in vivo. Neuron 67, 967-983.

Chen, Y.M., Wang, Q.J., Hu, H.S., Yu, P.C., Zhu, J., Drewes, G., Piwnica-Worms, H., and Luo, Z.G. (2006). Microtubule affinity-regulating kinase 2 functions downstream of the PAR-3/PAR-6/atypical PKC complex in regulating hippocampal neuronal polarity. Proc Natl Acad Sci U S A 103, 8534-8539.

Chen, Z., Gore, B.B., Long, H., Ma, L., and Tessier-Lavigne, M. (2008). Alternative splicing of the Robo3 axon guidance receptor governs the midline switch from attraction to repulsion. Neuron 58, 325-332.

Cheng, H.J., Nakamoto, M., Bergemann, A.D., and Flanagan, J.G. (1995). Complementary gradients in expression and binding of ELF-1 and Mek4 in development of the topographic retinotectal projection map. Cell 82, 371-381.

Chien, C.B., Rosenthal, D.E., Harris, W.A., and Holt, C.E. (1993). Navigational errors made by growth cones without filopodia in the embryonic Xenopus brain. Neuron 11, 237-251.

Choromanska, A., Chang, S.F., and Yuste, R. (2012). Automatic reconstruction of neural morphologies with multi-scale tracking. Frontiers in neural circuits 6, 25.

Cline, H., and Haas, K. (2008). The regulation of dendritic arbor development and plasticity by glutamatergic synaptic input: a review of the synaptotrophic hypothesis. The Journal of physiology 586, 1509-1517.

Cohen-Cory, S., and Lom, B. (2004). Neurotrophic regulation of retinal ganglion cell synaptic connectivity: from axons and dendrites to synapses. The International journal of developmental biology 48, 947-956.

Colamarino, S.A., and Tessier-Lavigne, M. (1995). The axonal chemoattractant netrin-1 is also a chemorepellent for trochlear motor axons. Cell 81, 621-629.

Colon-Ramos, D.A., Margeta, M.A., and Shen, K. (2007). Glia promote local synaptogenesis through UNC-6 (netrin) signaling in C. elegans. Science 318, 103-106.

Conde, C., and Caceres, A. (2009). Microtubule assembly, organization and dynamics in axons and dendrites. Nature reviews Neuroscience 10, 319-332.

Contractor, A., Rogers, C., Maron, C., Henkemeyer, M., Swanson, G.T., and Heinemann, S.F. (2002). Trans-synaptic Eph receptor-ephrin signaling in hippocampal mossy fiber LTP. Science 296, 1864-1869.

Corset, V., Nguyen-Ba-Charvet, K.T., Forcet, C., Moyse, E., Chedotal, A., and Mehlen, P. (2000). Netrin-1-mediated axon outgrowth and cAMP production requires interaction with adenosine A2b receptor. Nature 407, 747-750.

Costa, E., Davis, J., Grayson, D.R., Guidotti, A., Pappas, G.D., and Pesold, C. (2001). Dendritic spine hypoplasticity and downregulation of reelin and GABAergic tone in schizophrenia vulnerability. Neurobiology of disease 8, 723-742.

Craig, A.M., and Banker, G. (1994). Neuronal polarity. Annu Rev Neurosci 17, 267-310.

Dailey, M.E., and Smith, S.J. (1996). The dynamics of dendritic structure in developing hippocampal slices. J Neurosci 16, 2983-2994.

Dalva, M.B., McClelland, A.C., and Kayser, M.S. (2007). Cell adhesion molecules: signalling functions at the synapse. Nature reviews Neuroscience 8, 206-220.

Dalva, M.B., Takasu, M.A., Lin, M.Z., Shamah, S.M., Hu, L., Gale, N.W., and Greenberg, M.E. (2000). EphB receptors interact with NMDA receptors and regulate excitatory synapse formation. Cell 103, 945-956.

Davis, S., Gale, N.W., Aldrich, T.H., Maisonpierre, P.C., Lhotak, V., Pawson, T., Goldfarb, M., and Yancopoulos, G.D. (1994). Ligands for EPH-related receptor tyrosine kinases that require membrane attachment or clustering for activity. Science 266, 816-819.

de la Torre, J.R., Hopker, V.H., Ming, G.L., Poo, M.M., Tessier-Lavigne, M., Hemmati-Brivanlou, A., and Holt, C.E. (1997). Turning of retinal growth cones in a netrin-1 gradient mediated by the netrin receptor DCC. Neuron 19, 1211-1224.

de Wit, J., and Verhaagen, J. (2003). Role of semaphorins in the adult nervous system. Progress in neurobiology 71, 249-267.

Deiner, M.S., Kennedy, T.E., Fazeli, A., Serafini, T., Tessier-Lavigne, M., and Sretavan, D.W. (1997). Netrin-1 and DCC mediate axon guidance locally at the optic disc: loss of function leads to optic nerve hypoplasia. Neuron 19, 575-589.

Deitch, J.S., and Rubel, E.W. (1984). Afferent influences on brain stem auditory nuclei of the chicken: time course and specificity of dendritic atrophy following deafferentation. J Comp Neurol 229, 66-79.

Denk, W., Strickler, J.H., and Webb, W.W. (1990). Two-photon laser scanning fluorescence microscopy. Science 248, 73-76.

Dent, E.W., Gupton, S.L., and Gertler, F.B. (2011). The growth cone cytoskeleton in axon outgrowth and guidance. Cold Spring Harbor perspectives in biology 3.

Dickson, B.J. (2002). Molecular mechanisms of axon guidance. Science 298, 1959-1964.

Dickson, B.J., and Gilestro, G.F. (2006). Regulation of commissural axon pathfinding by slit and its Robo receptors. Annual review of cell and developmental biology 22, 651-675.

Dimitrova, S., Reissaus, A., and Tavosanis, G. (2008). Slit and Robo regulate dendrite branching and elongation of space-filling neurons in Drosophila. Developmental biology 324, 18-30.

Dotti, C.G., Sullivan, C.A., and Banker, G.A. (1988). The establishment of polarity by hippocampal neurons in culture. J Neurosci 8, 1454-1468.

Dunfield, D., and Haas, K. (2009). Metaplasticity governs natural experience-driven plasticity of nascent embryonic brain circuits. Neuron 64, 240-250.

Espinosa, J.S., Wheeler, D.G., Tsien, R.W., and Luo, L. (2009). Uncoupling dendrite growth and patterning: single-cell knockout analysis of NMDA receptor 2B. Neuron 62, 205-217.

Ewald, R.C., Van Keuren-Jensen, K.R., Aizenman, C.D., and Cline, H.T. (2008). Roles of NR2A and NR2B in the development of dendritic arbor morphology in vivo. J Neurosci 28, 850-861.

Fan, X., Labrador, J.P., Hing, H., and Bashaw, G.J. (2003). Slit stimulation recruits Dock and Pak to the roundabout receptor and increases Rac activity to regulate axon repulsion at the CNS midline. Neuron 40, 113-127.

Fazeli, A., Dickinson, S.L., Hermiston, M.L., Tighe, R.V., Steen, R.G., Small, C.G., Stoeckli, E.T., Keino-Masu, K., Masu, M., Rayburn, H.*, et al.* (1997). Phenotype of mice lacking functional Deleted in colorectal cancer (Dcc) gene. Nature 386, 796-804.

Filosa, A., Paixao, S., Honsek, S.D., Carmona, M.A., Becker, L., Feddersen, B., Gaitanos, L., Rudhard, Y., Schoepfer, R., Klopstock, T.*, et al.* (2009). Neuron-glia communication via EphA4/ephrin-A3 modulates LTP through glial glutamate transport. Nat Neurosci 12, 1285-1292.

Flanagan, J.G., and Vanderhaeghen, P. (1998). The ephrins and Eph receptors in neural development. Annu Rev Neurosci 21, 309-345.

Forsthoefel, D.J., Liebl, E.C., Kolodziej, P.A., and Seeger, M.A. (2005). The Abelson tyrosine kinase, the Trio GEF and Enabled interact with the Netrin receptor Frazzled in Drosophila. Development 132, 1983-1994.

Fox, G.Q., Pappas, G.D., and Purpura, D.P. (1976). Fine structure of growth cones in medullary raphe nuclei in the postnatal cat. Brain research 101, 411-425.

Friedlander, M.J., Stanford, L.R., and Sherman, S.M. (1982). Effects of monocular deprivation on the structure-function relationship of individual neurons in the cat's lateral geniculate nucleus. J Neurosci 2, 321-330.

Fritz, J.L., and VanBerkum, M.F. (2002). Regulation of rho family GTPases is required to prevent axons from crossing the midline. Developmental biology 252, 46-58.

Fu, W.Y., Chen, Y., Sahin, M., Zhao, X.S., Shi, L., Bikoff, J.B., Lai, K.O., Yung, W.H., Fu, A.K., Greenberg, M.E., and Ip, N.Y. (2007). Cdk5 regulates EphA4-mediated dendritic spine

retraction through an ephexin1-dependent mechanism. Nat Neurosci 10, 67-76.

Furrer, M.P., Kim, S., Wolf, B., and Chiba, A. (2003). Robo and Frazzled/DCC mediate dendritic guidance at the CNS midline. Nat Neurosci 6, 223-230.

Furrer, M.P., Vasenkova, I., Kamiyama, D., Rosado, Y., and Chiba, A. (2007). Slit and Robo control the development of dendrites in Drosophila CNS. Development 134, 3795-3804.

Gascon, E., Dayer, A.G., Sauvain, M.O., Potter, G., Jenny, B., De Roo, M., Zgraggen, E., Demaurex, N., Muller, D., and Kiss, J.Z. (2006). GABA regulates dendritic growth by stabilizing lamellipodia in newly generated interneurons of the olfactory bulb. J Neurosci 26, 12956-12966.

Georges, P.C., Hadzimichalis, N.M., Sweet, E.S., and Firestein, B.L. (2008). The yin-yang of dendrite morphology: unity of actin and microtubules. Mol Neurobiol 38, 270-284.

Gillette, T.A., Brown, K.M., and Ascoli, G.A. (2011). The DIADEM metric: comparing multiple reconstructions of the same neuron. Neuroinformatics 9, 233-245.

Gitai, Z., Yu, T.W., Lundquist, E.A., Tessier-Lavigne, M., and Bargmann, C.I. (2003). The netrin receptor UNC-40/DCC stimulates axon attraction and outgrowth through enabled and, in parallel, Rac and UNC-115/AbLIM. Neuron 37, 53-65.

Glaser, E.M., and Vanderloos, H. (1965). A Semi-Automatic Computer-Microscope for the Analysis of Neuronal Morphology. IEEE transactions on bio-medical engineering 12, 22-31.

Godenschwege, T.A., Simpson, J.H., Shan, X., Bashaw, G.J., Goodman, C.S., and Murphey, R.K. (2002). Ectopic expression in the giant fiber system of Drosophila reveals distinct roles for roundabout (Robo), Robo2, and Robo3 in dendritic guidance and synaptic connectivity. J Neurosci 22, 3117-3129.

Goslin, K., and Banker, G. (1989). Experimental observations on the development of polarity by hippocampal neurons in culture. J Cell Biol 108, 1507-1516.

Gotz, M., and Huttner, W.B. (2005). The cell biology of neurogenesis. Nature reviews Molecular cell biology 6, 777-788.

Greenough, W.T., and Volkmar, F.R. (1973). Pattern of dendritic branching in occipital cortex of rats reared in complex environments. Experimental neurology 40, 491-504.

Grueber, W.B., Jan, L.Y., and Jan, Y.N. (2003). Different levels of the homeodomain protein cut regulate distinct dendrite branching patterns of Drosophila multidendritic neurons. Cell 112, 805-818.

Gurdon, J.B., and Hopwood, N. (2000). The introduction of Xenopus laevis into developmental biology: of empire, pregnancy testing and ribosomal genes. The International journal of developmental biology 44, 43-50.

Haas, K., Jensen, K., Sin, W.C., Foa, L., and Cline, H.T. (2002). Targeted electroporation in Xenopus tadpoles in vivo--from single cells to the entire brain. Differentiation 70, 148-154.

Haas, K., Li, J., and Cline, H.T. (2006a). AMPA receptors regulate experience-dependent

dendritic arbor growth in vivo. Proc Natl Acad Sci U S A 103, 12127-12131.

Haas, K., Li, J., and Cline, H.T. (2006b). AMPA receptors regulate experience-dependent dendritic arbor growth in vivo. Proceedings of the National Academy of Sciences of the United States of America 103, 12127-12131.

Haas, K., Sin, W.C., Javaherian, A., Li, Z., and Cline, H.T. (2001). Single-cell electroporation for gene transfer in vivo. Neuron 29, 583-591.

Hansen, M.J., Dallal, G.E., and Flanagan, J.G. (2004). Retinal axon response to ephrin-as shows a graded, concentration-dependent transition from growth promotion to inhibition. Neuron 42, 717-730.

Harris, R., Sabatelli, L.M., and Seeger, M.A. (1996). Guidance cues at the Drosophila CNS midline: identification and characterization of two Drosophila Netrin/UNC-6 homologs. Neuron 17, 217-228.

Hausser, M., Spruston, N., and Stuart, G.J. (2000). Diversity and dynamics of dendritic signaling. Science 290, 739-744.

Henkemeyer, M., Itkis, O.S., Ngo, M., Hickmott, P.W., and Ethell, I.M. (2003). Multiple EphB receptor tyrosine kinases shape dendritic spines in the hippocampus. J Cell Biol 163, 1313-1326.

Hewapathirane, D.S., Dunfield, D., Yen, W., Chen, S., and Haas, K. (2008). In vivo imaging of seizure activity in a novel developmental seizure model. Experimental neurology 211, 480-488.

Higenell, V., Han, S.M., Feldheim, D.A., Scalia, F., and Ruthazer, E.S. (2011). Expression patterns of Ephs and ephrins throughout retinotectal development in Xenopus laevis. Dev Neurobiol.

Himanen, J.P., Chumley, M.J., Lackmann, M., Li, C., Barton, W.A., Jeffrey, P.D., Vearing, C., Geleick, D., Feldheim, D.A., Boyd, A.W.*, et al.* (2004). Repelling class discrimination: ephrin-A5 binds to and activates EphB2 receptor signaling. Nat Neurosci 7, 501-509.

Hivert, B., Liu, Z., Chuang, C.Y., Doherty, P., and Sundaresan, V. (2002). Robo1 and Robo2 are homophilic binding molecules that promote axonal growth. Molecular and cellular neurosciences 21, 534-545.

Hocking, J.C., Hehr, C.L., Bertolesi, G.E., Wu, J.Y., and McFarlane, S. (2010). Distinct roles for Robo2 in the regulation of axon and dendrite growth by retinal ganglion cells. Mech Dev 127, 36-48.

Hocking, J.C., Pollock, N.S., Johnston, J., Wilson, R.J., Shankar, A., and McFarlane, S. (2012). Neural activity and branching of embryonic retinal ganglion cell dendrites. Mech Dev 129, 125-135.

Hofmann, K., and Tschopp, J. (1995). The death domain motif found in Fas (Apo-1) and TNF receptor is present in proteins involved in apoptosis and axonal guidance. FEBS letters 371, 321-323.

Hong, K., Hinck, L., Nishiyama, M., Poo, M.M., Tessier-Lavigne, M., and Stein, E. (1999). A ligand-gated association between cytoplasmic domains of UNC5 and DCC family receptors converts netrin-induced growth cone attraction to repulsion. Cell 97, 927-941.

Hoogenraad, C.C., Milstein, A.D., Ethell, I.M., Henkemeyer, M., and Sheng, M. (2005). GRIP1 controls dendrite morphogenesis by regulating EphB receptor trafficking. Nat Neurosci 8, 906-915.

Horch, H.W., Kruttgen, A., Portbury, S.D., and Katz, L.C. (1999). Destabilization of cortical dendrites and spines by BDNF. Neuron 23, 353-364.

Hossain, S., Hewapathirane, D.S., and Haas, K. (2012). Dynamic morphometrics reveals contributions of dendritic growth cones and filopodia to dendritogenesis in the intact and awake embryonic brain. Dev Neurobiol 72, 615-627.

Irie, F., and Yamaguchi, Y. (2002). EphB receptors regulate dendritic spine development via intersectin, Cdc42 and N-WASP. Nat Neurosci 5, 1117-1118.

Ishii, N., Wadsworth, W.G., Stern, B.D., Culotti, J.G., and Hedgecock, E.M. (1992). UNC-6, a laminin-related protein, guides cell and pioneer axon migrations in C. elegans. Neuron 9, 873-881.

Jaffe, A.B., and Hall, A. (2005). Rho GTPases: biochemistry and biology. Annual review of cell and developmental biology 21, 247-269.

Jan, Y.N., and Jan, L.Y. (2010). Branching out: mechanisms of dendritic arborization. Nature reviews Neuroscience 11, 316-328.

Jarjour, A.A., Bull, S.J., Almasieh, M., Rajasekharan, S., Baker, K.A., Mui, J., Antel, J.P., Di Polo, A., and Kennedy, T.E. (2008). Maintenance of axo-oligodendroglial paranodal junctions requires DCC and netrin-1. J Neurosci 28, 11003-11014.

Jhaveri, D., Saharan, S., Sen, A., and Rodrigues, V. (2004). Positioning sensory terminals in the olfactory lobe of Drosophila by Robo signaling. Development 131, 1903-1912.

Jiang, H., Guo, W., Liang, X., and Rao, Y. (2005). Both the establishment and the maintenance of neuronal polarity require active mechanisms: critical roles of GSK-3beta and its upstream regulators. Cell 120, 123-135.

Jinushi-Nakao, S., Arvind, R., Amikura, R., Kinameri, E., Liu, A.W., and Moore, A.W. (2007). Knot/Collier and cut control different aspects of dendrite cytoskeleton and synergize to define final arbor shape. Neuron 56, 963-978.

Jones, C.A., London, N.R., Chen, H., Park, K.W., Sauvaget, D., Stockton, R.A., Wythe, J.D., Suh, W., Larrieu-Lahargue, F., Mukouyama, Y.S.*, et al.* (2008). Robo4 stabilizes the vascular network by inhibiting pathologic angiogenesis and endothelial hyperpermeability. Nature medicine 14, 448-453.

Jontes, J.D., and Smith, S.J. (2000). Filopodia, spines, and the generation of synaptic diversity. Neuron 27, 11-14.

Jurney, W.M., Gallo, G., Letourneau, P.C., and McLoon, S.C. (2002). Rac1-mediated endocytosis during ephrin-A2- and semaphorin 3A-induced growth cone collapse. J Neurosci 22, 6019-6028.

Kantor, D.B., Chivatakarn, O., Peer, K.L., Oster, S.F., Inatani, M., Hansen, M.J., Flanagan, J.G., Yamaguchi, Y., Sretavan, D.W., Giger, R.J., and Kolodkin, A.L. (2004). Semaphorin 5A is a bifunctional axon guidance cue regulated by heparan and chondroitin sulfate proteoglycans. Neuron 44, 961-975.

Kaufmann, W.E., and Moser, H.W. (2000). Dendritic anomalies in disorders associated with mental retardation. Cereb Cortex 10, 981-991.

Kayser, M.S., McClelland, A.C., Hughes, E.G., and Dalva, M.B. (2006). Intracellular and trans-synaptic regulation of glutamatergic synaptogenesis by EphB receptors. J Neurosci 26, 12152-12164.

Kayser, M.S., Nolt, M.J., and Dalva, M.B. (2008). EphB receptors couple dendritic filopodia motility to synapse formation. Neuron 59, 56-69.

Keleman, K., and Dickson, B.J. (2001). Short- and long-range repulsion by the Drosophila Unc5 netrin receptor. Neuron 32, 605-617.

Keleman, K., Rajagopalan, S., Cleppien, D., Teis, D., Paiha, K., Huber, L.A., Technau, G.M., and Dickson, B.J. (2002). Comm sorts robo to control axon guidance at the Drosophila midline. Cell 110, 415-427.

Keleman, K., Ribeiro, C., and Dickson, B.J. (2005). Comm function in commissural axon guidance: cell-autonomous sorting of Robo in vivo. Nat Neurosci 8, 156-163.

Kemphues, K. (2000). PARsing embryonic polarity. Cell 101, 345-348.

Kennedy, T.E., Serafini, T., de la Torre, J.R., and Tessier-Lavigne, M. (1994). Netrins are diffusible chemotropic factors for commissural axons in the embryonic spinal cord. Cell 78, 425-435.

Kennedy, T.E., Wang, H., Marshall, W., and Tessier-Lavigne, M. (2006). Axon guidance by diffusible chemoattractants: a gradient of netrin protein in the developing spinal cord. J Neurosci 26, 8866-8874.

Kidd, T., Bland, K.S., and Goodman, C.S. (1999). Slit is the midline repellent for the robo receptor in Drosophila. Cell 96, 785-794.

Kim, M.D., Jan, L.Y., and Jan, Y.N. (2006a). The bHLH-PAS protein Spineless is necessary for the diversification of dendrite morphology of Drosophila dendritic arborization neurons. Genes Dev 20, 2806-2819.

Kim, S., Burette, A., Chung, H.S., Kwon, S.K., Woo, J., Lee, H.W., Kim, K., Kim, H., Weinberg, R.J., and Kim, E. (2006b). NGL family PSD-95-interacting adhesion molecules regulate excitatory synapse formation. Nat Neurosci 9, 1294-1301.

Kolodkin, A.L., Matthes, D.J., and Goodman, C.S. (1993). The semaphorin genes encode a

family of transmembrane and secreted growth cone guidance molecules. Cell 75, 1389-1399.

Kolodkin, A.L., Matthes, D.J., O'Connor, T.P., Patel, N.H., Admon, A., Bentley, D., and Goodman, C.S. (1992). Fasciclin IV: sequence, expression, and function during growth cone guidance in the grasshopper embryo. Neuron 9, 831-845.

Komiyama, T., Sweeney, L.B., Schuldiner, O., Garcia, K.C., and Luo, L. (2007). Graded expression of semaphorin-1a cell-autonomously directs dendritic targeting of olfactory projection neurons. Cell 128, 399-410.

Konur, S., and Ghosh, A. (2005). Calcium signaling and the control of dendritic development. Neuron 46, 401-405.

Korobova, F., and Svitkina, T. (2010). Molecular architecture of synaptic actin cytoskeleton in hippocampal neurons reveals a mechanism of dendritic spine morphogenesis. Molecular biology of the cell 21, 165-176.

Kosik, K.S., and Finch, E.A. (1987). MAP2 and tau segregate into dendritic and axonal domains after the elaboration of morphologically distinct neurites: an immunocytochemical study of cultured rat cerebrum. J Neurosci 7, 3142-3153.

Lalli, G. (2014). Regulation of neuronal polarity. Experimental cell research 328, 267-275.

Lazar, G. (1973). The development of the optic tectum in Xenopus laevis: a Golgi study. Journal of anatomy 116, 347-355.

Lee, T., Winter, C., Marticke, S.S., Lee, A., and Luo, L. (2000). Essential roles of Drosophila RhoA in the regulation of neuroblast proliferation and dendritic but not axonal morphogenesis. Neuron 25, 307-316.

Li, W., Wang, F., Menut, L., and Gao, F.B. (2004). BTB/POZ-zinc finger protein abrupt suppresses dendritic branching in a neuronal subtype-specific and dosage-dependent manner. Neuron 43, 823-834.

Li, Z., Van Aelst, L., and Cline, H.T. (2000). Rho GTPases regulate distinct aspects of dendritic arbor growth in Xenopus central neurons in vivo. Nat Neurosci 3, 217-225.

Libersat, F., and Duch, C. (2002). Morphometric analysis of dendritic remodeling in an identified motoneuron during postembryonic development. J Comp Neurol 450, 153-166.

Lim, B.K., Cho, S.J., Sumbre, G., and Poo, M.M. (2010). Region-specific contribution of ephrin-B and Wnt signaling to receptive field plasticity in developing optic tectum. Neuron 65, 899-911.

Lim, B.K., Matsuda, N., and Poo, M.M. (2008a). Ephrin-B reverse signaling promotes structural and functional synaptic maturation in vivo. Nat Neurosci 11, 160-169.

Lim, Y.S., McLaughlin, T., Sung, T.C., Santiago, A., Lee, K.F., and O'Leary, D.D. (2008b). p75(NTR) mediates ephrin-A reverse signaling required for axon repulsion and mapping. Neuron 59, 746-758.

Lin, J.C., Ho, W.H., Gurney, A., and Rosenthal, A. (2003). The netrin-G1 ligand NGL-1

promotes the outgrowth of thalamocortical axons. Nat Neurosci 6, 1270-1276.

Liu, X.F., Tari, P.K., and Haas, K. (2009). PKM zeta restricts dendritic arbor growth by filopodial and branch stabilization within the intact and awake developing brain. J Neurosci 29, 12229-12235.

Lom, B., and Cohen-Cory, S. (1999). Brain-derived neurotrophic factor differentially regulates retinal ganglion cell dendritic and axonal arborization in vivo. J Neurosci 19, 9928-9938.

Long, H., Sabatier, C., Ma, L., Plump, A., Yuan, W., Ornitz, D.M., Tamada, A., Murakami, F., Goodman, C.S., and Tessier-Lavigne, M. (2004). Conserved roles for Slit and Robo proteins in midline commissural axon guidance. Neuron 42, 213-223.

Longair, M.H., Baker, D.A., and Armstrong, J.D. (2011). Simple Neurite Tracer: open source software for reconstruction, visualization and analysis of neuronal processes. Bioinformatics 27, 2453-2454.

Lowery, L.A., and Van Vactor, D. (2009). The trip of the tip: understanding the growth cone machinery. Nature reviews Molecular cell biology 10, 332-343.

Lu, J., Fiala, J.C., and Lichtman, J.W. (2009). Semi-automated reconstruction of neural processes from large numbers of fluorescence images. PloS one 4, e5655.

Lund, J.S., Holbach, S.M., and Chung, W.W. (1991). Postnatal development of thalamic recipient neurons in the monkey striate cortex: II. Influence of afferent driving on spine acquisition and dendritic growth of layer 4C spiny stellate neurons. J Comp Neurol 309, 129-140.

Ly, A., Nikolaev, A., Suresh, G., Zheng, Y., Tessier-Lavigne, M., and Stein, E. (2008). DSCAM is a netrin receptor that collaborates with DCC in mediating turning responses to netrin-1. Cell 133, 1241-1254.

Maletic-Savatic, M., Malinow, R., and Svoboda, K. (1999). Rapid dendritic morphogenesis in CA1 hippocampal dendrites induced by synaptic activity. Science 283, 1923-1927.

Mambetisaeva, E.T., Andrews, W., Camurri, L., Annan, A., and Sundaresan, V. (2005). Robo family of proteins exhibit differential expression in mouse spinal cord and Robo-Slit interaction is required for midline crossing in vertebrate spinal cord. Developmental dynamics : an official publication of the American Association of Anatomists 233, 41-51.

Mann, F., Harris, W.A., and Holt, C.E. (2004). New views on retinal axon development: a navigation guide. The International journal of developmental biology 48, 957-964.

Mann, F., Ray, S., Harris, W., and Holt, C. (2002). Topographic mapping in dorsoventral axis of the Xenopus retinotectal system depends on signaling through ephrin-B ligands. Neuron 35, 461-473.

Marler, K.J., Becker-Barroso, E., Martinez, A., Llovera, M., Wentzel, C., Poopalasundaram, S., Hindges, R., Soriano, E., Comella, J., and Drescher, U. (2008). A TrkB/EphrinA interaction controls retinal axon branching and synaptogenesis. J Neurosci 28, 12700-12712.

Marsick, B.M., Flynn, K.C., Santiago-Medina, M., Bamburg, J.R., and Letourneau, P.C. (2010). Activation of ADF/cofilin mediates attractive growth cone turning toward nerve growth factor and netrin-1. Dev Neurobiol 70, 565-588.

Mason, C., and Erskine, L. (2000). Growth cone form, behavior, and interactions in vivo: retinal axon pathfinding as a model. Journal of neurobiology 44, 260-270.

Mason, C.A., and Wang, L.C. (1997). Growth cone form is behavior-specific and, consequently, position-specific along the retinal axon pathway. J Neurosci 17, 1086-1100.

Mathers, L.H., Jr. (1977). Postnatal maturation of neurons in the rabbit superior colliculus. J Comp Neurol 173, 439-456.

Mathers, L.H., Jr. (1979). Postnatal dendritic development in the rabbit visual cortex. Brain research 168, 21-29.

Mattila, P.K., and Lappalainen, P. (2008). Filopodia: molecular architecture and cellular functions. Nature reviews Molecular cell biology 9, 446-454.

Matus, A., Bernhardt, R., and Hugh-Jones, T. (1981). High molecular weight microtubule-associated proteins are preferentially associated with dendritic microtubules in brain. Proc Natl Acad Sci U S A 78, 3010-3014.

Matus, D.Q., Pang, K., Marlow, H., Dunn, C.W., Thomsen, G.H., and Martindale, M.Q. (2006). Molecular evidence for deep evolutionary roots of bilaterality in animal development. Proc Natl Acad Sci U S A 103, 11195-11200.

McAllister, A.K. (2000). Cellular and molecular mechanisms of dendrite growth. Cereb Cortex 10, 963-973.

McAllister, A.K., Katz, L.C., and Lo, D.C. (1997). Opposing roles for endogenous BDNF and NT-3 in regulating cortical dendritic growth. Neuron 18, 767-778.

McAllister, A.K., Lo, D.C., and Katz, L.C. (1995). Neurotrophins regulate dendritic growth in developing visual cortex. Neuron 15, 791-803.

McLaughlin, T., and O'Leary, D.D. (2005). Molecular gradients and development of retinotopic maps. Annu Rev Neurosci 28, 327-355.

McMullen, N.T., Goldberger, B., and Glaser, E.M. (1988). Postnatal development of lamina III/IV nonpyramidal neurons in rabbit auditory cortex: quantitative and spatial analyses of Golgi-impregnated material. J Comp Neurol 278, 139-155.

Mehlen, P., and Furne, C. (2005). Netrin-1: when a neuronal guidance cue turns out to be a regulator of tumorigenesis. Cellular and molecular life sciences : CMLS 62, 2599-2616.

Meijering, E. (2010). Neuron tracing in perspective. Cytometry Part A : the journal of the International Society for Analytical Cytology 77, 693-704.

Meijering, E., Jacob, M., Sarria, J.C., Steiner, P., Hirling, H., and Unser, M. (2004). Design and validation of a tool for neurite tracing and analysis in fluorescence microscopy images.

Cytometry Part A : the journal of the International Society for Analytical Cytology 58, 167-176.

Miller, M. (1981). Maturation of rat visual cortex. I. A quantitative study of Golgi-impregnated pyramidal neurons. Journal of neurocytology 10, 859-878.

Miller, M., and Peters, A. (1981). Maturation of rat visual cortex. II. A combined Golgi-electron microscope study of pyramidal neurons. J Comp Neurol 203, 555-573.

Moore, A.W., Jan, L.Y., and Jan, Y.N. (2002). hamlet, a binary genetic switch between single- and multiple- dendrite neuron morphology. Science 297, 1355-1358.

Mumm, J.S., Williams, P.R., Godinho, L., Koerber, A., Pittman, A.J., Roeser, T., Chien, C.B., Baier, H., and Wong, R.O. (2006). In vivo imaging reveals dendritic targeting of laminated afferents by zebrafish retinal ganglion cells. Neuron 52, 609-621.

Munz, M., Gobert, D., Schohl, A., Poquerusse, J., Podgorski, K., Spratt, P., and Ruthazer, E.S. (2014). Rapid Hebbian axonal remodeling mediated by visual stimulation. Science 344, 904-909.

Murai, K.K., and Pasquale, E.B. (2003). 'Eph'ective signaling: forward, reverse and crosstalk. Journal of cell science 116, 2823-2832.

Myatt, D.R., Hadlington, T., Ascoli, G.A., and Nasuto, S.J. (2012). Neuromantic - from semi-manual to semi-automatic reconstruction of neuron morphology. Frontiers in neuroinformatics 6, 4.

Nakamura, F., Kalb, R.G., and Strittmatter, S.M. (2000). Molecular basis of semaphorin-mediated axon guidance. Journal of neurobiology 44, 219-229.

Nakamura, F., Tanaka, M., Takahashi, T., Kalb, R.G., and Strittmatter, S.M. (1998). Neuropilin-1 extracellular domains mediate semaphorin D/III-induced growth cone collapse. Neuron 21, 1093-1100.

Nakashiba, T., Ikeda, T., Nishimura, S., Tashiro, K., Honjo, T., Culotti, J.G., and Itohara, S. (2000). Netrin-G1: a novel glycosyl phosphatidylinositol-linked mammalian netrin that is functionally divergent from classical netrins. J Neurosci 20, 6540-6550.

Nakayama, A.Y., Harms, M.B., and Luo, L. (2000). Small GTPases Rac and Rho in the maintenance of dendritic spines and branches in hippocampal pyramidal neurons. J Neurosci 20, 5329-5338.

Nedivi, E., Wu, G.Y., and Cline, H.T. (1998). Promotion of dendritic growth by CPG15, an activity-induced signaling molecule. Science 281, 1863-1866.

Negishi, M., and Katoh, H. (2005). Rho family GTPases and dendrite plasticity. The Neuroscientist : a review journal bringing neurobiology, neurology and psychiatry 11, 187-191.

Nelson, R., Famiglietti, E.V., Jr., and Kolb, H. (1978). Intracellular staining reveals different levels of stratification for on- and off-center ganglion cells in cat retina. Journal of neurophysiology 41, 472-483.

Nguyen Ba-Charvet, K.T., Brose, K., Ma, L., Wang, K.H., Marillat, V., Sotelo, C., Tessier-Lavigne, M., and Chedotal, A. (2001). Diversity and specificity of actions of Slit2 proteolytic fragments in axon guidance. J Neurosci 21, 4281-4289.

Niell, C.M., Meyer, M.P., and Smith, S.J. (2004). In vivo imaging of synapse formation on a growing dendritic arbor. Nat Neurosci 7, 254-260.

Nieuwkoop, P.D., and Faber, J. (1994). Normal table of Xenopus laevis (Daudin) : a systematical and chronological survey of the development from the fertilized egg till the end of metamorphosis (New York: Garland Pub.).

Nishimura, T., Yamaguchi, T., Kato, K., Yoshizawa, M., Nabeshima, Y., Ohno, S., Hoshino, M., and Kaibuchi, K. (2005). PAR-6-PAR-3 mediates Cdc42-induced Rac activation through the Rac GEFs STEF/Tiam1. Nature cell biology 7, 270-277.

Parrish, J.Z., Emoto, K., Kim, M.D., and Jan, Y.N. (2007). Mechanisms that regulate establishment, maintenance, and remodeling of dendritic fields. Annu Rev Neurosci 30, 399-423.

Parrish, J.Z., Kim, M.D., Jan, L.Y., and Jan, Y.N. (2006). Genome-wide analyses identify transcription factors required for proper morphogenesis of Drosophila sensory neuron dendrites. Genes Dev 20, 820-835.

Pasterkamp, R.J. (2012). Getting neural circuits into shape with semaphorins. Nature reviews Neuroscience 13, 605-618.

Patapoutian, A., and Reichardt, L.F. (2001). Trk receptors: mediators of neurotrophin action. Current opinion in neurobiology 11, 272-280.

Peng, H., Long, F., Zhao, T., and Myers, E. (2011). Proof-editing is the bottleneck of 3D neuron reconstruction: the problem and solutions. Neuroinformatics 9, 103-105.

Peng, H., Ruan, Z., Atasoy, D., and Sternson, S. (2010). Automatic reconstruction of 3D neuron structures using a graph-augmented deformable model. Bioinformatics 26, i38-46.

Penzes, P., Beeser, A., Chernoff, J., Schiller, M.R., Eipper, B.A., Mains, R.E., and Huganir, R.L. (2003). Rapid induction of dendritic spine morphogenesis by trans-synaptic ephrinB-EphB receptor activation of the Rho-GEF kalirin. Neuron 37, 263-274.

Piper, M., Anderson, R., Dwivedy, A., Weinl, C., van Horck, F., Leung, K.M., Cogill, E., and Holt, C. (2006). Signaling mechanisms underlying Slit2-induced collapse of Xenopus retinal growth cones. Neuron 49, 215-228.

Polleux, F., Morrow, T., and Ghosh, A. (2000). Semaphorin 3A is a chemoattractant for cortical apical dendrites. Nature 404, 567-573.

Portera-Cailliau, C., Pan, D.T., and Yuste, R. (2003). Activity-regulated dynamic behavior of early dendritic protrusions: evidence for different types of dendritic filopodia. J Neurosci 23, 7129-7142.

Pratt, R.L., and Kinch, M.S. (2002). Activation of the EphA2 tyrosine kinase stimulates the

MAP/ERK kinase signaling cascade. Oncogene 21, 7690-7699.

Purpura, D.P. (1975). Normal and aberrant neuronal development in the cerebral cortex of human fetus and young infant. UCLA forum in medical sciences, 141-169.

Purves, D., and Hume, R.I. (1981). The relation of postsynaptic geometry to the number of presynaptic axons that innervate autonomic ganglion cells. J Neurosci 1, 441-452.

Rajan, I., and Cline, H.T. (1998). Glutamate receptor activity is required for normal development of tectal cell dendrites in vivo. J Neurosci 18, 7836-7846.

Rajan, I., Witte, S., and Cline, H.T. (1999). NMDA receptor activity stabilizes presynaptic retinotectal axons and postsynaptic optic tectal cell dendrites in vivo. Journal of neurobiology 38, 357-368.

Rajasekharan, S., and Kennedy, T.E. (2009). The netrin protein family. Genome biology 10, 239.

Rakic, P. (1975). Role of cell interaction in development of dendritic patterns. Advances in neurology 12, 117-134.

Redmond, L., Kashani, A.H., and Ghosh, A. (2002). Calcium regulation of dendritic growth via CaM kinase IV and CREB-mediated transcription. Neuron 34, 999-1010.

Rhee, J., Mahfooz, N.S., Arregui, C., Lilien, J., Balsamo, J., and VanBerkum, M.F. (2002). Activation of the repulsive receptor Roundabout inhibits N-cadherin-mediated cell adhesion. Nature cell biology 4, 798-805.

Rothberg, J.M., Hartley, D.A., Walther, Z., and Artavanis-Tsakonas, S. (1988). slit: an EGF-homologous locus of D. melanogaster involved in the development of the embryonic central nervous system. Cell 55, 1047-1059.

Rothberg, J.M., Jacobs, J.R., Goodman, C.S., and Artavanis-Tsakonas, S. (1990). slit: an extracellular protein necessary for development of midline glia and commissural axon pathways contains both EGF and LRR domains. Genes Dev 4, 2169-2187.

Ruchhoeft, M.L., Ohnuma, S., McNeill, L., Holt, C.E., and Harris, W.A. (1999). The neuronal architecture of Xenopus retinal ganglion cells is sculpted by rho-family GTPases in vivo. J Neurosci 19, 8454-8463.

Ruit, K.G., Osborne, P.A., Schmidt, R.E., Johnson, E.M., Jr., and Snider, W.D. (1990). Nerve growth factor regulates sympathetic ganglion cell morphology and survival in the adult mouse. J Neurosci 10, 2412-2419.

Sabatier, C., Plump, A.S., Le, M., Brose, K., Tamada, A., Murakami, F., Lee, E.Y., and Tessier-Lavigne, M. (2004). The divergent Robo family protein rig-1/Robo3 is a negative regulator of slit responsiveness required for midline crossing by commissural axons. Cell 117, 157-169.

Sabry, J.H., O'Connor, T.P., Evans, L., Toroian-Raymond, A., Kirschner, M., and Bentley, D. (1991). Microtubule behavior during guidance of pioneer neuron growth cones in situ. J Cell Biol 115, 381-395.

Schaupp, A., Sabet, O., Dudanova, I., Ponserre, M., Bastiaens, P., and Klein, R. (2014). The composition of EphB2 clusters determines the strength in the cellular repulsion response. J Cell Biol 204, 409-422.

Schmitt, A.M., Shi, J., Wolf, A.M., Lu, C.C., King, L.A., and Zou, Y. (2006). Wnt-Ryk signalling mediates medial-lateral retinotectal topographic mapping. Nature 439, 31-37.

Schwartz, P.M., Borghesani, P.R., Levy, R.L., Pomeroy, S.L., and Segal, R.A. (1997). Abnormal cerebellar development and foliation in BDNF-/- mice reveals a role for neurotrophins in CNS patterning. Neuron 19, 269-281.

Scott, E.K., and Luo, L. (2001). How do dendrites take their shape? Nat Neurosci 4, 359-365.

Seeger, M., Tear, G., Ferres-Marco, D., and Goodman, C.S. (1993). Mutations affecting growth cone guidance in Drosophila: genes necessary for guidance toward or away from the midline. Neuron 10, 409-426.

Segura, I., Essmann, C.L., Weinges, S., and Acker-Palmer, A. (2007). Grb4 and GIT1 transduce ephrinB reverse signals modulating spine morphogenesis and synapse formation. Nat Neurosci 10, 301-310.

Serafini, T., Colamarino, S.A., Leonardo, E.D., Wang, H., Beddington, R., Skarnes, W.C., and Tessier-Lavigne, M. (1996). Netrin-1 is required for commissural axon guidance in the developing vertebrate nervous system. Cell 87, 1001-1014.

Serafini, T., Kennedy, T.E., Galko, M.J., Mirzayan, C., Jessell, T.M., and Tessier-Lavigne, M. (1994). The netrins define a family of axon outgrowth-promoting proteins homologous to C. elegans UNC-6. Cell 78, 409-424.

Shamah, S.M., Lin, M.Z., Goldberg, J.L., Estrach, S., Sahin, M., Hu, L., Bazalakova, M., Neve, R.L., Corfas, G., Debant, A., and Greenberg, M.E. (2001). EphA receptors regulate growth cone dynamics through the novel guanine nucleotide exchange factor ephexin. Cell 105, 233-244.

Shewan, D., Dwivedy, A., Anderson, R., and Holt, C.E. (2002). Age-related changes underlie switch in netrin-1 responsiveness as growth cones advance along visual pathway. Nat Neurosci 5, 955-962.

Shi, S.H., Jan, L.Y., and Jan, Y.N. (2003). Hippocampal neuronal polarity specified by spatially localized mPar3/mPar6 and PI 3-kinase activity. Cell 112, 63-75.

Shimada, A., Mason, C.A., and Morrison, M.E. (1998). TrkB signaling modulates spine density and morphology independent of dendrite structure in cultured neonatal Purkinje cells. J Neurosci 18, 8559-8570.

Sholl, D.A. (1953). Dendritic organization in the neurons of the visual and motor cortices of the cat. Journal of anatomy 87, 387-406.

Sin, W.C., Haas, K., Ruthazer, E.S., and Cline, H.T. (2002). Dendrite growth increased by visual activity requires NMDA receptor and Rho GTPases. Nature 419, 475-480.

Smith, Z.D., Gray, L., and Rubel, E.W. (1983). Afferent influences on brainstem auditory nuclei

of the chicken: n. laminaris dendritic length following monaural conductive hearing loss. J Comp Neurol 220, 199-205.

Snider, W.D. (1988). Nerve growth factor enhances dendritic arborization of sympathetic ganglion cells in developing mammals. J Neurosci 8, 2628-2634.

Song, H., and Poo, M. (2001). The cell biology of neuronal navigation. Nature cell biology 3, E81-88.

Sotelo, C. (1975). Anatomical, physiological and biochemical studies of the cerebellum from mutant mice. II. Morphological study of cerebellar cortical neurons and circuits in the weaver mouse. Brain research 94, 19-44.

Sperry, R.W. (1963). Chemoaffinity in the Orderly Growth of Nerve Fiber Patterns and Connections. Proc Natl Acad Sci U S A 50, 703-710.

Stein, E., Cerretti, D.P., and Daniel, T.O. (1996). Ligand activation of ELK receptor tyrosine kinase promotes its association with Grb10 and Grb2 in vascular endothelial cells. The Journal of biological chemistry 271, 23588-23593.

Stein, E., Huynh-Do, U., Lane, A.A., Cerretti, D.P., and Daniel, T.O. (1998). Nck recruitment to Eph receptor, EphB1/ELK, couples ligand activation to c-Jun kinase. The Journal of biological chemistry 273, 1303-1308.

Stein, E., and Tessier-Lavigne, M. (2001). Hierarchical organization of guidance receptors: silencing of netrin attraction by slit through a Robo/DCC receptor complex. Science 291, 1928-1938.

Strasser, G.A., Rahim, N.A., VanderWaal, K.E., Gertler, F.B., and Lanier, L.M. (2004). Arp2/3 is a negative regulator of growth cone translocation. Neuron 43, 81-94.

Straznicky, K., and Gaze, R.M. (1972). The development of the tectum in Xenopus laevis: an autoradiographic study. Journal of embryology and experimental morphology 28, 87-115.

Sugimura, K., Satoh, D., Estes, P., Crews, S., and Uemura, T. (2004). Development of morphological diversity of dendrites in Drosophila by the BTB-zinc finger protein abrupt. Neuron 43, 809-822.

Takahashi, T., Fournier, A., Nakamura, F., Wang, L.H., Murakami, Y., Kalb, R.G., Fujisawa, H., and Strittmatter, S.M. (1999). Plexin-neuropilin-1 complexes form functional semaphorin-3A receptors. Cell 99, 59-69.

Takasu, M.A., Dalva, M.B., Zigmond, R.E., and Greenberg, M.E. (2002). Modulation of NMDA receptor-dependent calcium influx and gene expression through EphB receptors. Science 295, 491-495.

Tamamaki, N. (1999). Development of afferent fiber lamination in the infrapyramidal blade of the rat dentate gyrus. J Comp Neurol 411, 257-266.

Tan, Z.J., Peng, Y., Song, H.L., Zheng, J.J., and Yu, X. (2010). N-cadherin-dependent neuron-neuron interaction is required for the maintenance of activity-induced dendrite growth. Proc Natl

Acad Sci U S A 107, 9873-9878.

Tanaka, M., Ohashi, R., Nakamura, R., Shinmura, K., Kamo, T., Sakai, R., and Sugimura, H. (2004). Tiam1 mediates neurite outgrowth induced by ephrin-B1 and EphA2. The EMBO journal 23, 1075-1088.

Tear, G., Harris, R., Sutaria, S., Kilomanski, K., Goodman, C.S., and Seeger, M.A. (1996). commissureless controls growth cone guidance across the CNS midline in Drosophila and encodes a novel membrane protein. Neuron 16, 501-514.

Threadgill, R., Bobb, K., and Ghosh, A. (1997). Regulation of dendritic growth and remodeling by Rho, Rac, and Cdc42. Neuron 19, 625-634.

Tieman, S.B., Zec, N., and Tieman, D.G. (1995). Dark-rearing fails to affect the basal dendritic fields of layer 3 pyramidal cells in the kitten's visual cortex. Brain research Developmental brain research 84, 39-45.

Trachtenberg, J.T., Chen, B.E., Knott, G.W., Feng, G., Sanes, J.R., Welker, E., and Svoboda, K. (2002). Long-term in vivo imaging of experience-dependent synaptic plasticity in adult cortex. Nature 420, 788-794.

Triplett, J.W., and Feldheim, D.A. (2012). Eph and ephrin signaling in the formation of topographic maps. Seminars in cell & developmental biology 23, 7-15.

Tytell, M., Brady, S.T., and Lasek, R.J. (1984). Axonal transport of a subclass of tau proteins: evidence for the regional differentiation of microtubules in neurons. Proc Natl Acad Sci U S A 81, 1570-1574.

Vaughn, J.E., Barber, R.P., and Sims, T.J. (1988). Dendritic development and preferential growth into synaptogenic fields: a quantitative study of Golgi-impregnated spinal motor neurons. Synapse 2, 69-78.

Vaughn, J.E., Henrikson, C.K., and Grieshaber, J.A. (1974). A quantitative study of synapses on motor neuron dendritic growth cones in developing mouse spinal cord. J Cell Biol 60, 664-672.

Volkmar, F.R., and Greenough, W.T. (1972). Rearing complexity affects branching of dendrites in the visual cortex of the rat. Science 176, 1445-1447.

Wahl, S., Barth, H., Ciossek, T., Aktories, K., and Mueller, B.K. (2000). Ephrin-A5 induces collapse of growth cones by activating Rho and Rho kinase. J Cell Biol 149, 263-270.

Wang, T., Liu, Y., Xu, X.H., Deng, C.Y., Wu, K.Y., Zhu, J., Fu, X.Q., He, M., and Luo, Z.G. (2011). Lgl1 activation of rab10 promotes axonal membrane trafficking underlying neuronal polarization. Developmental cell 21, 431-444.

Whitford, K.L., Marillat, V., Stein, E., Goodman, C.S., Tessier-Lavigne, M., Chedotal, A., and Ghosh, A. (2002). Regulation of cortical dendrite development by Slit-Robo interactions. Neuron 33, 47-61.

Wills, Z., Emerson, M., Rusch, J., Bikoff, J., Baum, B., Perrimon, N., and Van Vactor, D. (2002). A Drosophila homolog of cyclase-associated proteins collaborates with the Abl tyrosine kinase

to control midline axon pathfinding. Neuron 36, 611-622.

Wimmer-Kleikamp, S.H., Janes, P.W., Squire, A., Bastiaens, P.I., and Lackmann, M. (2004). Recruitment of Eph receptors into signaling clusters does not require ephrin contact. J Cell Biol 164, 661-666.

Wong, K., Ren, X.R., Huang, Y.Z., Xie, Y., Liu, G., Saito, H., Tang, H., Wen, L., Brady-Kalnay, S.M., Mei, L.*, et al.* (2001). Signal transduction in neuronal migration: roles of GTPase activating proteins and the small GTPase Cdc42 in the Slit-Robo pathway. Cell 107, 209-221.

Wong, R.O., and Ghosh, A. (2002). Activity-dependent regulation of dendritic growth and patterning. Nature reviews Neuroscience 3, 803-812.

Woo, S., Rowan, D.J., and Gomez, T.M. (2009). Retinotopic mapping requires focal adhesion kinase-mediated regulation of growth cone adhesion. J Neurosci 29, 13981-13991.

Wu, G., Malinow, R., and Cline, H.T. (1996). Maturation of a central glutamatergic synapse. Science 274, 972-976.

Wu, G.Y., and Cline, H.T. (1998). Stabilization of dendritic arbor structure in vivo by CaMKII. Science 279, 222-226.

Wu, G.Y., and Cline, H.T. (2003). Time-lapse in vivo imaging of the morphological development of Xenopus optic tectal interneurons. J Comp Neurol 459, 392-406.

Wu, G.Y., Zou, D.J., Rajan, I., and Cline, H. (1999). Dendritic dynamics in vivo change during neuronal maturation. J Neurosci 19, 4472-4483.

Xiao, T., Staub, W., Robles, E., Gosse, N.J., Cole, G.J., and Baier, H. (2011). Assembly of lamina-specific neuronal connections by slit bound to type IV collagen. Cell 146, 164-176.

Xu, N.J., and Henkemeyer, M. (2012). Ephrin reverse signaling in axon guidance and synaptogenesis. Seminars in cell & developmental biology 23, 58-64.

Xu, N.J., Sun, S., Gibson, J.R., and Henkemeyer, M. (2011). A dual shaping mechanism for postsynaptic ephrin-B3 as a receptor that sculpts dendrites and synapses. Nat Neurosci 14, 1421-1429.

Yazdani, U., and Terman, J.R. (2006). The semaphorins. Genome biology 7, 211.

Yoshihara, Y., De Roo, M., and Muller, D. (2009). Dendritic spine formation and stabilization. Current opinion in neurobiology 19, 146-153.

Ypsilanti, A.R., Zagar, Y., and Chedotal, A. (2010). Moving away from the midline: new developments for Slit and Robo. Development 137, 1939-1952.

Zhou, F.Q., and Snider, W.D. (2006). Intracellular control of developmental and regenerative axon growth. Philosophical transactions of the Royal Society of London Series B, Biological sciences 361, 1575-1592.

Ziv, N.E., and Smith, S.J. (1996). Evidence for a role of dendritic filopodia in synaptogenesis and spine formation. Neuron 17, 91-102.

Zolessi, F.R., Poggi, L., Wilkinson, C.J., Chien, C.B., and Harris, W.A. (2006). Polarization and orientation of retinal ganglion cells in vivo. Neural development 1, 2.

Zou, D.J., and Cline, H.T. (1999). Postsynaptic calcium/calmodulin-dependent protein kinase II is required to limit elaboration of presynaptic and postsynaptic neuronal arbors. J Neurosci 19, 8909-8918.

Appendix: Dynamo Installation and Operation

Dynamo installation

1. Since Dynamo is a MATLAB plugin, a computer must have MATLAB installed prior to Dynamo installation. Dynamo uses the “Image processing toolbox” in MATLAB, so if not already installed, this toolbox must be included as well. Also, certain Dynamo functions require a C-compiler that can be accessed by MATLAB. Whether this already exists in the computer, can be checked by typing the following in the MATLAB command window:

```
>> mex  -setup
```

2. Once MATLAB is installed on the computer, the Dynamo folder can be downloaded from

http://haaslab.github.io/dynamo/installation.html.

Note: The folder is “unzipped” using a standard unzipping tool (i.e. WinZip or WinRar) and saved.

3. MATLAB needs to be run in “administrator” mode to set up Dynamo. This can be done by using right click on the MATLAB icon and clicking “Run as administrator”. Next, the Dynamo folder path needs to be added to MATLAB. This is done in MATLAB by clicking “File” -> “Set path” -> “Add with subfolders” -> Choose the Dynamo folder path. Clicking “Save” and “Close” saves the path. The path should remain saved on the computer even after MATLAB is closed, so the next time MATLAB is opened, the user can proceed directly to the next section, “Instructions for running Dynamo and loading image files”.

4. For time-lapse (4D) imaging, Dynamo has built-in tools to help with image alignment to account for drift during imaging.

Note: documentation including installation and usage instructions for Dynamo can be found online at http://haaslab.github.io/dynamo.

Dynamo initiation and loading image files

In this chapter examples, Dynamo prompts are in blue and user inputs are in red.

1. Dynamo toolbox is started by typing “Dynamo” + enter in the MATLAB command window. For example:

```
>> Dynamo
```

2. This displays the prompt:

```
Welcome to Dynamo!
```

Hit F1 while drawing for a list of hotkeys
Make sure you start drawing from the base of the dendritic tree!
Enter 's' to start a new stack, or 'l' to load a savefile, or 'c' to continue a new stack using the last timepoint from a finished stack,

s/l/c >>

3. A new project is started by typing “s” + enter. For example:

s/l/c >> s

This brings up a graphical user interface (GUI) to choose the file path to the images to be drawn. The user selects the location of the saved images.

For image stacks, it is suggested that the user has 2 images at a time, and uses a “treadmilling” approach for drawing. For example Image1 and Image2 can be opened and drawn. Then Image1 can be closed, but Image2 left open as reference. Next, Image 3 can be opened and drawn. This “treadmilling” method is simply a suggestion due to computer speed and screen size limitations (i.e. for a 13” screen with 4GB RAM, 1.70 GHz processor) and we have tested up to 13 image stacks open at a time in Dynamo in faster computers. The screen size can also be a limitation simply because fine details of neurons may be missed by the drawer if each image is too small, and zooming in and out continuously may be cumbersome.

If multiple files are selected (i.e. for 4D images), Dynamo asks whether to sort the files alphanumerically. If image files are labeled alphanumerically (i.e. based on time-points), the user should type “y” + enter. For example:

Sort filenames alphanumerically? y/(n) >> y

The order of drawing is important for time-lapse imaging, since this is how the program tracks dendritic processes over time.

Next, Dynamo prompts for resolution of acquired images in microns. For example, for a neuron with x and y resolution of 0.116 µm/pixel and a z-step size of 1.5µm:

Filename: ImageFile.tif
Enter the X pixel size (um) >>.116
Enter the Y pixel size (um) >>.116
Enter the Z step size (um) >>1.5
Opening image...
Preparing Data...
Done!

The user should now see the neuronal images displayed on the screen.

Note: Dynamo may also display a warning, such as:
Warning: Image is too big to fit on screen; displaying at 67% …
This simply refers to the program’s adjustment for image display, and can be ignored.

Optional: The user can manually organize images on the screen, or use the auto tiling option in Dynamo by first clicking on any image tab (where the image name is displayed) and then typing

“t”. The images should now be conveniently tiled on the screen.

6.3 Image alignment in Dynamo

For time lapse imaging, it is often necessary to align neuronal images (or image stacks) from one time-point to the next. Image drift can occur during image acquisition or, depending on the system under study, due to biological phenomena such as neuronal migration or shifting due to extracellular forces.

Dynamo has a built-in “landmarking“ tool to align images or image stacks in 3D. Importantly, this tool adjusts not only translational drift, but also image rotations. Landmarking refers to “landmarks” or consistent features present in all the images to be aligned.

Note: Landmarking should be done BEFORE starting to trace neurons, and it should be repeated for each newly opened image/image stack (i.e. for a new time-point). Also, landmarking should not be used for tracing single time-point images/image stacks.

1. Landmarking is started by first clicking on an image tab, and then typing the letter “l”. This should display the following prompt on top left corner of each image:

Adding Landmark 1: Hit Enter to Continue, L when finished.

2. Next, the user chooses a consistent landmark on the first image/image stack (i.e. a branch intersection or a consistent bending of a branch), and clicks that point. The same point is then clicked on each subsequent time-point. Once the point is clicked on all the images, the user presses enter to select the next landmark. Now, the prompt on the images should change to:

Adding Landmark 2: Hit Enter to Continue, L when finished.

3. This process is repeated for each additional landmark. In general, a minimum of 3 landmarks are suggested. For 3D image stacks, 4-7 landmarks are advisable. Once all the landmarks are completed, the user can type the letter “l” again to exit landmark mode.

Now the user can progress to the crux of the program, neural tracing.

Hint: The user is strongly advised to save the drawing at this stage, and for beginners, to save the files under different names along the way.

Neuronal tracing in Dynamo

Dynamo is designed to analyze not only individual dendritic components of a neuron, but the dendritic tree in its entirety, including connectivity of all the dendritic components. Since in a neuron, the entire dendritic tree of each neuron is physically connected, in Dynamo, the traced dendritic tree must be connected as well, and cannot exist as fragmented branches. However, the user can choose to selectively draw certain portions of the dendrites (i.e. apical dendrites only, basal dendrites only).

1. In Dynamo, tracing for time-lapse images must always be done in order, since tracing order provides critical dynamic morphometric analysis information. The starting point for tracing is

either the center of the soma, for neurons in which multiple dendrites emerge from the soma (i.e. neurons with apical and basal dendrites, basket cell neurons), or at the base of a dendritic tree, for neurons with a single primary dendrite.

Tracing is started by first clicking at the starting point, which causes a colored circle to appear, and clicking along the dendrite to the end of the dendritic tree. This should overlay a line (with circles along each of the clicked points) on top of the image. For 3D image stacks, to draw along the dendrite, the mouse scroll wheel or the numbers “1” and “2” can be used to navigate through the different z-planes. Points can be deleted by using right click on the point. To zoom in and out of images, commands “x” and “z” can be used respectively. Once zoomed in, “a”, “d”, “w”, and “s” keys are used to pan left, right, up, and down respectively (similar to many gaming commands). Importantly, while tracing, it is important to add sufficient points to capture all anatomical changes of the dendrite, but adding multiple points along straight lines will unnecessarily slow down the program.

Note: For 3D image stacks it is important to trace in the z-plane of focus. If a dendritic segment appears on several planes, it should be traced in the plane where it appears brightest. When on the plane with the tracing, the traced line will be a solid line, and when on a different plane, the traced line will be a dotted line.

2. To start a new branch, if there is already a colored dot at the intersection, a new branch can be started by first “activating” the dot by clicking on it. The activated dot is a different color than the rest of the dots along the dendrite. If a dot does not exist at the branchpoint, a dot can be inserted by using the “shift” + click at the branchpoint. Once activated, a new branch can be initiated by using either “right click” or “ctrl” + click on the new branch. The user should now see a short new branch. The rest of the new branch should be drawn with *left*, not right click, since more right clicks will be considered new branches.

Single points can be moved by using “shift + click” on the point and then clicking (without shift) on the new location. Also, segments of the dendritic tree can be moved by using “shift + click” on the beginning point of the dendritic segment to be moved, and then while holding down the “shift” key, clicking on the new location. Repeating these steps for tracing over dendrites and dendritic branches to cover all the branches will generate a skeletonized version of the dendritic tree.

Note: For convenience, Dynamo changes colors for different branches, although colors repeat. If a single branch shows up in multicolor, it should be redrawn (by either using the delete function, or if deleting creates confusion, then by restarting from a file saved before that branch was drawn).

3. For image files with multiple time-points, once the dendritic tree has been traced on the first time-point, the same dendritic tree will automatically appear on the next time-point. If the landmarking feature has been used properly, and the dendritic tree has not undergone dramatic morphological changes or shifting over the time-lapse interval, the user should find the skeletonized tree to be a close approximation of the neuronal image.

Thus, the user would be required to trace the entire dendritic tree only in the first time - point. For branches that are misaligned from the image, Dynamo has a built-in “auto-alignment” tool to adjust for any bending or shifting of the tree from the previous time-point. Auto-alignment is started by clicking on the first point on the part of the branch to be aligned and typing “r”. Dynamo command window should display the following prompt:

```
######################
#  Auto-alignment started #
#  Done!                  #
######################
```

This will automatically readjust the branch to match with the image and point out points that Dynamo could not find in “purple”. These “purple” points should then be manually moved to the proper place using the same method as described above.

4. Any dendritic additions and retractions, and annotation changes have to be adjusted manually for each time-point. A traced branch can be extended by first activating the branch endpoint, and then tracing the branch extension using left clicks. Similarly, branches can be added and subtracted, and points can be annotated to account for branch extension or retraction, by using the same method as in the first time-point.

Note: In time-lapse imaging, it is important that the auto-generated tree is used, rather than deleted and the dendritic tree redrawn, since Dynamo uses these modifications for dynamic morphometric calculations.

5. Any time during tracing, the user can alternatively view the tracing on the image plane only, or the complete tracing of the neuron by typing “v”.

Opening new time-points

To treadmill through image stacks, the user must close previous time-points and open the new time-points. The very last traced time-point should be left open as a reference for subsequent drawings. New image stacks are opened by using the “ctrl” + “o” command.

Note: It is important to use the landmark tool for each newly opened image BEFORE starting to trace or to make adjustments. Also, especially for new users, it is advisable to save files after finishing each time-point under different filenames.

Annotations

Often the user may want to differentiate various dendritic components, such as DGCs, basal dendrites, or apical dendrites. To make these distinctions, or any user-defined distinctions, there is an annotation feature in Dynamo. Any point along a dendrite can be annotated. Annotation is activated by clicking on a point and typing “q”. A dialog will open, allowing the user to type any custom annotation. For example, in Chapter 4, I have used the following annotations: “lam” to indicate lamellipodia, “basal” to denote basal dendrites”, “soma” for soma, “rootstart” and “rootend” to define the beginning and end of the primary dendritic branch angular orientation. These annotations can then be used both in pre-defined built-in Dynamo analyses as well as any user-defined custom analyses.

Saving files

Dynamo files are saved with the “ctrl” + s command.

Dynamo shortcuts

A list of all the Dynamo commands appears in Table 4. Also, during tracing, a list of commands can be attained by using the F1 key.

Command	Action
the letter "t"	Image tiling on screen
Left click	Add a point (i.e. to extend a dendrite)
"1" or "2"	"1" scrolls through image stacks in one direction, and "2" scrolls in the opposite direction
"x"	Zoom in
"z"	Zoom out
"a"	to pan left (panning only works when zoomed in)
"s"	to pan down (panning only works when zoomed in)
"d"	to pan right (panning only works when zoomed in)
"w"	to pan up(panning only works when zoomed in)
Click (to activate an existing point), followed by "ctrl" + click on another point	Branching
Click (to activate an existing point), followed by Shift + click on an adjacent point.	Add points to the dendritic tree
Shift + click on an existing point, followed by clicking on a new location	Moves existing point to the new location
Shift + click on an existing point, then while holding down shift, clicking on a new location	Moves the point and all downstream points to the new location.
Shift + click on an existing point, then click on a new branch	Reassigns the point and all downstream points to the new parent branch.
"l"	To enter or exit landmark mode.
"r"	Auto-alignment
"q"	To annotate a point
"f"	To show/hide annotations
"v"	To show/hide complete dendritic tree tracing
"3"	Show dendritic skeleton in 3D
Right click on a point	Deletes the point
Backspace	Undo
ctrl + "o"	Opens new images
ctrl + "s"	Saves drawing session
Click on the tab of one of the opened images, then press "F1" key	Shows Dynamo hotkeys

Table 4. List of Dynamo shortcuts

Analyses

It is critical that the neuronal tracings are done accurately follow the real dendritic structure since they are the basis for all analyses. Once these tracings are completed and saved, these files (referred to as 'savedata') can be analyzed in a multitude of different ways, using built-in and user-defined analysis functions.

Built-in functions

1. Dynamo Analysis GUI is started by typing "Dynamo_Analysis_GUI" in the MATLAB command window. For example:

```
>> Dynamo_Analysis_GUI
```

2. This brings up a GUI to choose the file path to the saved Dynamo tracing files. Once the user selects the location of the saved tracing files, the GUI prompts the user to choose the "output directory", where analysis outputs are saved.

3. Next, the "Dynamo Analysis Engine" GUI is displayed with a list of the selected tracing files, and a list of all the analysis functions (i.e. TDBL, motility, lifetime, etc.). For most analysis functions, several tracing savefiles can be analyzed simultaneously. For example, the "TDBL" or Total Dendritic Branch Analysis function displays the TDBL of each cell at all different time-points. Additional savefiles can be added to the Dynamo Analysis Engine, by clicking on the "Add Drawing Files" button. Next, the user selects the analysis function to be used from a scrollable list and clicks the "Go !" button.

4. Next, the "OPTIONS" GUI is displayed with customizable options specific to each analysis function. For example, for the Total Dendritic Branch Length analysis, the total length can be analyzed with or without including filopodia or basal dendrites. For the built-in analysis, the following annotations (capital letter sensitive) are used by default: "axon" denotes axon, "basal" denotes basal dendrites, and "soma" specifies the location of the soma. However, if the user wants to use different annotations, they can be set in the "OPTIONS" GUI under "Labels". For proper analysis, it is imperative that these annotations (or labels) are the same ones used while tracing the neurons. Once all the options are specified, the user clicks "Done".

5. A figure with the analysis output is displayed. Often in addition to these auto-generated figures, it may be necessary to access the raw numbers. Clicking on the figure tab to select the figure window, and then typing "x" exports the data as a MATLAB file, which shows up in the MATLAB workspace (i.e. "tdbl_export" MATLAB file is generated for the TDBL function). From here, the user can choose to manipulate this data directly in MATLAB or copy and paste the data to excel or statistical software.

Function	Description
added_subtracted_transitioned_Sharmin	Analysis of interstitial vs. branchtip filopodial turnover, differentiating between pre-existing and new filopodia, and interstitial filopodial trasition to branches.
added_subtracted_transitioned	Analysis of filopodial turnover (additions, retractions) and trasitions to branches. This function is useful for writing custom MATLAB functions. Please also see: 'added_subtracted_transitioned_DM' for further turnover analysis.
angular_sholl	Gives length or branchtip numbers at different angles from the root angle. Root angle defined by "rootstart" and "rootend" annotations.
branches_added_subtracted	Analysis of branches added and subtracted.
branch_motility	Motility of branches based on branch orientation.
Lifetime	Calculates lifetimes for pre-existing filopodia, new filopodia, and all filopodia. Pocesses other than filopodia (i.e. branches) have lifetimes of 'NaN', and filopodia that last until end of imaging have lifetimes of 'Inf')
motility_DM	Analysis of interstitial and branchtip filopodial motility (mean motility for each filopodia averaged over time-points), differentiating between pre-existing and new filopodia.
numFilo	Calculates interstitial and terminal filopodia number and filopodia density (filopodia/total dendritic branch length).
TDBL	Total dendritic branch length (TDBL) with options to include or exclude filopodia, basal dendrites, and axons.
Wireframe	Generates a skeleton structure of the traced neuron.

Table 5. Examples of Dynamo built-in functions.

User-defined functions

To write user-defined functions, the user needs to access data from ‘savedata’ files, which contain information on all xyz points, sub-branches of each point, and annotations. Each savedata file contains, fields called ‘state’, which refers to a specific time-point in the drawing file.

To become accustomed to the nature of the ‘savedata’ file, a new Dynamo user should open a saved neuronal tracing file and peruse though it. The Dynamo savedata, as with any MATLAB saved variables, can be loaded either by dragging it into the MATLAB workspace or by the following actions: “File” -> “Open” -> Choose savedata path. Once loaded, the user can navigate through savedata by double-clicking through various components and layers of this variable (i.e. “state”, “traits”) in the MATLAB “Variable Editor” similar to the way one navigates through folders in the Windows environment.

Structure of 'savedata' files

To access data for a specific time-point 2, the user would type 'savedata.state{2}'.The savedata.state component is a "cell array", a data type, which consists of as many cells as there are time points. For example, savedata.state{1} contains information for time-point 1, savedata.state{2} contains information for time-point 2, and savedata.state{n} refers to the same for time-point n. Each savedata.state{n} cell has 10 'fields' as shone in Figure 18.of which 'info' and 'tree' are useful in writing analysis functions; the other fields can be disregarded for most analysis purposes. To write a custom analysis function, a list of all the xyz coordinates for points that make up branch number 3 (branches are numbered according to the order at which it was traced) at time-point 2 can be obtained by 'savedata.state{2}.tree{3}{1}'. Similarly, the annotations for a specific point on the tree can be obtained by 'savedata.state{2}.tree{3}{3}' (Figure 19). Examples of how to use this variable to access relevant information for analysis and a breakdown of what each of the elements of the variable name means are shown in Figure 19

The following code demonstrates one way to calculate the length of branch 3 at time-point 2. The actual code is denoted in blue, whereas the lines following '%' is merely for explanatory purposes.

```
A = savedata.state{2}.tree{3}{1};
%obtain xyz coordinates for branch 3 at time-point 2 and save the values as 'A'.

B = diag([state.info.xres state.info.yres state.info.zres]);
%create a diagonal matrix composed of x,y,z resolutions (obtained from the microscope
%during imaging) and save the values as B.

C = diff(A*B);
% multiply image resolution by each coordinate and take the difference. 'diff' is a built-in
% MATLAB function

Distances = sqrt(sum(C.^2,2));
%take the Euclidean distance (formula = √(x^2 + y^2 + z^2)) between each point.

BranchLength = cumdist[0; cumsum(Distances)];
%obtain cumulative sum of distances between each point on the branch to obtain total
%branch length. Note: 'cumdist' and 'cumsum' are built-in MATLAB functions.
```

As shown in Figure 19, the savedata variable contains room for annotations. Annotations provide a way for users to demarcate any points on a neuron tracing. This can be useful, for example, to differentiate between apical and basal dendritic processes, or denote dendrites versus axons. Currently, the Dynamo built-in functions account for the following annotations: soma, basal, axon, and lamella. These were designed based on the needs of our lab, and can be modified in the source code.

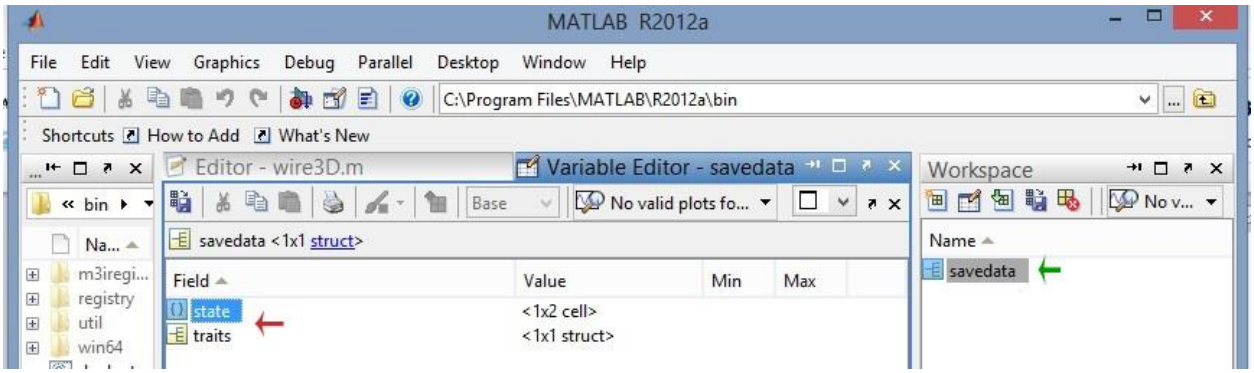

Figure 18. Loading savedata in MATLAB
Green arrow points to savedata (saved neural tracing file). Red arrows point to components of savedata.

New custom functions can be added to the “Dynamo_Analysis_GUI” tool by saving the new function in the “Dynamo/Analysis/Functions” folder as a MATLAB “.m” file. Each of the “Dynamo_Analysis_GUI” functions (listed inTable 5), appears as “.m” files in this folder. Before writing a new function, it may be helpful to take a look at the source code for an existing Dynamo built-in function. Function source code can be viewed or edited by typing “edit” followed by the function name in the MATLAB command window. For example, to open or edit the TDBL function source code:

```
>> edit TDBL
```

Please note that, in many cases, instead of writing functions from scratch, it may be easiest to modify existing functions and save it under a new name as a different function.

A

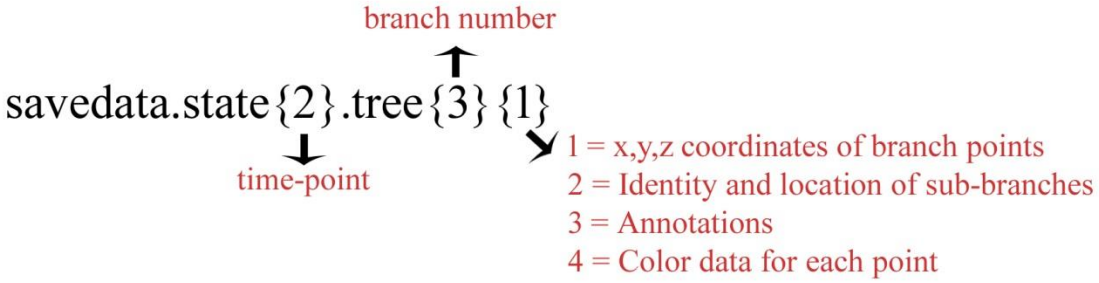

B

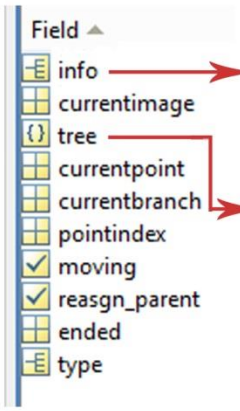

Field	Relevant content for writing analysis functions	Example syntax for accessing information
info	filename	savedata.state{2}.info.filename
	x resolution	savedata.state{2}.info.xres
	y resolution	savedata.state{2}.info.yres
	z resolution	savedata.state{2}.info.zres
tree	Branch info:	
	x,y,z coordinates of all the points on the branch	savedata.state{2}.tree{3}{1}
	Identity of sub-branches at each branch point	savedata.state{2}.tree{3}{2}
	Annotations (i.e. 'LAM', 'BASAL') at each branch point	savedata.state{2}.tree{3}{3}
	Color data for branch points (not relevant for analysis)	savedata.state{2}.tree{3}{4}

Examples shown for time-point 2.

Examples shown for time-point 2, branch 3.

Figure 19. Structure of the 'savedata' file and its components.
(A) Breakdown of elements of the 'savedata' files. (B) Structure of the 'savedata' variable, including descriptions of 'info' and 'tree', the 2 fields relevant for writing most custom analysis functions.